Eddy Current Techniques for Non-destructive Testing of Carbon Fibre Reinforced Plastic (CFRP)

A thesis submitted to The University of Manchester for the degree of
Doctor of Philosophy
in the Faculty of Engineering and Physical Science

2012

Xin Li

School of Electrical and Electronic Engineering

List of Contents

List of Figures

List of Tables

Abstract

This thesis describes research on the use of eddy current techniques for non-destructive testing of carbon fibre reinforced plastic (CFRP). The research has involved bulk conductivity testing, fibre direction characterization and 3D FEM modeling of the CFPR and eddy current probes geometry. In the conductivity testing, how the sample thickness, fibre volume content and fibre conductivity affects the signal from the eddy current has been evaluated. Eddy current testing shows good directionality as CFRP is an anisotropic material, thus is very suitable to characterize the fibre orientation. Direction sensitive probes have been developed and tested to reveal information about the fibre direction and layer. Computer FEM software has been used to analyze the magnetic field inside the sample and probes. Specific probe geometries have been designed depending on the electrical properties of the composites and testing requirement. The experiment, simulation and analysis results show very good agreement. However, when the measuring frequency increases, noises and parasitic capacitance inevitably become significant and have a negative influence on the results. Improvements and further research are proposed which are believed to make eddy-current techniques a more feasible and efficient measurement method, will contribute to the development and maintenance of light weight CFRP composites.

Declaration

No portion of the work referred to in the thesis has been submitted in support of an application for another degree or qualification of this or any other university or other institute of learning.

Copyright Statement

and/or Reproductions described in it may take place is available in the University IP Policy (see http://www.campus.manchester.ac.uk/medialibrary/policies/intellectual-property.pdf), in any relevant Thesis restriction declarations deposited in the University Library, The University Library's regulations (see http://www.manchester.ac.uk/library/aboutus/regulations) and in The University's policy on presentation of Theses.

Abbreviations

3D	Three Dimensions
AB	Air Bus
AC	Alternative Current
CFRP	Carbon Fibre Reinforced Plastic
CPU	Central Processing Unit
CT	Computed Tomography
DC	Direct Current
EDA	Engineering Design and Analysis
EEC	European Economic Community
ET	Eddy Current Testing
FCV	Fuel Cell Vehicles
FE	Finite Element
FEM	Finite Element Method
GPIB	General Purpose Interface Bus
GUI	Graphical User Interface
MT	Magnetic Particle Testing
NDT	Non-Destructive Testing
NMAB	National Materials Advisory Board
PC	Personal Computer
PT	Liquid Penetrant Testing
RAM	Random Access Memory
RT	Radiographic Testing
RTM	Resin Transfer Moulding
SAM	Scanning Acoustic Microscopy
UK	United Kingdom
US	United States

UT	Ultrasonic Testing
VBScript	Visual Basic Script

Publications

"Non-contact characterization of hybrid aluminium/carbon-fibre-reinforced plastic sheets using multi-frequency eddy-current sensors", Measurement and Science Technology, 21, 2010, 105708 (7pp)

"Non-Contact Characterisation of Carbon Fibre Reinforced Plastics in Hybrid Aluminium / CFRP Sheets Using Multi-frequency Eddy Current Sensors", IEEE International Instrumentation and Measurement Technology Conference, Singapore, 05/2009

"Characterization of Carbon Fibre Reinforced Plastic by Means of Eddy Current Non-Destructive Testing and FEM Modeling", 17^{th} World conference of Non-destructive Testing, ShangHai, 09/2008

Acknowledgment

First of all, I wish to express my great gratitude thanks to my academic supervisor Professor Anthony Peyton**,** school of electrical and electronic engineering, university of Manchester for his priceless supervision, guidance, understanding and constructive advice during my studying and living in Manchester. His rich experience and expertise are very valuable and essential to the completion of this project.

I am very grateful to my academic advisor Professor Philip Withers for his overall support and dedication into the project and my professional development.

I would like to say ‘Thank you’ to Dr Wuliang Yin and Dr Christos Ktistis for their helpful advices and willingness for open discussion.

Special thanks to everyone in E48 who lighten my UK life with their precious friendship and happiness.

Finally, I want to show my sincere appreciation to my family and fiancée for their support, patience and encouragement.

Chapter 1. Introduction

1.1 Motivation for the PhD Research

How to improve the performance of carbon fibre reinforced plastic (CFRP) material which is now widely used in aircraft and automobile industry is a big issue for current scientists and entrepreneurs. To make sure components made by CFRP material are working in proper conditions, it is necessary to carry out non-destructive inspection and monitoring of the components during certain periods. However, the limitation of non-destructive methods for the inspection of CFRP composites is a major problem for many practical applications of the material, especially in the aircraft industry.

CFRP is a composite made with carbon fibres embedded in a polymer, commonly an epoxy matrix. The fibres, which are usually 7 to 15 μm in diameter, are bundled together to form a tow, which can then be woven into a fabric or laid down unidirectionally to form a lamina. A single lamina has a thickness of about 0.05-0.2 mm, and so in order to obtain usable mechanical engineering components, many laminae are stacked in same or different directions to form a laminate. This fibre directionality contributes to the electrical anisotropy in CFRP, which means the composite electrical conductivity is typically much higher in the fibre direction and lower perpendicular to fibre direction, with the electrical conductivity ratio being several orders of magnitude.

To non-destructively characterize CFRP structure and optimize its manufacturing, various inspection techniques have been studied and developed such as ultrasonics, scanning acoustic microscopy, embedded optical fibre, microwave technique scanning and DC or AC conductivity measurement. Eddy current testing has gained interest for in-service inspection and rapid quality control because it is fast, simple, portable and non-contacting [1,2]. Some recent work has been published [3-6], which introduces the application of eddy current testing on various fields including aerospace, manufacture, and quality monitoring.

Compared with other developed and well used non-destructive testing methods, eddy current testing is proved to be a very useful tool in inspection as it possesses advantages over other technique on cost, developing period and efficiency. Also, eddy current testing instruments are able to achieve in-service inspection and non-contact testing. In addition, by virtue of electromagnetic principles, eddy current testing is more suitable for electrical conductive material such as CFRP which possesses conductivity resulting from the carbon fibres. Considering all of above factors, eddy current testing is thought of as a very promising method for non-destructive characterization of CFRP material.

1.2 Aims

The limitation of non-destructive methods for the inspection of CFRP is a major problem involving many practical applications of the material, especially in the aircraft industry. The study of this project is directed towards non-destructive characterization of CFRP using eddy current methods. The relationship between the signal from different types of inductive probes and the microstructure of CFRP samples has been studied. The measurement of a bulk equivalent electrical conductivity of the material is based on the Deeds and Dodd’s analytic solution, which provides the fundamentals for prediction and detection of fibre fracture and material defects. Fibre direction characterization will also be performed on unidirectional and multidirectional CFRPs using a highly directional probe. Based on these, detection of

CFRP defects can be realized. In addition, 3D finite element method (FEM) computer simulations have been developed to demonstrate the coupling of the probes and samples, and to support the experimental method. This project is aimed to build up a methodology of eddy current testing for characterization of CFRP and look forward to developing a set of testing systems.

1.3 Achievement of The Project

The main achievement of this project was successfully developing and applying eddy current method to non-destructive characterization of CFRP material. The method was based on Dodd and Deeds theory of determining equivalent bulk conductivity using eddy current coils, as well as by virtue of CFRP material's electrical conductivity and anisotropy. An eddy current testing system consisting of all the devices and equipments, eddy current probes, and controlling computer was designed and put into use in the project. All operation including measurement configuration, probe setup, scanning control, signal processing and result analysis could be executed through the interface which was programmed in MatLab environment. This system in cooperation with various probe designs was able to carry out bulk conductivity testing, fibre direction characterization and lift-off measurement. 3D FEM models of the CFRP samples, eddy current probes and measurement environment have been developed. The modeling results had a good agreement with measurement ones, which proved the theory and the performance of measurement system. The 3D models were also beneficial to simulate and predict the performance of more complicated samples and measurement conditions. What is more, this eddy current method has also been applied to the non-destructive characterization of hybrid aluminium/CFRP material and the material's properties could be obtained. As the outcomes of this project, three papers have been published on international conferences and scientific journals which have been listed in previous Publications part.

1.4 Organization of the Thesis

The research work and results are discussed in the following chapters.

Chapter 2 gives fundamental introduction to the non-destructive testing techniques and the requirement from the industries and research bodies for non-destructive testing. Following, the background knowledge of CFRP material including its formation, performance, application in industry, and structural and electrical properties are presented. The last part of this chapter is focused to discuss the non-destructive characterization of CFRP and the current popular methods with results and comparisons.

Chapter 3 describes in details the theory and principle of eddy current testing. The change of the impedance of eddy current coil indicated the information of the sample under inspection. At the same time, the side effects such as the skin effect and phase lag need to be taken into consideration. In the study of coil's impedance, the coil can be indicated as an equivalent parallel RLC circuit with a resistor in series with an inductance. To carry out eddy current testing, the basic system consists of excitement generating devices, probe, and measurement instruments.

Chapter 4 presents the details of eddy current system including the system configuration, probe design, measurement operation and result analysis. A practical solution for measuring conductive plate with circular air-cored coil is proposed based on Dodd and Deeds' formulas, by which the electromagnetic property of the material can be calculated considering most of the measurement parameters and a set of fundamental equations can be achieved. According to the measurement aims, two types of probes are designed and used to make use of the electrical conductivity and anisotropy of CFRP material. This chapter also introduces the development of an advanced measurement system for more accuracy, stability, automation and flexibility.

Chapter 5 discusses the 3D FEM modeling and simulation for characterization of CFRP. The geometry of probes and tested samples are modeled and the parameters are set up in the simulation software. To achieve the communication between simulation software and computers, an interface using the Visual Basic Script program is developed. In term of resource cost and result accuracy, it needs to find out an optimal simulation configuration. The modeling technique can provide the characterization with high flexibility and accuracy with access to the properties of probe, sample and simulation, which in turn supports the analytic and experimental results.

Chapter 6 introduces the application of the eddy current method on the non-destructive characterization of hybrid aluminium/CFRP material. In order to inspect various properties of the material, two specific types of eddy current probes are designed for different purposes. Both the measurement and simulation results can support the outcome of the analysis. To link the bulk conductivity with the conductivity tensor, a formula is proposed and verified. Also, the lift-off effect is studied and eliminated by a balance formula.

Chapter 7 concludes the results and achievements of the whole PhD research project. The future work including probe design, improvement to system development and damage inspection are also proposed.

Chapter 2. Background of NDT and CFRP

Non-destructive testing involves extensive knowledge of techniques in various subjects and it is impossible to present full details in a single PhD thesis. However, a brief review is provided in this chapter to help present the relevant background and give a better understanding of this research work. CFRP (carbon fibre reinforced plastic) is a composite material which is widely used for engineering applications. This chapter also presents information on CFRP which is expected to make readers more familiar with this material.

2.1 Overview of Non-Destructive Testing (NDT)

2.1.1 Requirement for Testing

During the process of manufacturing, it is possible that defects and flaws of various natures and sizes can be introduced into the materials and components which may result in the malfunction or failure of the final product. On the other hand, during service, the industrial component may suffer quality decrease and risk of failure due to the presence of other imperfections such as fatigue and impact cracks. These defects and flaws may even result in further accidents and individual injury. Therefore, for the purpose of high product quality and less cost, at the manufacturing stage, it becomes necessary to find proper and reliable examination to detect mis-assembled or malfunctioned components, missing or displaced parts, to measure spacings and so on;

and regular health monitoring and flaw/defect detection during the components or products' service are required to prolong their working time and avoid breaking down or bigger loss. Table 2.1 summarizes some possible flaws and defects occurring in the components and products during their different stages [7].

Manufacture stage	machining faults, heat treatment defects, welding defects, stress cracks
Assembly stage	missing part, wrongly assembled parts, additional welding and stress cracks
Service stage	fatigue, corrosion, stress corrosion, wear, creep, thermal instability

Table 2.1 Possible flaws and defects in the components and products during their different stages

To be stricter, the terms 'defect' and 'flaw' should be defined from a technical view. It is difficult to say which one is more suitable to a particular occasion than another, as in many dictionaries, a flaw is even defined as a defect. A defect, explained by EEC (European Economic Community) [8], indicates the group of imperfections which can make the component defective or unserviceable, while the word 'flaw' represents any imperfection which is classified to be non-rejectable. Hence, according the definitions, it is incorrect to call an imperfection as an acceptable defect. Although there is no uniform standard by which to distinguish both, common sense and the evaluation method can be helpful [9]. In applications relating to quality-control or fitness-for-purpose in which the evaluation is carried out to decide rejectable component or product, these two terms make a considerable difference and can not be interchanged.

Testing can be found in many places in everyday life and industry, and examples include:

- Aircraft skins are subject to corrosion and stress corrosion cracking.
- Food and medical products require high standard inspection before they are bought by the consumers.
- Underground pipelines need regular checking to detect cracks.
- Drink machines check the inserted coins for the total amount.
- Airports use security gate to detect threat objects carried by passengers.

- Pipes in industrial plants may be subject to erosion and corrosion from the products they carry.
- Concrete structures may be weakened if the inner reinforcing steel is corroded.
- Doctors use medical devices to image patients' organ.
- The wire ropes in suspension bridges are subject to weather, vibration, and high loads, so testing for broken wires and other damage is important.

2.1.2 Destructive and Non-destructive

To carry on testing work, there are a wide range of choice of testing methods, some of which are destructive and some non-destructive [10].

By definition, destructive testing is described as a method in which the specimen is destroyed or mechanically changed in order to get the maximum information about the specimen's structure or performance under different loads. Sometimes, the testing is carried out under the simulated service conditions and environments to obtain a precise result which is only specific to the specimen under examination. Moreover, this method can provide direct access to the specimen's inner structure and the response to outer changes, therefore the most detailed information can be obtained.

A natural consequence of destructive testing is that the specimen cannot be used any more in service due to the damage from the testing process. According to its nature, destructive testing is most suitable and economic for specimens which are mass produced in an identical form, as the cost of damaging a small amount of specimens can be ignored.

Non-destructive testing, in principle, is a form of testing, examination or evaluation made on an object to study the absence or presence of conditions or imperfections that possibly make an impact on the function of serviceability of the objects in the way that will not cause any kind of change or alteration on the performance of the object [11]. The science of non-destructive testing incorporates all the technology for detection and measurement of significant properties and imperfections, in items ranging from research specimens to finished hardware and products [1].

Where the tested object needs to remain its original condition or the inspection is made in-service, non-destructive testing has the advantage of producing desirable information at lower cost than destructive tests, as the testing cost incurred is very often negligible compared to the possible financial and human loss caused by the product failure and malfunction. As a very broad, interdisciplinary field, non-destructive testing involves subjects like chemistry, electronic and electrical engineering, mathematics, material science, physics. So, for a specific application, choosing a suitable method or a combination of several methods makes a big impact on the final results. Also, for particular object, the testing method may be variable at different stages of the product life cycle, often with notable difference between manufacturing and service stages.

In fact, non-destructive testing is being performed by every person in the daily life and human body can be looked as the most unique and versatile nondestructive testing device so far [11]. Even in such a simple process as cooking at home consists of a series of non-destructive tests taken by a human's complicated sensing system. By smelling the odour, observing the color and feeling the temperature, the cook is able to determine if the food is ready to serve. As an extension to the human senses, non-destructive testing is well developed though the use of advanced electronic instrumentation and other specific equipment.

For the non-destructive testing to be well controlled and optimized, some factors need to be considered. These include: 1. the inspected object must be testable. Every NDT method has its own requirements and limitations, as well as specification for the tested object. Before beginning a test, the object should meet the certain needs of the specific method and be accessible to the testing tool. 2. The testing process must be carried out following secured procedures. To make the non-destructive testing successful and effective, it is necessary to perform the testing following the approved procedure which has been developed according to the specific requirement and specification. 3. The equipment works without problem. It is very essential to make sure that all the equipment is in good conditions and can operate properly. What is more, periodical check is required that all the equipments are under control. 4. Documentation is adequate. The entire testing documentation which includes a primary part such as calibration data, equipment and component description, procedure followed and flaw or defect detected, etc should be produced. In addition, the documentation should be easy to read and interpret. 5. Operator is properly qualified. Most of the non-destructive testing is hands-on work, so the skill, knowledge and experiment of the operator are very important. The individuals need to be trained well before starting the testing so that the testing can be performed in the correct way and the result is reliable.

In general, non-destructive testing is regarded as a more advanced method than destructive testing and has been used more widely in many fields. But destructive testing also can find its application in some specific cases where destructive shows advantages over its peers. The table 2.2 presents the comparison between destructive and non-destructive testing.

Non-destructive testing	
Advantages	**Limitations**
The tested object is not altered so could be used after testing.	The result may depend on the capability of the operator.
Many non-destructive testing systems are portable so that it is easy to get close to the object.	Evaluation of some result is subjective.
In general, non-destructive testing costs less.	Approved procedure is essential.
It is able to inspect material's internal structure and the surface.	
Component can be tested in service.	
Destructive testing	
Advantages	**Limitations**
Destructive testing is able to be applied for various service conditions.	Most destructive testing specimen can not be in service after examination.
The destructive testing data is quantitative usually.	The result is only for the tested object.
The result is very useful for the purpose of design.	Destructive costs are more as it needs large and expensive equipments in a laboratory environment.
The testing data from the specimen is reliable and accurate.	
The result can help make predictions4.	

Table 2.2 List of advantages and limitations of two testing techniques

By use of NDT methods and techniques, it is possible to decrease the factor of ignorance about a material without decreasing the factor of safety in the finished product [2]. In general, the purpose of NDT will fall into one of the following categories:

- Determination of material properties.
- Detection, characterization, location and sizing of discontinuities/defects.
- Determining quality of manufacture or fabrication of a component/structure.
- Checking for deterioration after a period of service for a component/structure.

The origin of defects in a material can take place during the manufacturing stage, or during assembly, installation, commissioning or during in-service [3]. These defects, in turn, result in deterioration of mechanical properties, crack initiation and propagation, leaks in pressurized components and catastrophic failures [4]. The types of defects that NDT is applied to, can be classified into three major groups:

- Inherent defects - introduced during the initial production of the base or raw material.
- Processing defects - introduced during processing of the material or part.
- Service defects - introduced during the operating cycle of the material or part.

The kind of defects or structural variations which may exist in these three groups are, cracks, surface and subsurface, arising from a large number of cases; porosity; tears; machining, rolling and plating defects; laminations; lack of bond; inclusions; segregation; lack of penetration in welds; fatigue defects; seams; blow holes, gross shrinkage etc.

2.1.3 Benefits of NDT

The benefits derived from NDT to industry are numerous [5]. Increased serviceability of equipment and materials will result through the application of NDT techniques by finding and locating defects which may cause malfunctioning or breakdown of equipment [6]. Provided a reliable relationship is found between the measured NDT parameter and process variables, the technique can be used to improve the product quality and process efficiency [12].

Non-destructive testing can also be beneficial in reducing the frequency of unscheduled maintenance which usually is more expensive than regularly scheduled maintenance. Often, NDT can be used to inspect questionable parts whilst they are still in site on the equipment, thereby preventing an unscheduled and unnecessary shutdown if the part is in fact defect free. With assurance that there is no defect present, the equipment may continue operating without fear of failure.

Additionally, scheduled maintenance periods may be lengthened with the proper use of NDT in the maintenance cycle. Knowing from an inspection that crucial parts are not approaching failure may allow the machine to operate safely for a longer period of time. Less frequent maintenance may be more cost-effective provided that the cost of operation is not increased due to an unexpected failure.

During manufacturing stages, NDT can be used to detect defects at various stages during production, by means of off-line measurements. While there are clear benefits in this approach, it has the drawback that off-line measurements interrupt the process stream and reduce the productivity [13]. A better way would be monitor for incipient defect formation on-line. For example, on-line monitoring and control of the welding process has the potential to improve weld quality and increase productivity in automated welding.

In summary, modern non-destructive testing techniques can be used by manufacturers to

- Ensure the integrity and reliability of a product.
- Prevent accidents and saving lives.
- Ensure customer satisfaction.
- Aid in product design.
- Control manufacturing processes.
- Lower manufacturing costs.
- Maintain uniform quality level.

2.1.4 Growth of NDT Techniques

One key event in the development history of NDT was the boiler explosion that happened in Hartford, Connecticut, US in March of 1854, in which 21 persons were killed and more than 50 people were seriously injured. This catastrophic accident, as well as other dramatic failures drew awareness and appeal for safety. This was a significant turning point in the importance and process of inspection and non-destructive testing. As following, inspection laws for industry and relevant organization have emerged [11]. Initially progress was slow due to the lack of suitable inspection technique and as technology advanced, the majority of the NDT methods which are used at present made significant progress in the late 1930s/early 1940s, and the growth accelerated during the Second World War, the tremendous need for inspection and testing greatly boosted the development and application of non-destructive testing both in industry and the military.

One of the earliest applications of NDT was the detection of surface cracks in railcar wheels and axles. The parts were soaked in thinned oil, then cleaned and dusted with a fine white powder. When a crack was present, the oil would seep out from the crack and turn the white powder brown providing visual indicating that the component was flawed. This was the forerunner of modern liquid penetrant testing.

X-rays were discovered in 1895 by Wilhelm Conrad Roentgen(1845-1923) who was a Professor at Wuerzburg University in Germany [11]. Soon after his discovery, Roentgen produced the first industrial radiograph when he imaged a set of weights in a box to show his colleagues. In 1920, Dr. H. H. Lester from Watertown Arsenal in Boston started his research in developing X-ray techniques to inspect the castings, welds and armour plate in purpose of enhancing the quality of material used in the army. His work and research outcome made the foundation of the industrial radiography for metal inspection.

In 1929, the Magnaflux Corporation was established based on the use of magnetic particle testing principles which exploited the result of electromagnetic conduction and induction experiments performed by Professor A. V. Deforest and F. B. Doane [11]. The devices designed from this company provided an advanced method to detect surface discontinuities in ferromagnetic materials, especially applied in the railway track inspection, which is still in use today.

The uses of radium for gamma radiography found its application in the industry from the 1930s. Dr. Robert F. Mehl was developing a method by which the detection of discontinuities in materials could be performed by use of radium [11]. At that time, this task could not be achieved by low energy X-ray. Early X-ray devices can only generate low energy X-rays which make the exposure time on structures very long. However, in the 1940s, as a big breakthrough, the first million volt X-ray machines were designed for industry which could generate higher energy to perform inspection for thicker material.

When a material gets stressed, it will generate noise and when the noise density increases, there is an indication that the object is getting close to failure. Based on this phenomenon, the first research study of acoustic emission testing was carried out by Dr. Joseph Kaiser as his PhD thesis in Germany during the 1950s [11]. His study showed the fact that the acoustic emission events happened as result of small failures in a material which was subject to the stress. These early experiments were done in the audible frequency range, however, as electronic systems advanced the frequency increased and present day acoustic emission testing is made at very high audio or ultrasonic frequencies to provide a valuable method to inspect in-service characteristics of many materials and structures.

Eddy current testing for non-destructive characterization had its origin in 1831, when Michael Faraday discovered the principles of electromagnetic induction [11]. The first documented eddy current test was taken by E. E. Hughes in 1879, in which he could find the difference between various metals by applying multi-frequency electromagnetic induction. In 1926, the first eddy current instrument showed was designed to measure metal thickness. During the Second World War and the early 1940s, there was a large development on eddy current testing due to military demand. More advanced instruments with impedance plane signal have been introduced by Forster in 1950s, which can distinguish between a number of parameters.

Since the 1920s, NDT has developed from a laboratory demonstration to an indispensable tool of production [14]. The real revolution in NDT took place during World War II. The progress in materials engineering in identifying new and improved materials subsequent to a number of catastrophic failures during this period, such as the brittle fracture of Liberty ships, necessitated the requirement to test and improve material properties. This requirement resulted in a wider application of the then existing NDT methods and techniques and also paved the way for development of new methods and techniques. Electronic inspection techniques such as ultrasonic and eddy current testing started with the initial rapid developments in instrumentation spurred by technological advances following World War II. Significant improvements have also been made both in the NDT equipment and in the specific techniques used [15]. As NDT techniques improve the performance reliability of components through periodic in-service inspections, which is able to prevent premature and catastrophic failures [16, 17], the method has become a vital ingredient of modern engineering practice contributing significantly to overall safety, reliability and confidence at economic cost [18].

2.1.5 NDT Methods

Although, there has no clearly defined boundary for non-destructive testing [8], traditionally, it is considered that there are five major and established methods: liquid penetrant testing, magnetic particle testing, radiographic testing, ultrasonic testing and eddy current testing. They have their effectiveness and efficiency enhanced by conversion to electronic, computerized, or robotic operation. Further, a large number of even new and more specialized methods have been investigated, developed and found to have applications in particular fields, such as for example thermography.

2.1.5.1 Liquid Penetrant Testing (PT) [8]

PT is thought of as one of the most widely used non-destructive testing method in the detection of surface discontinuities in nonporous solid materials. Today, it is still very popular in surface NDT testing as it is effective for both magnetic and nonmagnetic materials. In industry, PT is applied to detect surface-breaking discontinuities like laps, folds and cracks in almost any materials with a non-absorbent surface. In engineering materials, many cracks look very small on surface opening width even though they could be very deep inside. So, although they give just little information on the surface, the potential consequence may be very serious and result in big failure on the strength of the components. In the case where it is difficult to detect the cracks by normal visual inspection, PT is an effective alternative.

In manual operation, the penetrants are usually solutions with color or fluorescent dyes in oil-based liquids. Another option is water-washable penetrants without oil. The penetrant wetting the surface can seep into the open cracks. Then the excess liquid is removed from the surface and a white developer is put on. The developer draws out the liquid in the cracks which carries a dye of a fluorescent substance. Therefore, the characteristics of the penetrant are related to information of the inspected cracks.

2.1.5.2 Magnetic Particle Testing (MT) [8]

MT usually requires electrical equipment to generate a magnetic field. Only metals which can be magnetized are tested by MT. The flaws do not have to be open to the surface but must be close to it. MT works best for flaws which are elongated rather than round. An internal magnetic field is generated in the tested specimen. In locations where flaws (non-magnetic voids) exist, some of the field will leak out of the specimen and bridge the voids through the air. Magnetic (iron) particles, dusted over the magnetized area, are attracted by the leakage or external fields, and the build-up of the particles gives an indication of the presence of a flaw.

2.1.5.3 Radiographic Testing (RT) [8]

The safety hazard inherent in RT dictates a special installation in which the material density and thickness set the limits of usefulness. The strength of RT is its ability to detect internal, non-linear flaws whereas the two dimensional views sometimes a drawback of the technique. RT uses penetrating radiation and works on the principle that denser or thicker materials will absorb more radiation of it. The specimen is placed between a source of radiation and a sheet of radiographic film or detector array. A flaw present anywhere within the specimen will absorb less radiation than the specimen itself. The flaw's presence and location will be indicated on the film by an area of higher or darker exposure.

2.1.5.4 Ultrasonic Testing (UT) [8]

Any material which transmits mechanical vibration can be tested. UT detects both linear and non-linear flaws and permits three dimensional interpretation. The UT instrument converts electrical pulses into mechanical vibrations or pulses. These pulses travel across the tested specimen and reflect from flaws because of their different acoustic nature. The returning reflected pulses are re-converted to electrical energy and displayed as signals or images. The position and size of these signals correspond to the position and size of the flaws.

2.1.5.5 Eddy Current Testing (ET) [8]

ET instruments are usually small and portable. The method is used only on electrically conductive materials, and only a small area can be inspected at a time. An energized electromagnetic coil induces an AC magnetic field into the tested specimen. The fluctuating magnetic field generates a circulating electric eddy current. The presence of a flaw increases the resistance to the flow of eddy currents. This is indicated by a deflection on the measuring instruments.

2.1.6 Summary of NDT Techniques

Each method can be completely characterized in terms of five principal factors:

- Energy source or medium used to probe the test object (such as X-rays, ultrasonic waves or thermal radiation).
- Nature of the signals, image or signature resulting from interaction with the test object (attenuation of X-rays or reflection of ultrasound, for example).
- Means of detecting or sensing resulting signals (photo emulsion, piezoelectric crystal or inductance coil).
- Method of indicating or recording signals (meter deflection, oscilloscope trace, radiograph or image).
- Basis for interpreting the results (direct or indirect indication, qualitative or quantitative, and pertinent dependencies).

The objective of each test method is to provide information about the following material parameters:

- Discontinuities (such as cracks, voids, inclusions, delaminations).
- Structure or mal-structure (including crystalline structure, grain size, segregation, misalignment).
- Dimensions and metrology (thickness, diameter, gap size, discontinuity size).

- Physical and mechanical properties (reflectivity, conductivity, elastic modulus, sonic velocity).
- Composition and chemical analysis (alloy identification, impurities, elemental distributions).
- Stress and dynamic response (residual stress, crack growth, wear, vibration).
- Signature analysis (image content, frequency spectrum, field configuration).

These methods are among the major tools of quality control and can find wide application in quality programs in industries such as aerospace, automotive, defense, pipe line, power generation, preventative maintenance, pulp and paper, refinery, and shipbuilding. Another classification system used by the National Materials Advisory Board (NMAB), Ad Hoc Committee on Non-destructive Evaluation divided methods into six major categories: visual, penetrating radiation, magnetic-electrical, mechanical vibration, thermal and chemical-electrochemical [19, 20]. A summary for the major methods are shown in the Table 2.3.

NDT method	Applications	Advantages	Limitations
Penetrant Testing	Solid nonabsorbent material having uncoated surfaces that are not contaminated.	Easy and inexpensive. Very sensitive and versatile. Minimal training required.	The discontinuities must be open to the surface. Surface must be relatively smooth and free of contaminants.
Magnetic Particle Testing	Be used for surface and slightly subsurface discontinuities in ferromagnetic materials.	Easy to operate and the equipment is inexpensive. Highly sensitive and very fast.	The inspection area is limited to surface and subsurface. Ferromagnetic materials only.
Radiography Testing	Be used for almost any materials, shapes and structures manufactured or in-service.	Offer permanent record and high sensitivity. Widely used and accepted.	The inspection thickness is relied on the material density. The orientation of discontinuities is

			important. And radiation is sometimes harmful.
Ultrasonic Testing	If the condition of sound transmission and surface finish are good and the object shape is not complex, it can be used for most materials.	The precise and sensitive results can be achieved very quickly. Material information such as thickness, depth and flaw can be got only from one side of the object.	In many cases, there has no permanent record. Testing requires couplant.
Eddy Current Testing	All conductive materials can be inspected.	Absolutely noncontacting, easy to operate. The testing is fast and versatile.	Measured signal is hard to interpret. Penetration depth, lift-off effect and surface condition need to be considered.

Table 2.3 Comparison of major NDT methods

When deciding on an NDT technique for an inspection task, the first thing needing to consider is whether it is suitable for detecting the existing discontinuities with sufficiently high probability. For many tasks, a single NDT method is sufficient to solve an inspection problem, however some times, more than one method is also employed to provide additional information and enhance the inspection reliability [21]. In addition, the choice of inspection equipment is a process including a few considerations [22].

- The equipment must have sufficient capability and at the same time be easy to calibrate, maintain and operate.
- The equipment also needs to be able to work in tough environment conditions of the inspection.
- The equipment should provide ease of signal interpretation and recording.
- The equipment should be portable if necessary.

2.2 Carbon Fibre Reinforced Plastic

2.2.1 Introduction to CFRP

CFRP, short for Carbon Fibre Reinforced Plastic, is a kind of composite material made up of carbon fibre and another or more materials at the macroscopic level, which is able to combine the best of the properties from each and as a result, CFRP shows better performance than its components [23]. On the purpose of developing a new advanced material for aircraft which should be stiff, light and strong, the researchers at the Royal Aircraft Establishment, Farnborough, UK produced carbon fibre in 1963-64 [24]. Taking full advantage of the anisotropy, CFRP combines a low specific weight with excellent mechanical properties and durability, and has been serving in the aerospace, automotive and shipbuilding industries for almost four decades. Furthermore, in last two decades, more and more attention and effort from research institutes and industries has been paid to CFRP composites as load-bearing components, particularly in aerospace and automobile applications [25]. On the other hand, the intensive increase in the availability of improved matrix materials which work as the supporting material in CFRP e.g., high performance thermoplastics and the progress in the development of fast and reliable processing techniques are boosting CFRP’s development and application widely.

As other materials, defects in CFRP occurring during in-service use may significantly affect the mechanical properties of composites then result in malfunction [26]. So, such defects as impact, matrix cracking and delamination must be detected at an early stage in order to prevent accident and reduce costs caused by failure of a component. To make sure the material systems working properly both initially and in-service, non-destructive material characterisation needs to meet higher demands [27, 28], such as airworthiness requirements for civil aircraft metal structures are well defined by certification authorities [29]. The development of inspection techniques and a proper understanding of the meaning of the results for the functional properties of composite components will be a prerequisite for their application.

2.2.2 Structure and Electrical Properties of CFRP

Carbon fibres are made in the form of bundles, called strands or tows containing, usually, 10^4 discrete filaments, which are typically 7 to 15 μm in diameter [30]. Carbon fibre composites are made with carbon fibres embedded in a polymer, commonly epoxy. These stiff and strong fibres carry the loads to which the component or structure is submitted. The matrix has low stiffness and low strength and it contributes to the shape of the component. The plastic matrix is used to transfer loads to the fibres and between them as it's another important task [23].

In a CFRP composite, a single layer has a thickness of about 0.05 to 0.2 mm, and consequently, in order to obtain usable engineering mechanics components, some layers are stacked one by one to form a lamina, as shown in Figure 2.1. A lamina with fibres in only one direction is called a unidirectional lamina. Alternatively, a few laminae with fibres in different directions are used to form a laminate. The directions of the fibre in each part of the mechanical component need to be chosen by the designer to offer the component required properties and minimum cost.

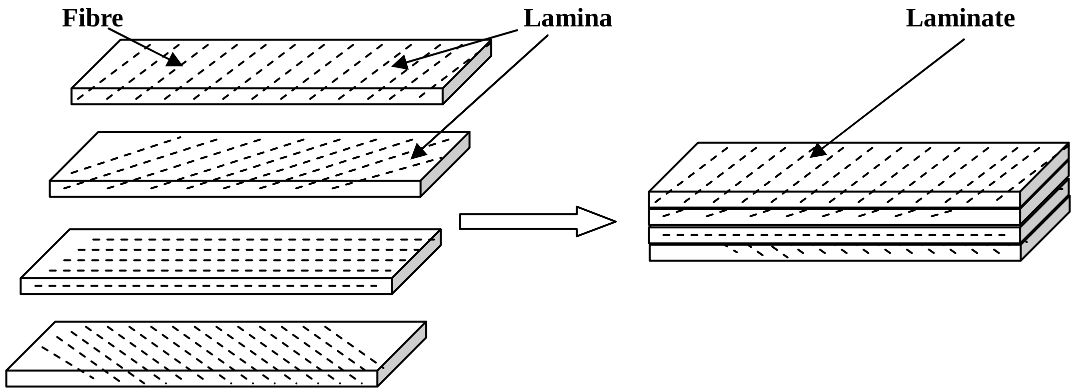

Figure 2.1 Stacking of single lamina to form a laminate

One basic and common method to fabricate a laminate is to spread fibres which are normally distributed in rolls of layers. Then, as defined in the design process, layers are stacked in a mould and the liquid epoxy mixed with a curing agent is poured into mould. The step of pouring the epoxy on the fibres could be carried out by several methods: by hand (manually spreading epoxy through fibre layers) or automatically spreading the epoxy using a vacuum process called Resin Transfer Moulding or RTM. Finally, under controlled temperature and pressure conditions the liquid epoxy cures after some time. Although all the constituents are same, the final composites may have different mechanical properties when applying different manufacturing. Somewhat, these differences are related to the fibre volume fraction, and the presence of micro-bubbles or voids. For example, the void or air micro-bubbles generated during non-uniform epoxy spreading could be reduced or even eliminated by combing a RTM process and pressure controlled epoxy curing cycle. Compared with metals, CFRP composites present strong anisotropy in electrical conductivity which is relatively high in the fibre direction and low perpendicular to fibre direction [31]. A comparison of conductivity between various materials is shown in Table 2.4.

Material	**Conductivity(10^4 s/m)**	**Direction of measurement**
Copper	5900	n/a
Aluminum	3500	n/a
Iron	1000	n/a
Graphite	13	n/a
Carbon	3	
Carbon fibre	4-17	
Unidirectional CFRP	0.9-1.5 0.01-0.2	Parallel Perpendicular

Table 2.4 Conductivity of metal and CFRP

From the above table, it can be seen that the conductivity of unidirectional CFRP composites is lower than that of metals by a factor of about 1000, while the conductivity in cross fibre direction is further lower by up to more than 100 times. Under ideal condition, if do not take coupling capacitance between fibres into account, in CFRP, the current can only flow through individual carbon fibers, as the fibers are surrounded by insulating polymer. However, because of the presence of inter-fiber contact points, the current may flow from fibre to fibre (Figure 2.2 (a)). So, the total electrical impedance of a piece of CFRP material is an assemblage of the impedance of all fibers and their structure (Figure 2.2 (b)). Due to its internal structure, for unidirectional CFRP laminates, the electrical properties are anisotropic, which means that along fiber direction (0^0 direction), the conductivity of the composite is calculated by total single-fiber conductivity and fiber-volume fraction [32], while the conductivity is relatively small perpendicular to fibers (90^0 direction). The current switch between fibres depends on the existence and number of inter-fiber contact points. Some resistance values of CFRP material are shown in Table 2.5 [32]. According to various manufacturing and processing procedures, they may be different.

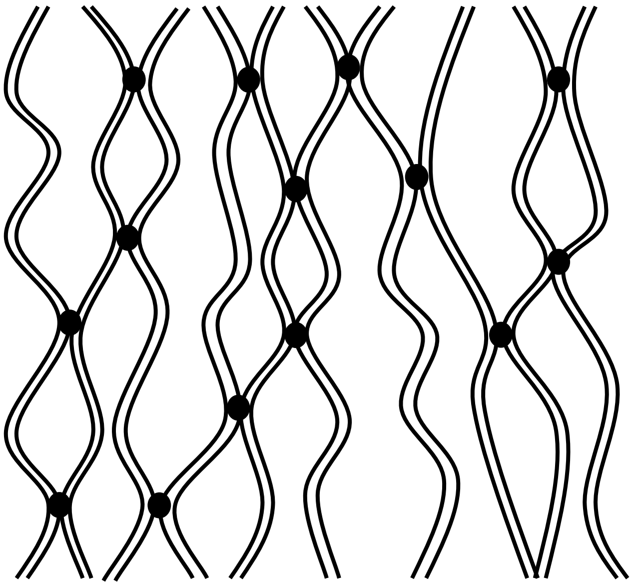

(a)

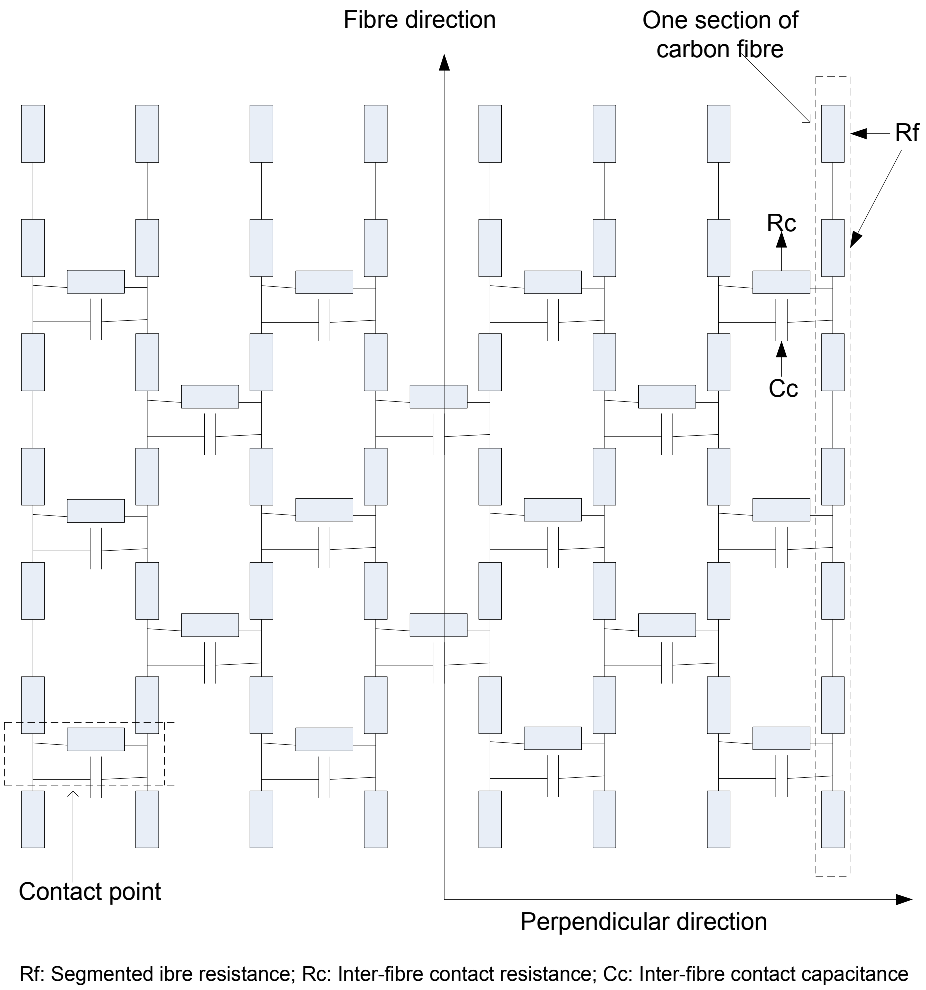

(b)

Figure 2.2 (a) Schematic representation of a unidirectional CFRP with contact points between two parallel fibres; (b) Electrical model of contacting carbon fibres [33]

Material	**Fiber content (vol. %)**	**0^0 (Ω-cm)**	**90^0 (Ω-cm)**	**$90^0/0^0$ (Ω-cm)**
Carbon/epoxy	55	0.08	0.4	50
Carbon/epoxy	65	0.0025	1	400
Carbon/epoxy	*	0.0021	0.95	450

Table 2.5 Resistivity of CFRPs [32]

*Average value for commonly used samples with fiber content from 60% to 65%

As can be seen, there is a very high anisotropy in the electrical resistance of CFRP.

The $90^0/0^0$ electrical resistance ratio ranges from 50 to 500. It has also been proved by experiments that the resistance of CFRP increases with the appearance of internal damage, such as fiber breakage and delamination [34]. Research results show that the change of electrical resistance can indicate the presence of damage in CFRP. Further, the damage could be better defined and classed by extension of the measurements such as fiber breakage or delamination, damage size and position.

2.2.3 Defects in CFRP

A particular component has various physical and mechanical properties and also there have different damage mechanism, as is the case for CFRP. Figure 2.3 presents some of the defects which may change the material properties and adversely influence the performance of the component. These include planar flaws running parallel to the surface (delamination, ceramic debonding), perpendicular flaws (cracks of the matrix or of the patches) and volume imperfections (pores, voids, inclusions). Their existence can have a great impact on the performance of the material. From the figure, it can be seen that some defects are similar and sometimes it is not easy to tell one from another. As the effects of different defects are various and a corresponding method is needed to deal with each one, it is very important to distinguish one type of defect from others. The detail of some typical defects will be introduced in the following sections.

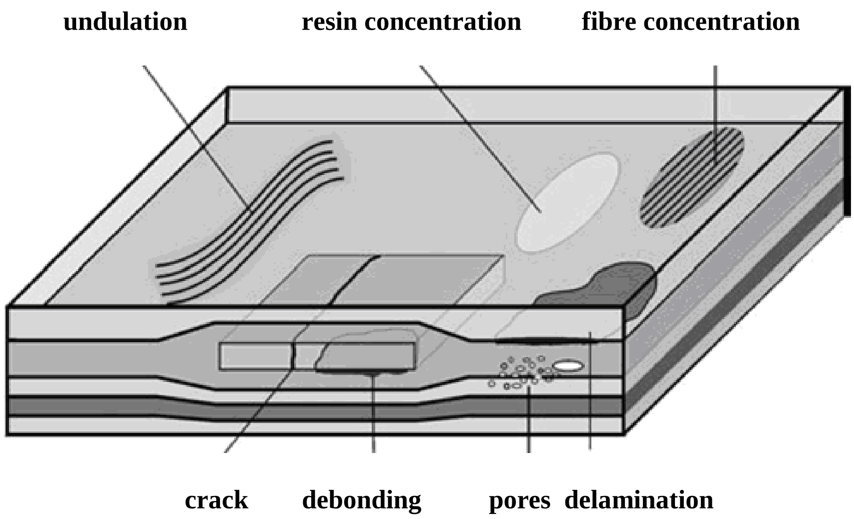

Figure 2.3 Typical flaws in CFRP [35]

2.2.3.1 Impact Damage

This kind of defect is a result of foreign object damage such as stone, bird strike, dropping of an object, etc. Consequently, this defect will result in matrix cracks, fibre breaking and delamination in CFRP composites. The impact defect can reduce the CFRP's residual strength by up to 50% [36]. CFRP sample with various impact damages is shown in Figure 2.4. As can be seen in the following figures, some low-energy impacts often cause internal defects and matrix breakage on the back surface of the composite without modifying the top surface of the component. However, for component in-service inspection, it is highly possible that the probe can only get access to one side of the tested object which makes it very hard to detect the defects. This type of defects which are caused by low-energy impacts is one of the most difficult defects to detect, and of primary importance to the structural integrity of composites.

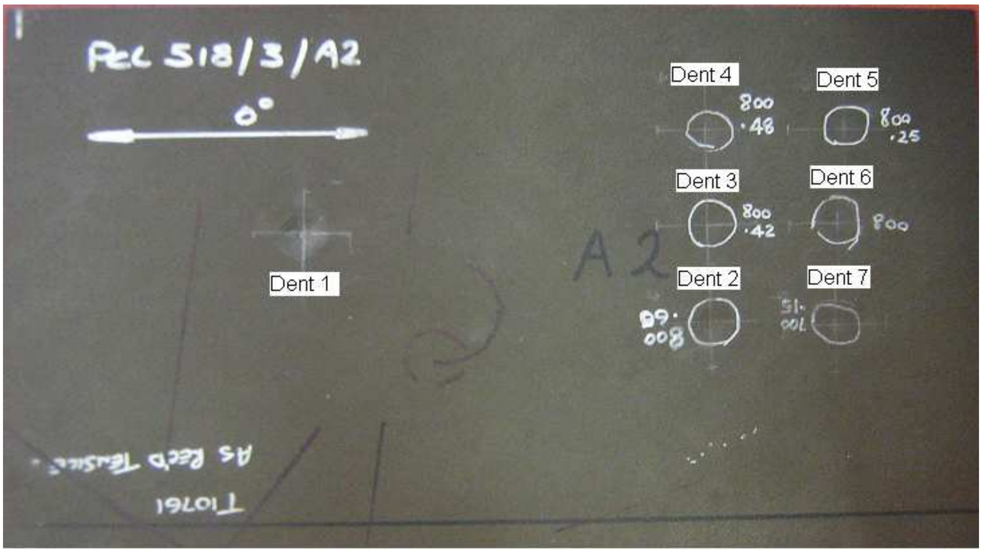

(a) Front side

(b) Back side

Figure 2.4 CFRP sample holding seven impact damages with different dents

2.2.3.2 Fibre Breakage

In tension, most fibres tend to fracture in a brittle manner, without any yield or flow [37]. As the loading on materials accumulating, damage is initiated at failure points of weaker fibres which break during initial loading. The shear stresses around the breaks cause the resin and the interfaces to degrade and promote cracks which propagate along the fibre-matrix interfaces. The cracks affect the ability of the material to redistribute load as it becomes further damaged and so more fibres break which lead to further resin damage and ultimate failure. So detecting the broken fibre at the early stage is very important for avoiding further functional failure of material.

Figure 2.5 shows the scanning electron micrograph in which it can be seen that carbon fibres are deformed and broken by impact energy.

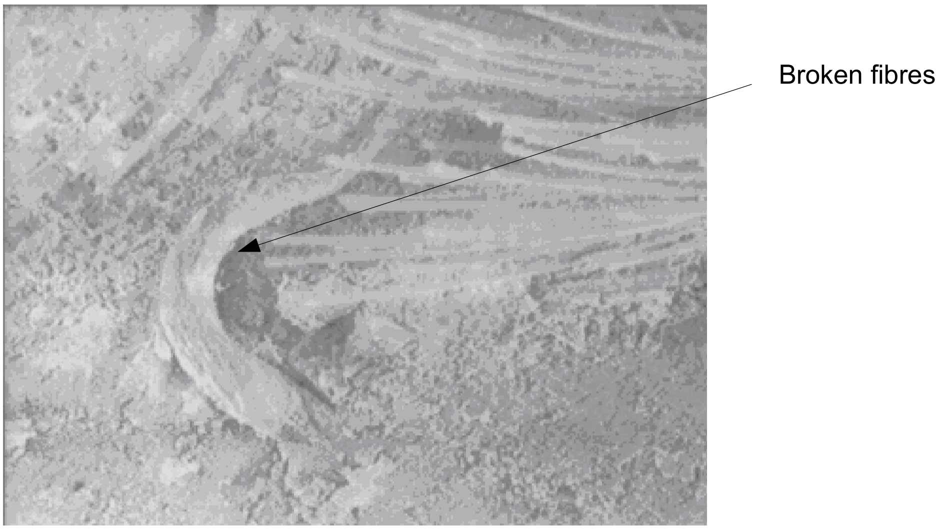

Figure 2.5 View of deformed and broken carbon fibre by impact energy [36]

2.2.3.3 Delamination

In definition, delamination means the lack of adhesion between two layers of carbon fibres laminates [38]. As, the delamination resistance of CFRP composite laminates is low, delaminations often takes place resulting from slight out-of-plane impacts [39]. Delamination can bring many problems on CFRP performance such as large reductions in strength and stiffness of the CFRP laminates, and deterioration of the structural reliability of the CFRP. It can also cause worse failure because delaminations are usually difficult to detect visually or sometimes even invisible. When applying eddy current testing for delamination detection, it is difficult to be sensitive to the delamination if measurement is carried on the fibre conductivity, because the eddy currents are flowing parallel to the laminates making the currents very slightly changed by the delamination. However, in CFRP, there actually exist resistive and capacitive couplings, which occur both between the fibres of laminate and between different laminate. Thus, these couplings generate inter-fibre and inter-laminar currents, which can be modified and measured under certain frequency when delaminations happen.

The Figure 2.6 gives a micrograph view of delamination which clears shows how delamination modifies the CFRP's inner structure.

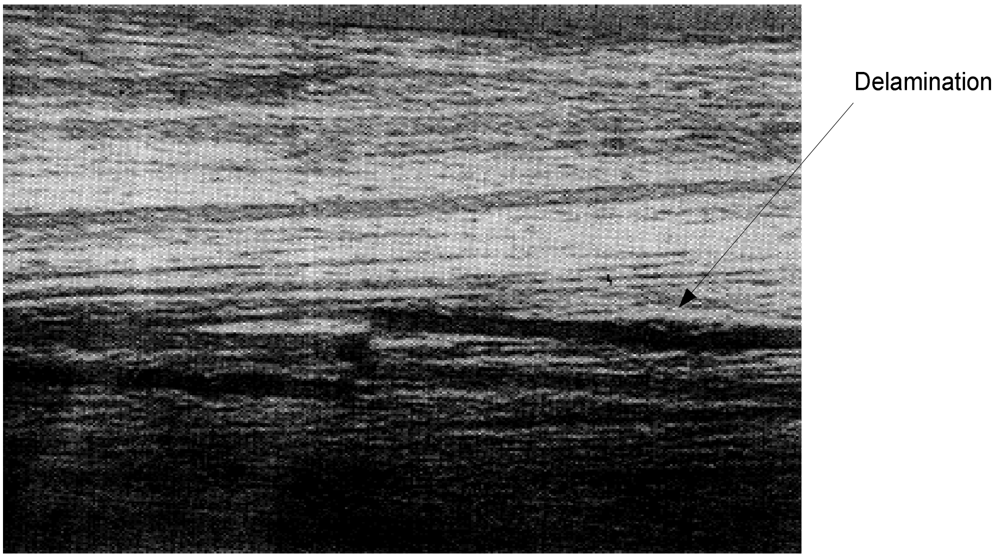

Figure 2.6 View of delamination between fibre layers [40]

2.2.3.4 Voids

There have several types of voids occurring in composite materials. Some large ones can be produced during the manufacturing process of the component by gross defects, while small ones are often found adjacent to the fibres because of incomplete infiltration during processing or cavitations during deformation. In addition, void also can be seen in matrix-rich part or regions between laminate where no fibre exists. Voids exist in all forms of composite with variations in their incidence depending on fabrication route and matrix type. Figure 2.7 shows the detail of the micro structure of a small CFRP region with void. An obvious area of voids can be seen around fibres and matrix. This can reduce the mechanical and electrical performance of the composite.

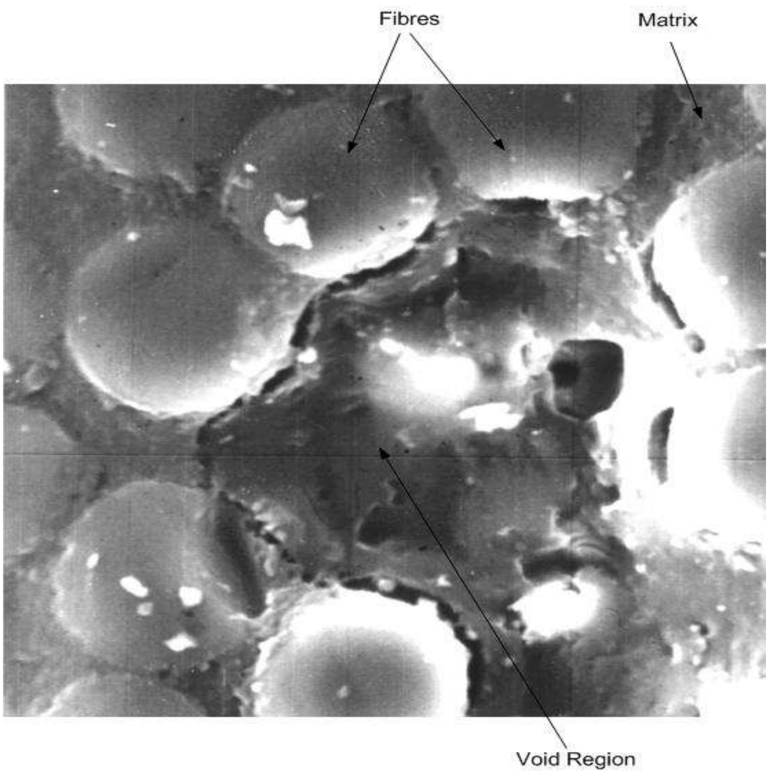

Figure 2.7 Structure of a small CFRP region with void [40]

2.3 Non-Destructive Characterization of CFRP Structure

To improve the performance and to increase the reliable lifetime of a structure, it is necessary to analyze and describe quantitatively the damage process. As essential prerequisites to guarantee the performance of the component during its lifetime, non-destructive testing (NDT) is able to optimize the CFRP structure such as ply sequence, fibre orientation, local fibre and epoxy concentrations and manufacturing process [35]. NDT is also able to detect the defects in material including planar flaws, perpendicular flaws and volume imperfections.

In the past couple of decades, both research institutes and industry have studied the NDT characterization of CFRP and made considerable progress [41-46]. As discussed in previous section, how to choose the NDT method is dependent on the specific requirement and conditions of the material and the application. However, there are some well developed and commercially viable NDT methods for CFRP characterization, which are the eddy current method, ultrasonic NDT and scanning acoustic microscopy [38]. In addition, X-ray inspection and thermography are also effective method for CFRP characterization. A brief introduction to background and application of these methods is shown as follows.

2.3.1 Ultrasonic NDT

Ultrasonic NDT typically involves the following steps. First, mechanical vibrations are generated by converting electric energy into ultrasound using a transducer containing a piezoelectric crystal in a frequency range which can not be heard by the human ear. Next, the ultrasonic wave is transmitted through the inspected CFRP objects and is finally reflected onto the back surface of the object. Last, the same transducer or separate receivers collects the wave signal and sends it to instrument for analysis. To improve the penetration of the ultrasonic signal within the object, before the scan starts, a couplant such as water or some kind of gel may be applied between the transducer and the material. The ultrasonic wave’s properties are sensitively related to direction of propagation, polarization and anisotropy of material properties [47]. In order to present different flaws and structures in CFRP, various presentation techniques are applied in ultrasonic inspection. While time-based graph, called A-scan or B-scan is used to interpret the output signal, a C-scan, which is a representation of multiple scans is useful to provide more information and produce a plan view of the object. For example, it can be realized that projection C-scans with varying gate width and B-scans of different sections are generated in real time, and at the same time the evaluation of phase information or measurement of geometric parameters are carried on at the A-scan at the same screen [47].

For the inspection of CFRP objects, it is suggested to employ high frequency (up to 25 MHz), and highly focused transducers with suitable ultrasonic equipment (bandwidth up to 100 MHz) [47] in order to obtain high axial and lateral resolution. During ultrasonic inspections, the sound beam propagates in a direction along the axis of the reinforcement fibres [48]. Then the received ultrasonic signals are saved in a computer which is able to digitize the signal at high frequency and capture full waveform. The reports suggest that transmitting frequency of 5 to 20 MHz should be chosen for inspection of objects with thickness from 2.5 to 13.0 mm [49]. Also, the research taken in [50] showed that since the attenuation of waves propagating perpendicular to the plies was sensitive to the interlaminar quality of the inspected object, it could provide the information to identify and interpret damages. Also, the modification by the multi-layer structure of objects on ultrasonic parameters such as refraction, intensity, reflection, wave velocity and scattering should be considered because it may have negative impact on the efficiency and quantification of ultrasonic scanning in defect location.

As one of the most commonly used NDT methods for characterization of CFRP composites currently in industry, ultrasonic techniques are able to successfully detect flaws and provide structural features of CFRP composites, which can help optimize the materials, structures and manufacture.

2.3.2 Scanning Acoustic Microscopy (SAM)

As a high resolution ultrasonic imaging technique, scanning acoustic microscopy operates at higher frequencies ranging from 30 MHz to 2 GHz. The frequency is sufficiently high in order to provide a resolution comparable to optical microscopy in opaque objects, therefore this technique offers a very useful NDT tool for examing the microstructure of CFRP composites. Some previous work proved that in term of defect detection, scanning acoustic microscopy is very sensitive to interfacial debondings and microscopic crack damage growth [51, 52]. Such systems are comparable to conventional ultrasonic C-scan method but an extremely focused lens is used in order to improve spatial resolution. A single transducer is used in pulse-echo mode, in which the same transducer emits and receives ultrasonic waves. The transducer moves linearly, parallel to the surface of the specimen. The sample is immersed in a water tank and a computer controlled scanning system is used to inspect the area. A C-scan of the area inspected can be displayed on a monitor screen from which hard copy can be produced and data saved on disk for archiving.

2.3.3 Eddy Current Testing

Eddy current testing is an electromagnetic NDT method which consists of bringing a coil carrying an electrical current to proximity of a conductive material [53]. Eddy currents are induced in the specimen under test by electromagnetic induction. They will decay exponentially with depth below the surface of a material. If the structural integrity of the material is modified due to the presence of a flaw, a change in eddy current phase and amplitude will occur. This change can be observed on an oscilloscope for instance and defect characteristics determined. It has recently been demonstrated that eddy currents could be used for the inspection of composite materials [54-56]. Previous work on the use of eddy current techniques for composites testing have shown that fibre damage with or without matrix cracking can be detected [57], variations in fibre volume fraction revealed [56] and determination of fibre orientation achieved [58]. The detection of low energy impact damage (0.5 J) in CFRP materials has been achieved and the sensitivity of the technique could be potentially better than any other widely used NDT technique, such as ultrasonics, radiography or infrared thermography [59].

An example of the performance of the three methods is demonstrated in Figure 2.8.

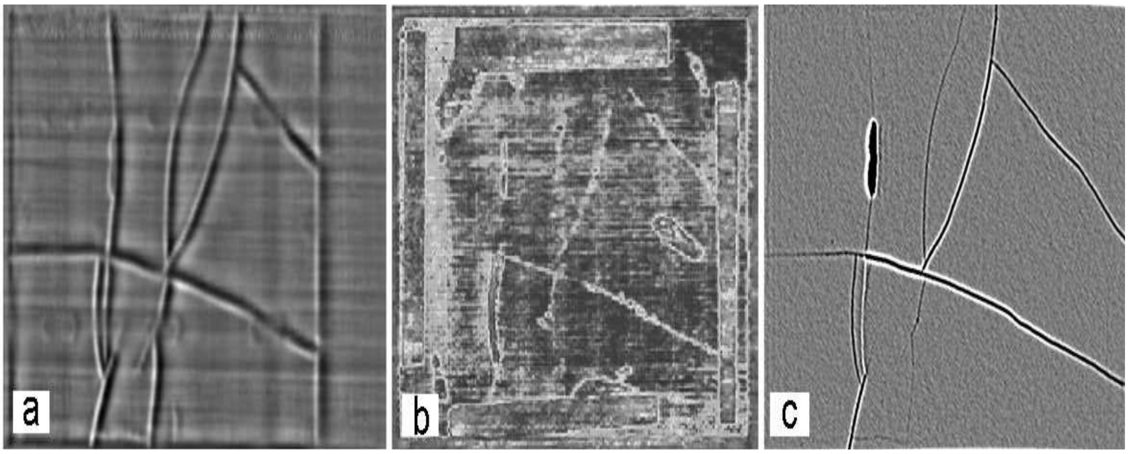

Figure 2.8 (a) Eddy current, (b) radiography and (3) ultrasonics testing of a broken specimen ($57 \times 42 \times 0.2$ mm^2) [35]

According to the previous work and study by researchers, the details of advantages and limitations of the three NDT methods employed have been summarized up in Table 2.6.

	Advantages	**Limitations**
Ultrasonic C-scan	1. Signal output in an ease to interpret image format. 2. Rapid automated inspection. 3. Well recognized NDT method by industry. 4. Can also be used to detect deep internal defects. 5. Effective detection and characterization of both delamination and interlaminar cracks. 6. Good signal reproducibility.	1. High signal attenuation and scattering. 2. Expensive apparatus. 3. Calibration time consuming. 4. Highly skilled and experienced operator required. 5. Sensitivity and resolution can be limited for surface defects. 6. Improving result with water immersion.
Scanning acoustic microscopy	1. Automated inspection. 2. Allows inspection of different layers of composites. 3. Signal in an image format. 4. Adequate for the inspection of	1. Expensive apparatus. 2. Time consuming calibration. 3. System not portable. 4. Highly skilled and experienced operator required.

	opaque material.	5. Signal interpretation sometimes difficult. 6. No distinction between delamination and interlaminar cracks. 7. Improving result with water immersion (difficult for on-site testing of large structures). 8. Limited signal reproducibility. 9. High signal attenuation and scattering.
Eddy current testing	1. Easy to interpret color coded image. 2. Non-contact testing. 3. Low cost. 4. High signal reproducibility. 5. Inspection results not very dependent upon the operator skills and experience. 6. Delamination unambiguously detected. 7. Portable system (laboratory and on-field testing is possible). 8. No water immersion of the sample required.	1. Detect mainly surface and subsurface defects. 2. Limited to composites containing carbon fibres or other conductive fibres. 3. Difficult to distinguish between delamination and interlaminar cracks.

Table 2.6 Advantages and limitations of three NDT methods

We can see that each NDT method presents some advantages and limitations in term of defect detectability and characterization. Eddy current testing is proven to be well suitable for in-service inspection and rapid control of the structural integrity of composites. Although distinguishing between different types of defects may be difficult, the low cost of such systems make them a worthwhile alternative to more costly method such as SAM or ultrasonic C-scan. In the two methods, water immersion is a key requirement for optimum inspection which may be difficult to achieve and costly for in-service inspection. Besides the above three most popular NDT methods, there have some other potential NDT methods for characterization of CFRP which are introduced briefly as below. They have their own advantages and show excellence in specific areas where x-ray method is able to produce 3D image and thermography image is good at characterization of layers and interfaces.

2.3.4 X-Ray Inspection

X-rays are generated during acceleration of electrons or by deceleration of electrons in solid-state materials. X-ray inspection is a method to produce image of a three dimensional body in a two-dimensional plane, so the object's detail is superposed in a radiographic projection. As a result, structures resembling defects, called by artifacts are caused by these super-impositions. Then, the artifacts as well as real structures are distinguished from real defects by image processing [60]. X-ray transmission is applied in modern industrial quality control by two different ways [60]:

- Two-dimensional radioscopic transmission imaging (projection technique).
- Three-dimensional Computed tomography (CT) which can generate 3D images, represent density distribution of objects and provide spatial information. With the help of CT, understanding of production process failure, component and module inspection, and dimensional measuring of hidden geometrical outlines can be achieved.

By scanning the CFRP objects with X-rays, it is possible to detect flaws or damage concealed deep inside. By using CT, an in-depth view into the CFRP components' three-dimensional structure can be captured which in turn, enables the position and volume of fibers to be detected as well with matrices and inclusions. An image of x-ray inspection of CFRP is shown in Figure 2.9.

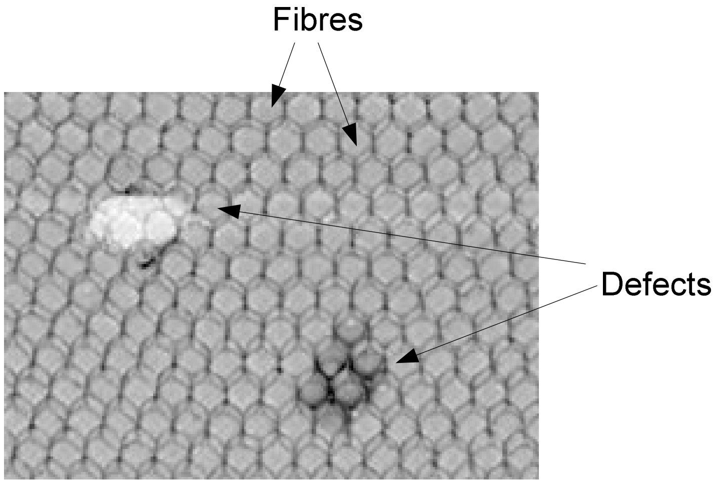

Figure 2.9 X-ray inspection of CFRP [60]

2.3.5 Thermography

During thermography inspection, the surface of the tested object is heated by a short flash (pulse thermography) or periodically (lockin thermography). Then the produced heat flux is studied. The presence of defects like delaminations or voids disturbs the heat flux which causes the temperature difference at the surface. An infrared camera is used to detect the difference. And the acquired temperature sequence is transformed by Fourier to improve the signal-to-noise-ratio of the resulting images significantly. Also, a phase image is generated by Fourier calculation to map the local delay between excitation and thermal response, which can reveal hidden boundaries and thermal features of the inspected object. The advantage of the phase image over others such as amplitude or single images is that it is not sensitive to some surface properties like varying emission coefficient, or to inhomogeneous heat flux resulting from non-uniform illumination or surface topography. To characterize the adhesive joint, it is important to distinguish the layer's properties from the interface beneath's properties. In some report [61], scientists are able to determine the sample thicknesses and the interface parameters by taking at least two lock-in measurements at different modulation frequencies. Figure 2.10 shows the thermography inspection image which is easy to interpret the sample layers and interfaces.

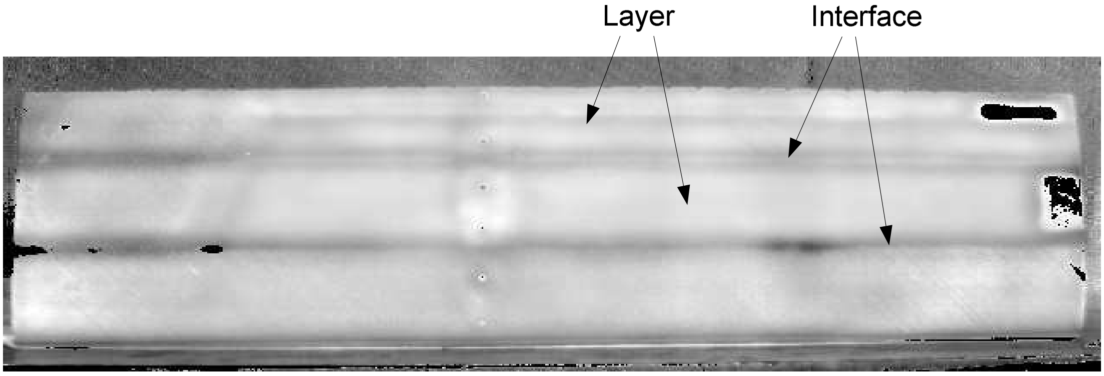

Figure 2.10 Thermography inspection of CFRP layers and interfaces [61]

2.4 Defect Detection by Eddy Current Testing

Massive effort has been made in studying advanced NDT techniques capable of detecting defects in CFRP composites including ultrasound [77, 78], shearography [79] and X-ray [40]. In industry especially aerospace, some traditional methods such as visual inspection, coin tapping, and ultrasonic pulse echo and low-energy radiography are already in use. More recently, late technologies like ultrasonic phased array scanning [80], electrical potential technique [81, 82], near-field microwave [83], lamb waving sensing [84] and electrical resistance change method [85, 86] are catching more and more attention from research labs and industry. However, CFPR composites' heterogeneous and anisotropic composition makes their structures too complicated to inspect by conventional non-destructive testing methods.

An application of eddy current testing which has rapidly grown in importance is the detection and sizing of surface and subsurface defects in materials. With recent improvements in design of electrical equipment and probes, the method is both more reliable and accurate. Eddy current flaw detection can test objects of almost any shape and size with help of development of more recent techniques such as multi-frequency testing. As discussed previously, when the structural property of conductive material is modified because of the presence of a flaw, a change in eddy current phase and amplitude will occur which is being monitored and can be observed by measurement equipment and then the defect characteristics could be analyzed. It has recently been demonstrated that eddy currents methods could be used for the inspection of composite materials [87, 88]. Previous work on the use of eddy current techniques for composites testing have shown that fibre damage with or without matrix cracking can be detected [89], and variations in fibre volume fraction is also successfully revealed [88]. Using eddy current testing, low energy impact damage (0.5J) in CFRP materials can be detected with better sensitivity than other popular NDT technique such as radiography, ultrasonic, and infrared thermography [90].

To detect the flaw in CFRP, one simple way is to scan the inspected object using a single-coil probe of appreciate design and keep the lift-off constant. Then look into the output signals to check if there has any abrupt change due to sharp discontinuities in structure, i.e. in the parameters μ and σ, where they are the magnetic permeability and the electrical conductivity respectively. When a defect or any kind of discontinuity occurs in the object in which eddy current is induced, the paths of the currents are diverted and changes in impedance of the coil take place in a way in accordance the nature of the defect. It is already proved that the parallel defects such as planar cracks and delaminations which are in the same direction as the eddy currents is difficult to detect, so care should be taken in directing the axis of the coil or use other type of probe. Effort has been made to predict the relation between changes and defect's size and shape using analytic methods [91]. And, realistic results have been obtained by the following modeling techniques:

- Theoretically by the use of numerical methods;

- Mechanically by introducing artificial defects;
- Coupled mechanical and electrical models [86].

One of the most important issues in eddy current testing is how to generate eddy currents in the inspected object and received them back, which is largely dependent on the design and setup of the eddy current probe. The configuration of the probes could be a single coil with air core, or a pair of coils with several turns which are wound on formers of specific material and used as transmitter and receiver respectively. For certain application, there may have wide range of choice for the coil number, former material, former shape and the probe size. This section will give a further discussion on some designs of eddy current probes for detecting different defects in CFRP.

2.4.1 Surface Scanning Probe for Vertical Defects [92]

The use of surface-scanning probes is required for the precise location of vertical defects such as fibre breakage and cracks, and they are most effective with plane surfaces. With curved surfaces, it is important that the diameter of the probe is small enough to ensure that the surface beneath it is effectively plane, so that lift-off is constant to within the accuracy required for the measurement.

Some proposed probes for detecting vertical defects are shown in Figure 2.11. Absolute probes (Figure 2.11(a)) contain a single coil and are widely used due to their versatility. Since absolute probes are sensitive to things such as conductivity, permeability and liftoff, and the inspection process are comparatively easy to perform; they are the most used probes for material defect inspection.

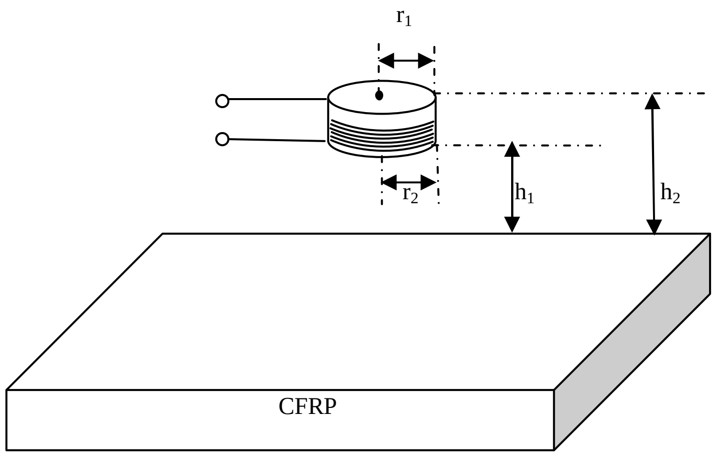

(a) Single-coil absolute probe

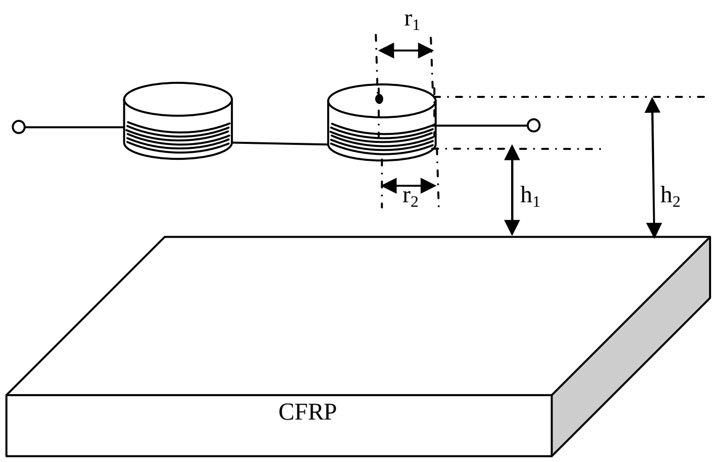

(b) Defferential probe

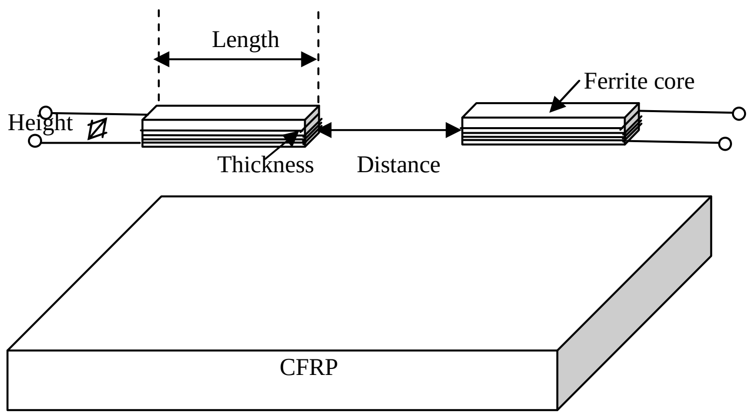

(c) Transmitter and receiver coil pair

Figure 2.11 Probe design for inspecting vertical defects

The inductance of a coil at a given frequency can be considerably increased by introducing a ferrite core which has a high magnetic permeability and a low electrical conductivity, thus increasing the sensitivity of measurement. This is because ferrite is ferromagnetic; the magnetic flux produced by the coil prefers to travel through the ferrite as opposed to the air. Therefore, the ferrite core concentrates the magnetic field near the center of the probe. This, in turn, concentrates the eddy currents near the center of the probe. Probes with ferrite cores tend to be more sensitive than air core probes and less affected by probe wobble and lift-off.

Differential probes (Figure 2.11(b)) have two active coils usually wound in opposition. When the two coils are over a flaw-free area of test sample, there is no differential signal developed between the coils since they are both inspecting identical material. However, when one coil is over a defect and the other is over good material, a differential signal is produced. They have the advantage of being very sensitive to defects. Probe wobble signals are also reduced with this probe type. There are also disadvantages to using differential probes. Most notably, the signals may be difficult to interpret. For example, if a flaw is longer than the spacing between the two coils, only the leading and trailing edges will be detected due to signal cancellation when both coils sense the flaw equally.

For enhanced sensitivity, a coil pair (Figure 2.11(c)) which have separate transmitting and receiving coil windings, may be used if deep penetration of eddy current is required in the material under test [92] and they are sensitive to the fibre breakage because of their high directionality.

2.4.2 Probe for Planar Defects [92]

Planar cracks and delaminations which are orientated in the same direction as the eddy currents are more difficult to find with conventional probes which are more sensitive to vertical defects, because planar defects are virtually no diversion of eddy current generated by those probes and have little of no effect on the impedance of the probes. However, defects of this kind, which parallel to the surface, may be detected with the use of a gap probe seen at Figure 2.12. Gap probe consists of a ferrite yoke through which a magnetic flux is excited by means of a pair encircling coils. When the lower end of the yoke is in contact with the material surface, the latter completes the magnetic circuit and eddy currents flowing in planes perpendicular to that surface appear. This probe has advantage of close electromagnetic coupling with the object under test.

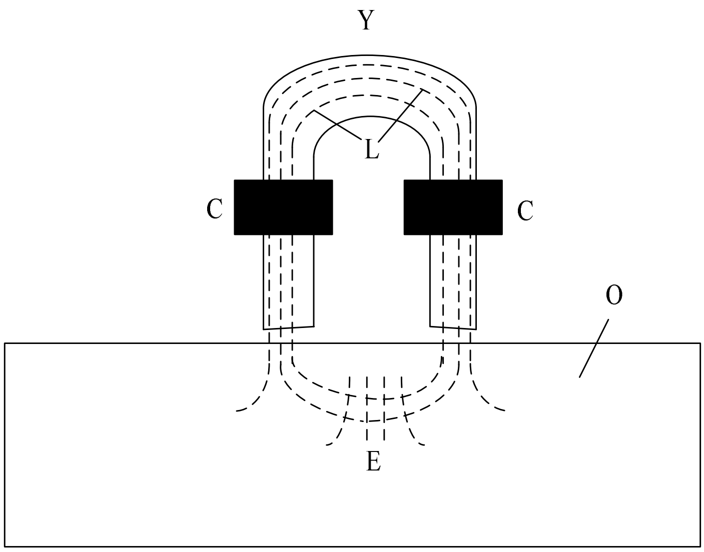

Figure 2.12 Gap Probe. C: coil; Y: ferrite yoke; O: object under test;

L: lines of magnetic flux; E: planes of eddy current flow

2.5 Conclusion

In the last several decades, NDT techniques have been increasingly developed and intensively applied in industry. However, more advanced and reliable NDT methods are still urgently required to meet the demand in rapidly growing industries such as aerospace, automobile and medical device. Among the popular and comparatively mature NDT methods, eddy current testing owns advantages over others in such as cost, development period and efficiency and eddy current instrument can realize in-service and non-contact testing. Eddy current testing is expected to help provide a more complete picture of the structural integrity and properties of the objects being tested [62]. To improve the performance of CFRP, it is necessary to take inspection on the materials both during the manufacturing process and service time. Considering the cost and efficiency, non-destructive characterization is proved as a vey useful tool to make sure CFRP component working properly without failure. The following chapters are focusing on the discussion of non-destructive characterization for CFRP materials using eddy current techniques.

Chapter 3. Eddy Current Testing

3.1 Introduction

For non-destructive testing, a number of electrical methods are available, which include resistance measurement, electrical conductivity measurement, and the use of triboelectic, thermoelectric, exoelectron effects, potential-drop methods and eddy current testing [8]. To get the desired information from electrical methods, it is necessary to correlate the electromagnetic properties with the proper measured material properties because all the electrical NDT methods are indirect. To achieve good correlation, it is necessary to ensure that the test conditions are well controlled and the, instruments are well calibrated on test specimens. However, the major issue of electrical NDT methods lies in the difficulty to define an electromagnetic property as a function of one and only one material property of interest.

A fundamental requirement for eddy current testing is that the inspected object is able to induce a distribution of currents in it. Thus, only materials with sufficient electrical conductivity can be tested using this method. In eddy current testing, a probe carrying changing current is placed in close proximity to the material to produce a changing electromagnetic field, then the eddy currents will be generated within the inspected materials in response to the applied electromagnetic field. These currents are compelled to flow in closed loops within the inspected material and in turn, themselves can generate magnetic fields in the way that is to reduce the applied electromagnetic field. Finally, both the original electromagnetic field and the induced field are detected by electromagnetic induction in a coil, or a system of coils. In many cases the same coil is used both to excite the eddy currents and also to detect their fields.

In brief, the Figure 3.1 shows the steps of eddy current testing for characterization of CFRP. Amplitude of the signals tells about the defects severity and phase angle with respect to a known reference give information about the defect location or depth. Defects that are parallel to eddy current flow may not produce a significant change in signals i.e. detected with a poor sensitivity.

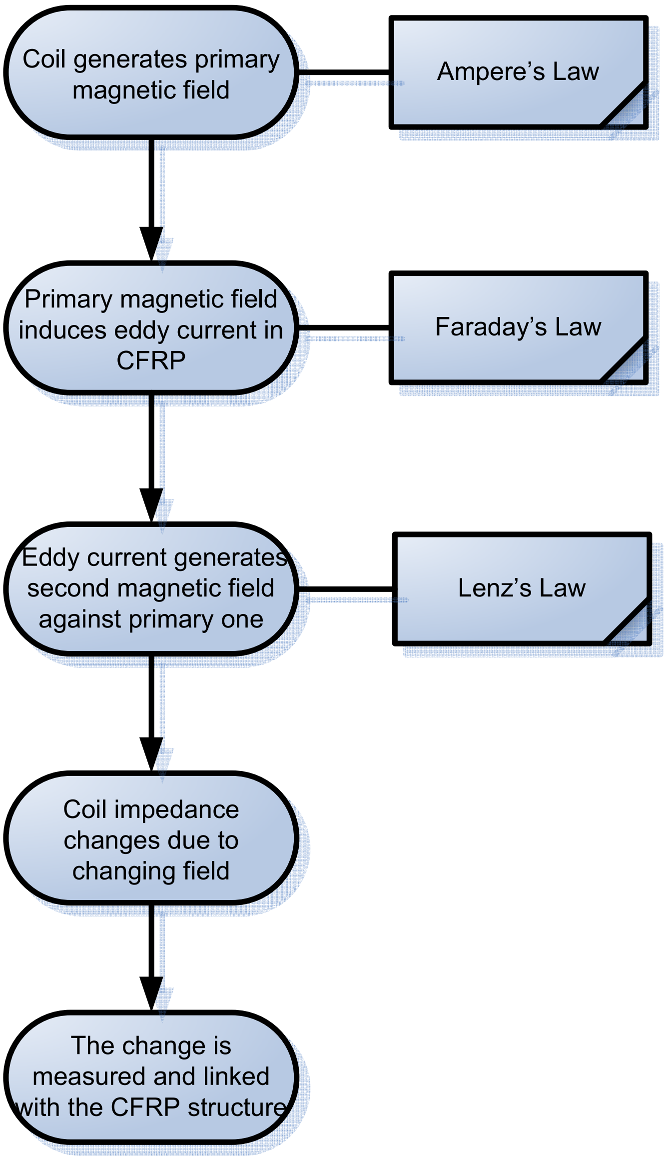

Figure 3.1 Process of the eddy current testing for characterization of CFRP

From the discovery of eddy currents by Foucault, electrical engineers keep showing great interests in their effects, and eddy current techniques can be considered to be a separate subject in the field of electromagnetism. Indeed, no one who deals with electrical engineering, either theoretically or practically, can ignore eddy currents because of their two-folded nature, that is, they can be either desired or undesired. In one field of applied electricity they are consciously generated, and in others they are detrimental and should be avoided or reduced.

In the past years, efforts have been put into the research of eddy current inspection of CFRP and the results have been reports. A method was developed to reconstruct current distribution in CFRP from the magnetic field for the better understanding of eddy current propagation in [63]. The method was to measure the z-component of magnetic field using a receiver coil and from the 2-D magnetic field the current distribution can be calculated by taking the partial derivative of the field. They also described about fibre orientation measurements with high angular resolution, some fundamentals of testing for de-lamination, cracks and fibre fracture. They concluded that special static and rotary probes are required to use the electrical anisotropy of such composites.

Also researchers found a signal perpendicular to the fibre orientation and termed it plateau effect [33]. It is a result of capacitive connections between the fibres and increases as frequency increase as we know capacitive reactance $1/\omega C$ is inversely proportional to frequency which means at high frequency there will be higher conductivity i.e. higher current density.

An approach using normalisation and two reference signals to reduce the lift-off problem with pulsed eddy current techniques is intruduced in [64]. Experimental testing was done based on proposed approach. Results show that significant reduction in the lift-off effect has been achieved mainly in metal loss and sub surface slot inspection.

In [65], the study was focused on developing a method on non contact eddy current based SQUID (super conducting quantum interference device, has high magnetic sensitivity in even low frequency range) NDT method for thick carbon fibre composites. The advantage with SQUID is that it can help in detecting deep lying defects in electrically conductive materials. Electric conductivity of CFRP is lower than metals by a factor of thousands, so strong field or high frequency field is necessary to induce enough eddy current. In case of thick samples the low frequency field is required to induce an eddy current at a deeper part because of skin effect.

As experimental characterization of multidirectional fibre composites based on eddy current testing using HTS (high temperature superconductivity) dc SQUID magnetometers was presented in [66] and is used to detect damage not visible to naked eye (impact energy less than 2J in 4 mm thick CFRP composites, in unshielded environment). The study on the effect of impact far from the point of impact finds that magnitude of magnetic field in the vicinity of defect center shows no significant variation and the change with distance looked quite similar to perfect sample. They related the slope $d\theta / dx$ of magnetic phase to the severity of the damage.

This research work aims to employ and develop eddy current techniques for the characterization and reconstruction of defects within Carbon Fibre Reinforced Plastics (CFRP), especially on bulk conductivity measurements, directionality characterization, fault detection and imaging. In this chapter, some basic theoretical analysis and mathematic derivation will be presented related to eddy current technology.

3.2 Fundamental and Parameters of Eddy Current Testing

3.2.1 Introduction

The major task of eddy current testing (ECT) is the observation of the interaction between electromagnetic fields and inspected objects. To achieve this, the basic requirements are:

- A coil or system of coils carrying alternating current.
- Objected with electrical conductivity.
- Measurement method for current or voltage in the coil(s).

In ECT, the coil or coils can be in various configurations, in which the coils may be constructed as part of a probe which moves above the surface of inspected object, or is fixed on a bobbin to move along the inside of a tube or hole, or be wound in solenoid form to encircle a specimen such as a bar or tube.

The exciting frequency is chosen depending on the conductivity of the inspected object, the measuring depth and so on. The properties of the object then modify the electromagnetic fields and the resultant current has relation with some of the physical properties of the inspected object which is shown below [10]:

- The proximity of the exciter coil to the material
- The proximity of the sensing coil to the material and to the exciter coil
- The radius of the exciter coil for circular shapes or other relevant dimensions for other shapes
- The flaws in the material
- The radius of the sensing coil for circular shapes or other relevant dimensions for other shapes

- The numbers of turns on the coils, which directly affect the strength of the applied field that generates the eddy currents and the induced sensing coil voltage
- The proximity of the system to the edges of the material or any other physical change in the material that could alter the path of eddy currents
- Material dimensions such as thickness, radius, etc

In addition to above physical properties, there are several electromagnetic properties that need to be considered [10]:

- The source frequency or frequencies, which are also the eddy current and magnetic field frequencies
- The electrical conductivity(σ) of the inspected material and its changes ($\Delta\sigma$)
- The relevant magnetic permeability (μ) and its changes ($\Delta\mu$)
- The anisotropy of the electromagnetic properties.

The process of eddy current testing is to find out and set up the testing parameters optimally in order to test both the desired material parameters such as changes in conductivity or permeability, and imperfections, coating thickness and other properties; and in parallel, to reduce the possible noise and unwanted or non-relevant signal from the receiving devices.

3.2.2 Basic Eddy Current Testing Principles

Two electrical quantities used to characterise the status and condition of the testing coils are expressed as ohmic resistance R and the inductance L. Then, the reactance can be

$$X_L = 2\pi fL$$

$$L = L_S + L_M \tag{3.1}$$

In the above equations, f is the frequency of exciting ac current while L is the combination of self inductance of the coil L_S and mutual inductance L_M. Providing the absence of capacitance, the impedence Z can be formed by combining the resistance and inductance together using the following equation

$$Z = [R^2 + (2\pi f L)^2]^{1/2} \tag{3.2}$$

It can be seen that coil impedance is a complex vector quantity which is also written in another common form

$$Z = R + iX \quad \text{where } i = (-1)^{1/2} \tag{3.3}$$

The impedance can be usefully plotted on the complex impedance plane, where the real part of the impedance is resistance R and the imaginary part is X. Then, the phase angle θ is

$$\tan\theta = 2\pi f L / R \tag{3.4}$$

On the graph, the resistance is plotted on the x-axis and the inductance is plotted on the y-axis, thus the coil impedance can be indicated by a point, or phasor (shown in Figure 3.2). P1 in Figure 3.2 represents the original state of the coil when there has no conductive object in the electromagnetic field. However, if an object with certain electrical conductivity is put close to the coil, the field is modified which is indicated by the change on properties of the testing coil. Thus, the coil has new impedance shown by P2 on the plot, with different values of phase angle, resistance and inductance.

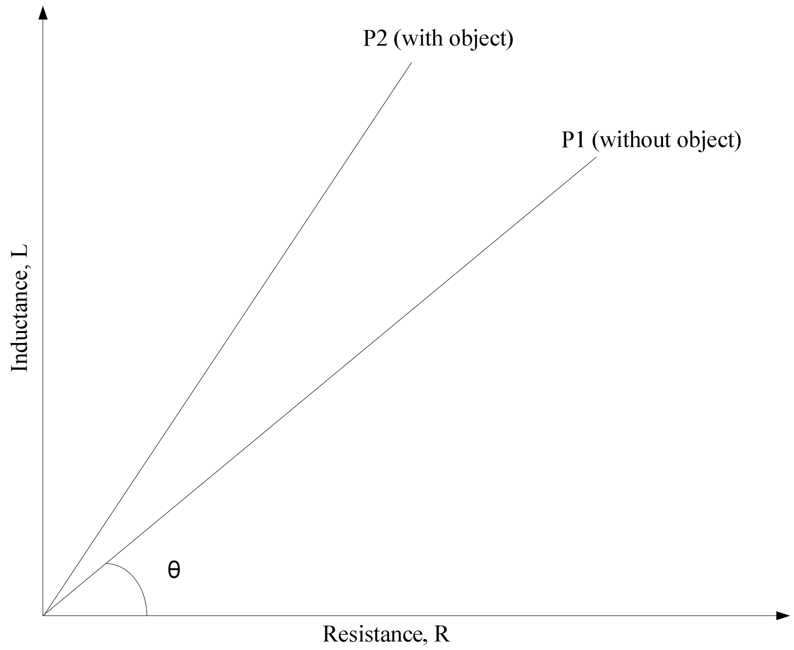

Figure 3.2 Complex impedance plane of a coil carrying a.c. current

When multiple different frequencies are used, the impedance plane plot can be normalized so that all the phasors are more clearly presented. Here, the resistance and inductance of the coil with no target is as L_S, then the normalized values are achieved by $R/\omega L_S$ and $\omega L/\omega L_S$ (ω is the angular frequency and equal to $2\pi f$). The diagram can be produced by plotting the normalized values, i.e. $\omega L/\omega L_S$ against $R/\omega L_S$. The normalization can help avoid having to plot every set of values when changing the coil or specimen's properties. However, if the frequency and coil properties are not variable, it is more convenient to choose the non-normalized impedance plane display.

Figure 3.3 shows how a normalized impedance curve may appear in response to the change of testing frequency. This is ideal frequency response when the measurement conditions are fixed. However, the distortion will occur if there has any changes of sample conductivity and coil configuration, or damage in samples. It needs practical skill and experience to distinguish these factors using this curve.

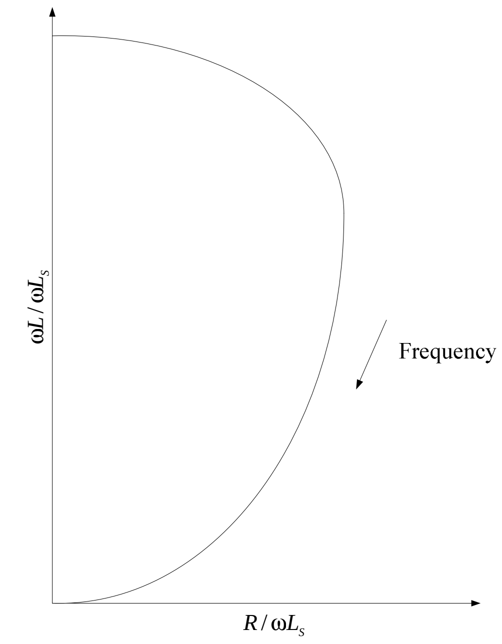

Figure 3.3 Normalized impedance plane showing the frequency response of a conducting, non-magnetic target

In Figure 3.4, it shows how the coil impedance responds to the sample conductivity and lift-off when it is put above a conductive sample. The conductivity line (solid line) illustrates how the conductivity of the sample influences the normalized impedance, fixing the testing frequency and lift-off. From the figure, it can be found that when the coil is put in the air, the solid curve goes to the top end, assuming an ideal coil; while as the sample conductivity increases, the curve goes to the bottom end. The lift-off lines (broken lines) in figure 3.4 give the information about coil lift-off at four sample conductivity values. When the testing frequency and the sample conductivity are fixed, change of the lift-off can result in the coil impedance change alone one of the broken lines (not necessary the ones shown in the figure 3.4) relevant to a specific conductivity value. The broken lines finally reach the conductivity line as the coil touch the surface of sample which means the lift-off is zero. The point at which the broken line reaches the conductivity lines is related to the sample conductivity.

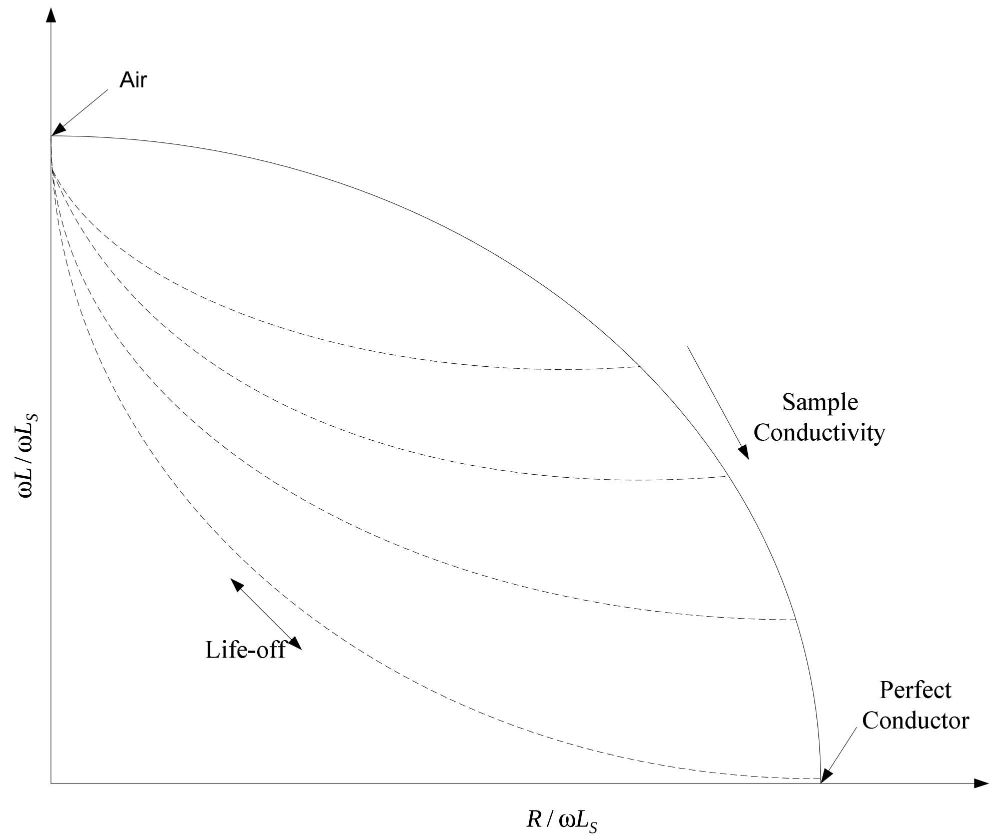

Figure 3.4 Normalized impedance plane showing the conductivity and lift-off response

3.3 Skin Effect and Phase Lag

When eddy currents are produced in a conductive material, they are not distributed uniformly throughout the inspected object [7]. Instead, they tend to be concentrated near to the surface adjacent to the coil, and become less intense as the distance away from the surface increases. Eventually, the eddy current effect becomes negligible and can be ignored above certain distance from the surface. So, this is called the skin effect.

For a simple planar geometry, as the distance from the object surface grows, the eddy current density decreases exponentially. The depth below the surface at which the intensity of the eddy current is reduced to (1/e) of its surface value (approximately 37 percent) is defined as the standard depth of penetration, δ for plane material, where e=2.718, and the value of δ can be obtained from

$$\delta = (\pi f \mu \sigma)^{-1/2} \tag{3.5}$$

where f is the testing frequency

μ is the magnetic permeability of the inspected object

σ is the electrical conductivity of the inspected object.

For particular test object, μ and σ values may be constant. So, the standard depth of penetration for a given material is actually a function of the testing frequency, f .

Table 3.1 shows some typical values of δ for various materials [8], with the values of δ plotted over a larger frequency range in Figure 3.5 [7]. Clearly, the standard penetration depth is not a constant for a given material as it changes with the testing frequency. For a target plate with a thickness less than approximately three times the standard penetration depth, the distribution of the eddy current will be affected by the thickness of the plate. Figure 3.6 shows a few examples of the eddy current distribution in plates of different thickness and shows how the distribution is affected by a thin plate.

In the inspection for thin objects (around or below 3δ), a variation of the thickness can result in the change on the value of the coil impedance. This implies that an eddy current system, if calibrated by a known standard, can be an accurate tool to measure the thickness of a thin object. In turn, the value of δ, along with the plate thickness, are important factors to decide the testing frequency used in eddy current applications.

Frequency / ***Material***	0.001MHz	0.01MHz	0.05MHz
Copper	2.00	0.64	0.28
Aluminium	2.65	0.84	0.04

Titanium	12.00	3.80	1.67
Steel	0.50	0.15	0.07
Graphite	45.00	13.00	6.20

Table 3.1 Depth of penetration, δ (mm) [8]

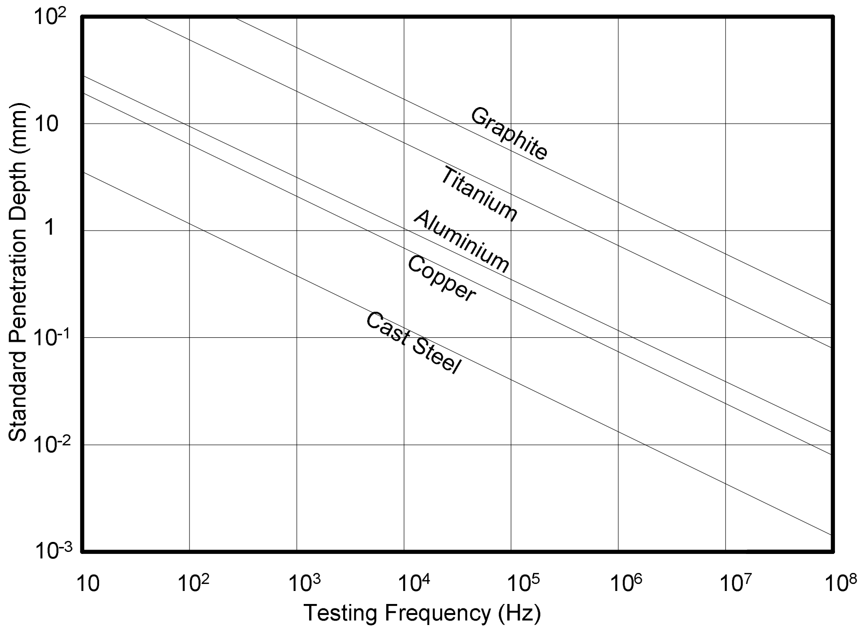

Figure 3.5 Standard Penetration Depth vs. Testing Frequency [7]

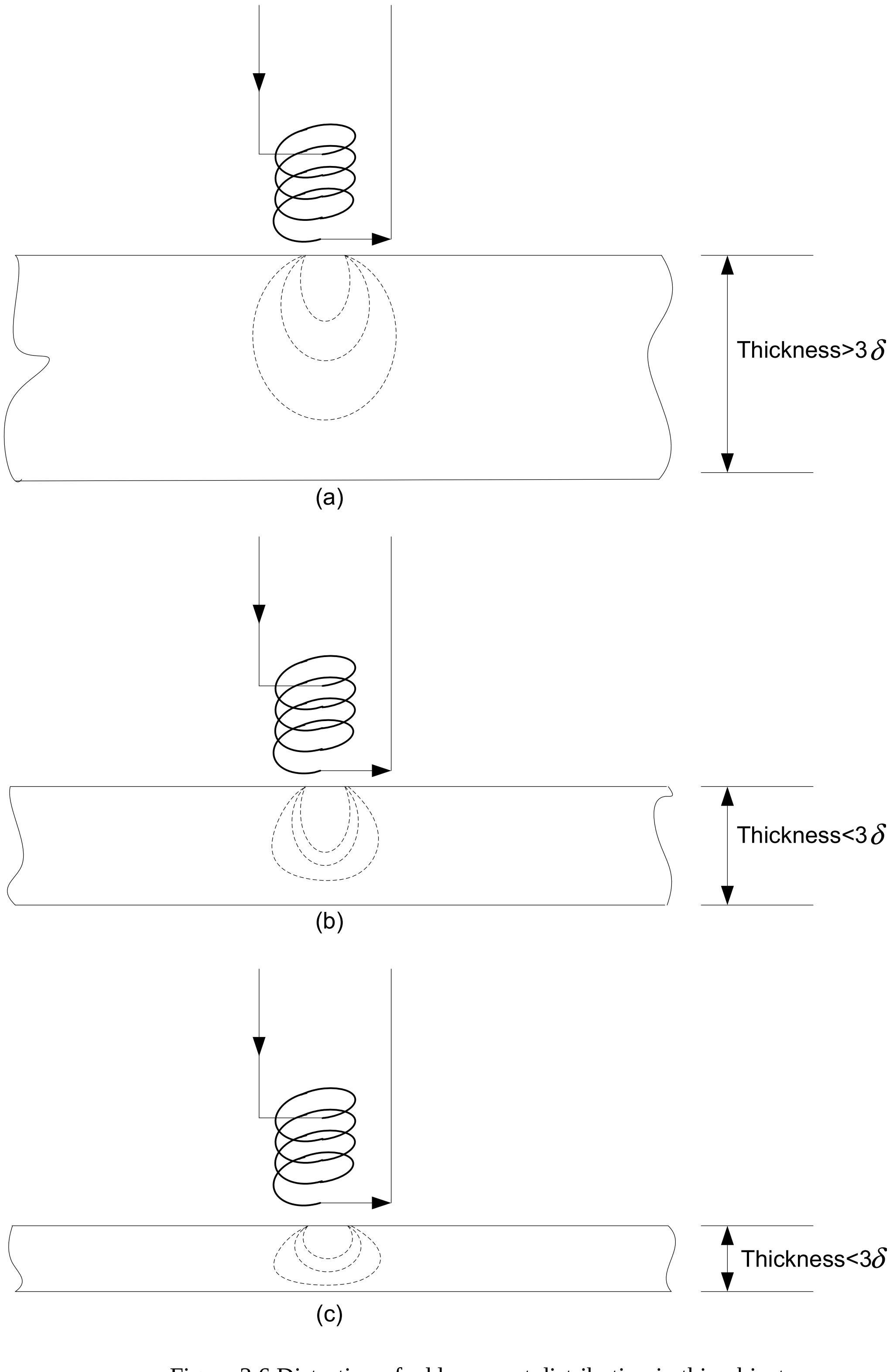

Figure 3.6 Distortion of eddy current distribution in thin objects

(a) Object with thickness more than 3δ ; (b) Object with thickness less than 3δ ;

(c) Object with thickness much less than 3δ

So far, only the magnetic of the eddy currents has been considered. However, as the distance from the coil increases and the deeper that the eddy currents reach into the material, the bigger is the phase change of the eddy current density compared to the surface, which is called phase lag. For objects whose thickness is much larger than three times standard penetration depth, the phase lag is

$$\beta = x/\delta \text{ (in rad) or}$$

$$\beta = 57.5x/\delta \text{ (in degrees)} \tag{3.6}$$

where x is the depth of eddy current into the material. So, for every standard penetration depth, the magnitude of eddy current density is reduced by $1/e$ (37 percent) and the phase lags by 57.5 degrees.

3.4 Coil Impedance

The coil impedance contains much information about the object under testing, so it is of great importance to understand how to represent this value by mathematic derivation and equations.

3.4.1 Coil Resistance

As a conductor with finite electrical conductivity, coils also process electrical resistance. For DC, the resistance is calculated by

$$R = \rho l / A(ohm) \tag{3.7}$$

where ρ is the DC resistivity of the coil (ohm.m)

l is the length of the coil (m)

A is the cross section area of the wire (m^2).

The resistance of the wire carrying AC current can increase with frequency rising up due to the proximity and skin effect. The proximity effect is that when currents flow through one or more nearby conductors such as a wound coil of wire, the distribution of current within the first conductor is constrained to smaller regions. The value of AC resistance may be ten times of the DC resistance of the same wire.

3.4.2 Coil Inductive Reactance

In an alternating current system, the coil also shows self inductance along with electrical resistance as a result of the changing flux in the coil. The self inductance is defined as the flux change per unit current, so it can be derived by

$$L_S = d(N\phi)/dI \tag{3.8}$$

For an air-cored cylindrical coil with finite length D, the flux can be calculated by $\phi = BA$, where B is magnetic flux density. Providing the relation between B and magnetic field intensity H, $B = \mu_0 H$, thus $\phi = \mu_0 HA$. In definition, $H = NI/D$, so $N\phi = \mu_0 N^2 IA/D$. From the above evolution, the self inductance is

$$L_S = \mu_0 N^2 A/D \tag{3.9}$$

If the coil has finite length, a geometrical factor K is add into equation (3.9), so the self inductance is

$$L_S = K\mu_0 N^2 A/D \tag{3.10}$$

A coil excited by alternating currents at angular frequency ω can produce electromagnetic field in itself, which in turn changes the flux in the coil. This modifies the property of the coil and introduces another form of opposition to current flow, called the inductive reactance X_L

$$X_L = \omega L = 2\pi fL \tag{3.11}$$

The value of X_L is zero when frequency is zero and is directly proportional to frequency. To derive the equation (3.11), consider that an alternating source $I = I_0 \sin \omega t$ is connected to a pure inductor of which the self inductance is L_S and the resistance is zero. The generated voltage can be represented by $e = -Nd\phi / dt$. Giving $Nd\phi = L_S dI$, e is also equal to

$$e = -L_S dI / dt \tag{3.12}$$

With $I = I_0 \sin \omega t$, it can be

$$e = -(\omega L_S) I_0 \cos(\omega t) = -(\omega L_S) I_0 \sin(\omega t + 90) \tag{3.13}$$

According to Lenz's Law, the exciting voltage should be equal on the value and opposite on the direction, so it is

$$E = (\omega L_S) I_0 \sin(\omega t + 90) \tag{3.14}$$

Using rms form, the (3.14) could be

$$E_{rms} = (\omega L_S) I_{rms} \tag{3.15}$$

So, the equation (3.11) can be obtained as

$$E_{rms} / I_{rms} = \omega L_S = 2\pi f L_S \tag{3.16}$$

Thus, a specific value inductance reactance at a certain frequency can be calculated by equation (3.11) giving the value of frequency and inductance. Also, it can be noticed that the voltage in the coil is always leading the exciting current by 90 degree according to equations (3.13) and (3.14).

3.4.3 Coil Impedance

When an alternating current I is applied on a coil, it goes through both resistance and inductive reactance of the coil, thus across the two parts produces the voltages which are IR and $I\omega L$ (L contains both self inductance and mutual inductance), respectively. The voltage across L is ahead of it across R by 90°, which can be seen on Figure 3.7. So, the total voltage across circuit, E is

$$E = I\sqrt{\omega^2 L^2 + R^2} \tag{3.17}$$

According to Ohm's Law, the total impedance of the coil is

$$Z = \frac{E}{I} = \sqrt{\omega^2 L^2 + R^2} \tag{3.18}$$

and the phase θ can be derived by

$$\tan\theta = I\omega L / IR = \omega L / R = 2\pi f L / R \tag{3.19}$$

So, the exciting current lags the voltage on the inductance by 90° and the total circuit voltage by θ. Given that the impedance is able to measured by an instrument, according to Figure 3.7, the resistance and inductance can be achieved by

$$X_R = |Z|\cos\theta$$

$$X_L = |Z|\sin\theta \tag{3.20}$$

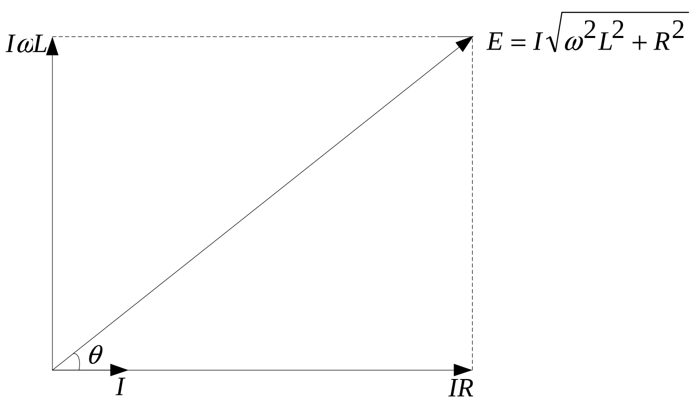

Figure 3.7 Diagram of impedance for coil

In order to get more accurate result, the coil capacitance needs to be considered, particularly in the case that long cables are used. In definition, the capacitive inductance X_C is given by

$$X_C = 1/\omega C = 1/2\pi fC \tag{3.21}$$

where C is the coil stray capacitance in unit farad. And the capacitive reactance produces a voltage across in with 90 degree lagging behind the exciting current. A parallel RLC circuit with resistor in series with inductance can indicate the total coil impedance, seen in Figure 3.8.

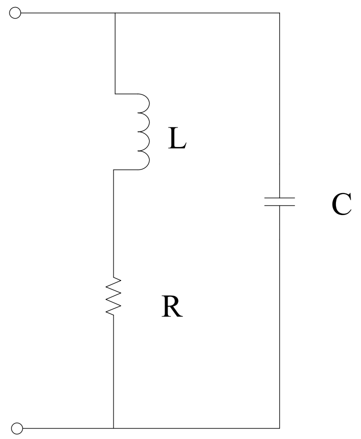

Figure 3.8 RLC circuit indicating coil impedance

Thus, the total impedance of the circuit containing resistance, inductance and capacitance is

$$Z = \sqrt{\frac{R^2 + (\omega L)^2}{(1-\omega^2 LC)^2 + (\omega CR)^2}} \tag{3.22}$$

and the phase angle is

$$\tan\theta = \frac{\omega L - \omega C[R^2 + (\omega L)^2]}{R} \tag{3.23}$$

When

$$\omega = \omega_0 = \sqrt{\frac{1}{LC} - (\frac{R}{L})^2} \tag{3.24}$$

the total impedance get maximum value, which is so called resonance and ω_0 is called resonance frequency. Many circuits benefit from operating under this condition. Figure 3.9 shows the coil impedance's frequency response. When the frequency is close to zero, the total impedance is equal to the resistance in the circuit, so the circuit is resistive. The maximum value of the circuit impedance occurs when the frequency is set to resonance frequency. On the left half of the curve, the impedance changes mainly according the inductive reactance $X_{L,}$ while on the right half, it relies on the capacitive reactance $X_{C.}$

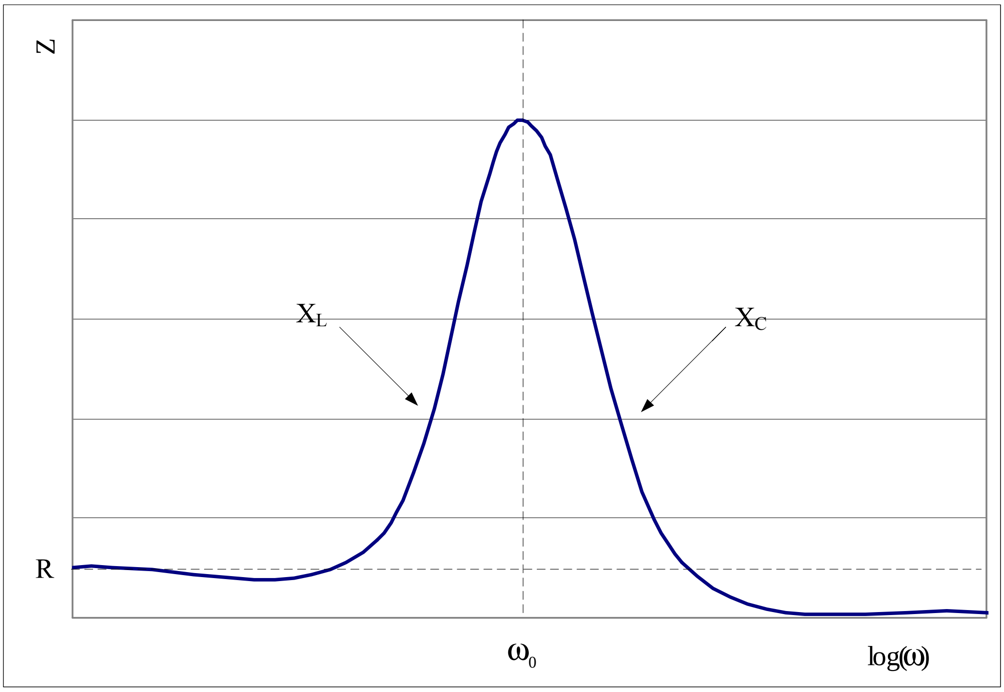

Figure 3.9 Frequency response of coil impedance

3.5 Equipment Requirements

A highly complicated eddy current system can contain excitement generating devices, measuring instruments, probe using coil or coil set, probe scanning device, reference standard, control equipment, and recording devices, among which the basic three parts are excitement generating devices, probe, and measurement instruments.

Figure 3.10 (a) depicts an eddy current testing system with a basic configuration. An oscillator generates alternating currents flowing through the probe, and then produces a changing electromagnetic field and eddy currents in the object under test. At the same time, the property of the coil is also being monitored by the measurement instrument; here a simple voltmeter. Any changes on the coil property can be captured and shown by the voltmeter, which may indicate the existence of a conductive object close to the coil or the presence of defects in the object.

Figure 3.10 shows various coil configurations. In Figure 3.10 (a), the exciter coil also serves as the sensing coil, so that the voltmeter detects changes in self-inductance. In Figure 3.10 (b), a separate receiver, coil is used. This coil can be inside, close to, or remote from the transmitter coil, and can be split into a differential or “cross-axis” configuration as in Figure 3.10 (c). By using a matched pair of coils, the differential coil configuration is able to perform a comparison. Both coils are set to be coupled to the inspected object, by comparing one pitch of the inspected object to another. However, if a signal is received by both coils together, it can not be detected. Only the signal that sensed by one of the coils can be treated. Thanks to its nature of coupling and comparing, the differential coil is able to effectively suppress temperature and lift-off noise. However, the shortcoming is that it cannot provide any signal when a defect is detected by both coils simultaneously. In the cross-axis coils configuration, there have a pair of adjacent coils interacting with the inspected object, with the coil axes oriented 90^{o} to each other in order to generate sensitivity to defects of all orientations. Cross-axis coils can be placed in a side-by-side configuration as in Figure 3.10 (c). They can generate eddy currents at two directions, where the eddy currents produced by one coil is parallel to the inspected object and the eddy currents by the other flow perpendicular to the object.

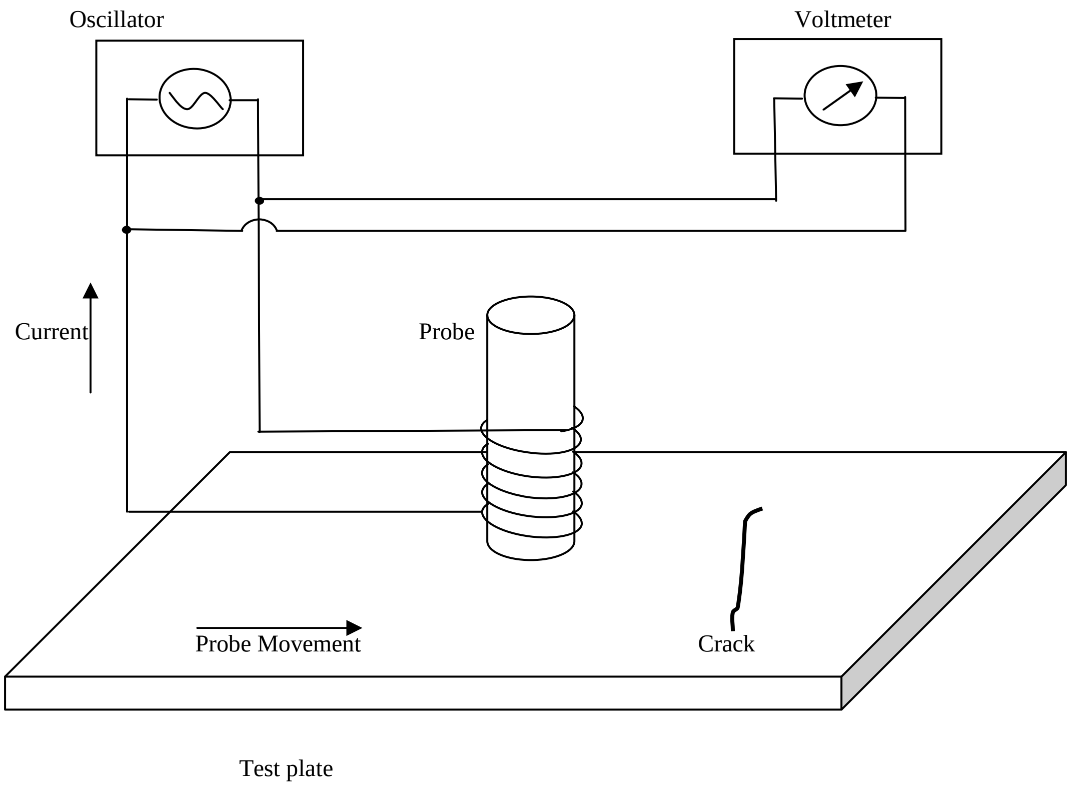

(a) Single coil configuration

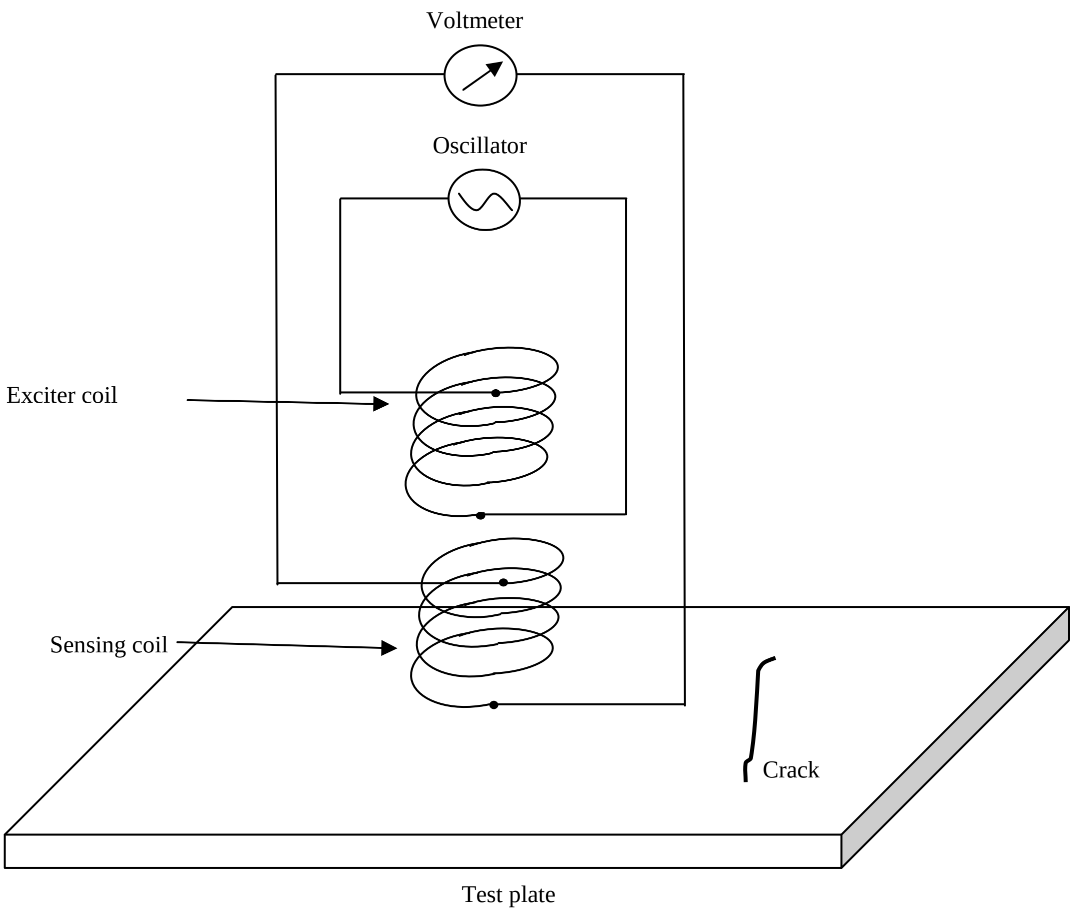

(b) Separate coils configuration

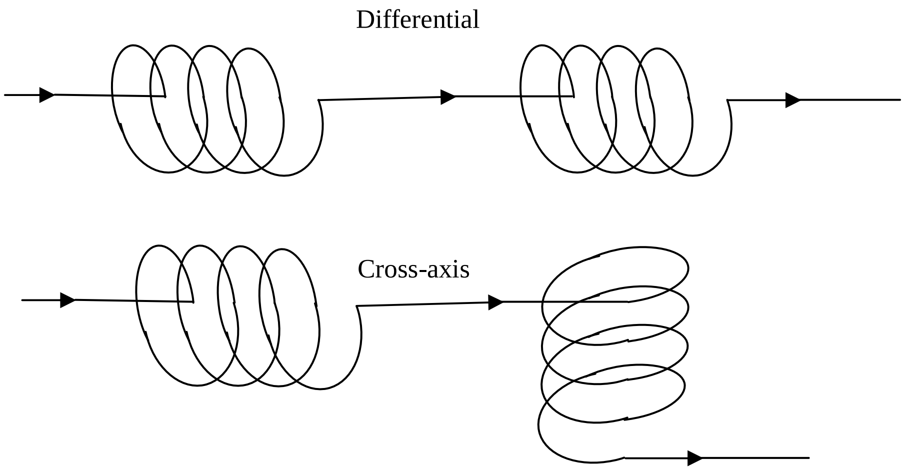

(c) Differential and Cross-axis configuration

Figure 3.10 Various eddy current testing configurations

The oscillator working as function generator here generally produces a sinusoidal waveform with desired frequencies being dependent upon the application and object properties. The oscillator is expected to have a wide range of working frequency, because the eddy current testing may be operated at a frequency from several kHz to several MHz or higher. Voltage measurements consist of amplitude and phase difference measurements from the transmitter coil current. When the electromagnetic field is modified by some reason such object conductivity, distance between probe and object, thickness, and defects, the impedance of the coil is changed. As a result, this change will be detected and received by the receiver coil, and result in the change on the reading of the voltmeter. Thus the voltmeter is able to successfully capture and reflect the modification of the inspected object. For better results, the signal is brought into more advanced equipment for analysis and display. Compared with the standard reference, a good understanding of the object properties can be achieved.

The probe must also be configured to suit the application. This requires some prior evaluation of the task, with such items as size, orientation, impedance at various frequencies, the presence or absence of ferrite cores, the nature of suspected flaws, and the suppression of non-relevant indications all being taken into consideration.

3.6 Governing Equations

Eddy currents are defined in the general theory of electromagnetism and can be deduced from Faraday's Law as well as from Maxwell's equations [67]. The eddy current problem can be considered as a result of electromagnetic induction with electromotive force induced in an electrical conductor.

Before quoting the field equations, the following assumptions are made, normally used in eddy current analysis:

- The displacement current is neglected
- Conducting objects are treated macroscopically
- The structure of media is homogeneous
- The thermal non-linearity is ignored if not considered
- The magnetic permeability μ of the conducting media is constant.

Under the above assumptions, the equations describing eddy currents represent fundamental laws of electromagnetism and are as follows [68]:

$$\nabla \times \boldsymbol{E} = -\frac{\partial \boldsymbol{B}}{\partial t} = -\frac{dB}{d\boldsymbol{H}}\frac{\partial \boldsymbol{H}}{\partial t} \tag{3.25}$$

$$\nabla \times \boldsymbol{H} = \boldsymbol{J} \tag{3.26}$$

$$\nabla \cdot \boldsymbol{B} = 0 \tag{3.27}$$

In a conductor, the electric field strength is linked to the current density by Ohm's law

$$\boldsymbol{J} = \sigma \boldsymbol{E} \tag{3.28}$$

where σ is the conductivity. The constituent equation relating $\boldsymbol{B}$ and $\boldsymbol{H}$ can be written in the form

$$\boldsymbol{B} = \mu \boldsymbol{H} \tag{3.29}$$

where μ is the product $\mu_0\mu_r$ for a linear material.

An additional constraint on $\boldsymbol{J}$ is imposed by the law of conservation of charge, which in the absence of free electric charge, gives

$$\nabla.\boldsymbol{J} = 0 \tag{3.30}$$

This is the field equivalent of Kirchhoff's current law.

For the purpose of solution, the first-order differential equations involving both $\boldsymbol{H}$ and $\boldsymbol{E}$ are combined to give a second-order equation in $\boldsymbol{H}$ or $\boldsymbol{E}$ only. Combining equations (3.26) and (3.28) we obtain

$$\nabla\times(\nabla\times H) = \nabla\times(\sigma\boldsymbol{E}) \tag{3.31}$$

or

$$\nabla(\nabla.\boldsymbol{H}) - \nabla^2\boldsymbol{H} = \sigma(\nabla\times\boldsymbol{E}) + (\nabla\sigma)\times\boldsymbol{E} \tag{3.32}$$

The first term can be obtained by expanding (3.27) with (3.29) to give

$$\nabla.\mu\boldsymbol{H} = \mu(\nabla.\boldsymbol{H}) + \boldsymbol{H}.(\nabla\mu) = 0$$

so that

$$\nabla.\boldsymbol{H} = -\boldsymbol{H}.\frac{1}{\mu}\nabla\mu$$

Thus, with the aid of (3.25), (3.32) become

$$\nabla^2\boldsymbol{H} = \sigma\frac{d\boldsymbol{B}}{d\boldsymbol{H}}\frac{\partial\boldsymbol{H}}{\partial t} - \nabla(\boldsymbol{H}.\frac{1}{\mu}\nabla\mu) - \frac{1}{\sigma}(\nabla\sigma)\times(\nabla\times\boldsymbol{H}) \tag{3.33}$$

Inside a linear magnetic or nonmagnetic material of constant conductivity, (3.32) reduces to the simpler form, which describes a diffusion equaiton

$$\nabla^2\boldsymbol{H} = \sigma\mu_0\mu_r\frac{\partial\boldsymbol{H}}{\partial t} \tag{3.34}$$

As a direct consequence of (3.26) it is often useful to define a magnetic vector potential $\boldsymbol{A}$ for which

$$\nabla\times\boldsymbol{A} = \boldsymbol{B} \text{ and } \nabla.\boldsymbol{A} = 0 \tag{3.35}$$

Substituting for $\boldsymbol{B}$ in (3.25) we obtain

$$\nabla\times(\boldsymbol{E} + \frac{\partial\boldsymbol{A}}{\partial t}) = 0$$

which, after integration, yields

$$\boldsymbol{E} = -\frac{\partial \boldsymbol{A}}{\partial t} - \nabla \boldsymbol{V} \tag{3.36}$$

Where $\boldsymbol{V}$ is a scalar potential.

It is possible to derive a second-order differential equation in $\boldsymbol{A}$ by taking the curl of (3.35), so that

$$\nabla(\nabla.\boldsymbol{A}) - \nabla^2 \boldsymbol{A} = \nabla \times \mu \boldsymbol{H} = \mu(\nabla \times \boldsymbol{H}) + \nabla \mu \times \boldsymbol{H}$$

But $\nabla.\boldsymbol{A}$ is zero by definition, and so using (3.26), (3.28), and (3.36), we obtain

$$\nabla^2 \boldsymbol{A} = \sigma\mu(\frac{\partial \boldsymbol{A}}{\partial t} + \nabla \boldsymbol{V}) - \frac{1}{\mu}(\nabla\mu) \times (\nabla \times \boldsymbol{A}) \tag{3.37}$$

or the simpler linear form in terms of $\boldsymbol{J}$,

$$\nabla^2 \boldsymbol{A} = -\mu \boldsymbol{J} \tag{3.38}$$

which has the formal solution

$$\boldsymbol{A} = \int_v \frac{\mu \boldsymbol{J}}{4\pi r_p} dv \tag{3.39}$$

where r_p is the distance between the incremental volume dv and the field point P.

We can now see the difficulty of solving the integral equation for time-dependent problems because $\boldsymbol{J}$ is related to $\boldsymbol{A}$ via Ohm’s law and (3.36), and so $\boldsymbol{A}$ appears in the integrand of (3.39). Alternatively, substituting (3.39) in (3.36), we have

$$\boldsymbol{J} = -\int_v \frac{\sigma\mu}{4\pi r_P} \frac{\partial \boldsymbol{J}}{\partial t} dv - \sigma \nabla \boldsymbol{V} \tag{3.40}$$

where the time derivative can be taken inside the volume integral if the system is stationary.

The vector Laplacian in (3.33) and (3.37) has a well-known expansion in rectangular coordinates, and in circular-cylindrical coordinates the following components

$$(\nabla^2 \boldsymbol{H})_r = \frac{\partial^2 \boldsymbol{H}_r}{\partial r^2} + \frac{1}{r}\frac{\partial \boldsymbol{H}_r}{\partial r} - \frac{\boldsymbol{H}_r}{r^2} + \frac{1}{r^2}\frac{\partial^2 \boldsymbol{H}_r}{\partial \psi^2} - \frac{2}{r^2}\frac{\partial \boldsymbol{H}_\psi}{\partial \psi} + \frac{\partial^2 \boldsymbol{H}_r}{\partial z^2} \tag{3.41}$$

$$(\nabla^2 \boldsymbol{H})_\psi = \frac{\partial^2 \boldsymbol{H}_\psi}{\partial r^2} + \frac{1}{r}\frac{\partial \boldsymbol{H}_\psi}{\partial r} - \frac{\boldsymbol{H}_\psi}{r^2} + \frac{1}{r^2}\frac{\partial^2 \boldsymbol{H}_\psi}{\partial \psi^2} - \frac{2}{r^2}\frac{\partial \boldsymbol{H}_r}{\partial \psi} + \frac{\partial^2 \boldsymbol{H}_\psi}{\partial z^2} \tag{3.42}$$

$$(\nabla^2 \boldsymbol{H})_z = \frac{\partial^2 \boldsymbol{H}_z}{\partial r^2} + \frac{1}{r}\frac{\partial \boldsymbol{H}_z}{\partial r} + \frac{1}{r^2}\frac{\partial^2 \boldsymbol{H}_z}{\partial \psi^2} + \frac{\partial^2 \boldsymbol{H}_z}{\partial z^2} \tag{3.43}$$

3.7 Boundary Conditions

When solving partial differential equations in a given region it is necessary to specify sufficient information on the boundary of the region to make the solution unique. A convenient linear form of the equation for the vector potential can be obtained by combing (3.27), (3.35) and (3.36) to give

$$\nabla \times (\nabla \times \boldsymbol{A}) = \mu \boldsymbol{J} = -\sigma\mu(\frac{\partial \boldsymbol{A}}{\partial t} + \nabla \boldsymbol{V}) \tag{3.44}$$

Suppose two solutions $\boldsymbol{A_1}$ and $\boldsymbol{A_2}$ satisfy (3.44). Their difference C will satisfy

$$\nabla \times (\nabla \times \boldsymbol{C}) = -\sigma\mu \frac{\partial \boldsymbol{C}}{\partial t} \tag{3.45}$$

The boundary conditions must be such that they ensure that $\boldsymbol{C}$ is zero everywhere in the given region. The solution of (3.44) will then be unique.

The required conditions can be found with the aid of Gauss's theorem applied to a vector $\boldsymbol{P} \times curl\boldsymbol{Q}$, which gives

$$\begin{aligned} \oint_s (\boldsymbol{P} \times (\nabla \times \boldsymbol{Q})).\boldsymbol{n}ds &= \int_v \nabla.(\boldsymbol{P} \times (\nabla \times \boldsymbol{Q}))dv \\ &= \int_v (\nabla \times \boldsymbol{P}).(\nabla \times \boldsymbol{Q}) - \boldsymbol{P}.(\nabla \times (\nabla \times \boldsymbol{Q}))dv \end{aligned} \tag{3.46}$$

Let $\boldsymbol{P} = \boldsymbol{Q} = \boldsymbol{C}$ and incorporating (3.45), (3.46) becomes

$$\int_v |\nabla\times\boldsymbol{C}|^2 dv + \frac{1}{2}\frac{d}{dt}\int_v \sigma\mu|\boldsymbol{C}|^2 dv = \oint_s (n\times\boldsymbol{C}).(\nabla\times\boldsymbol{C})ds$$

$$= -\oint_s (n\times(\nabla\times\boldsymbol{C})).\boldsymbol{C}ds \qquad (3.47)$$

If the surface integrals are zero, we have

$$\int_v |\nabla\times\boldsymbol{C}|^2 dv + \frac{1}{2}\frac{d}{dt}\int_v \sigma\mu|\boldsymbol{C}|^2 dv = 0 \qquad (3.48)$$

The integrands of (3.48) are always positive and the time derivative of the second integral cannot always be negative. Therefore, we can conclude that $\boldsymbol{C} = 0$ everywhere and the solution of (3.46) is unique. Thus, the problem of finding the required boundary conditions has been reduced to that of finding the conditions under which the surface integrals of (3.47) are zero.

It can be shown that

$$\oint_s (n\times\boldsymbol{H})ds = \int_v (\nabla\times\boldsymbol{H})dv = \int_v \boldsymbol{J}dv \qquad (3.49)$$

which is a generalization of Ampere's law. The specification of the surface tangential vector component of H is sufficient to ensure the uniqueness of the magnetic field.

3.8 Conclusion

In chapter, the discussion mainly focuses on the theory of eddy current testing. By generating eddy currents in the inspected specimen and interacting with it through the electromagnetic field, the probe with transmitter and receiver coils can obtain the information about the specimen properties, its inner structure and health conditions fast and easily. For different inspection tasks, a specifically designed probe is used and some theory is also referred to. In eddy current testing, the normalized complex impedance plane is mostly used as it is able to represent important information in one plot. The skin effect is a very important phenomenon that needs much consideration as it is one of the factors when determining the testing frequency and also it provides a very useful method to measure the specimen's thickness. The basic configuration of an eddy current testing system is introduced in this chapter. A wide range of choice for the devices and coils configuration is available, but the basic components include excitement generating devices, probe set, and measurement instruments. Detailed mathematic calculation for coil impedance and eddy current are also discussed in the last couple of sections for a better understanding of the principles and provides the prerequisite background and theoretical tools for further applications.

Chapter 4. Eddy Current Techniques for Characterization of CFRP

4.1 Introduction

Previous chapters have given introductions to CFRP material and eddy current testing techniques. In this chapter, the solution to non-destructive characterization of CFRP using eddy current methods is discussed in detail. Based on Dodd and Deeds' formulas, the bulk conductivities can be evaluated by circular coil. Also, using specific designed probes, the fibre direction, layer sequence, and stacking can be characterized. The detection of impact damage on CFRP samples is described as well. The eddy current inspection system is developed combining devices, probes, scanning equipments and controlling computer with GUI interface programmed in MatLab. The measurement results are presented and can give the information of the inspected samples' properties and health condition.

4.2 Analytical Techniques and the Dodd & Deeds' Formulation

4.2.1 Background Knowledge

Eddy current testing is based on electromagnetic principles, and can detect the effects of a conductive object without contacting it [69]. This method has been used in a range of technological applications such as thickness measurement, quality inspection, coating and surface treatment [70-73].

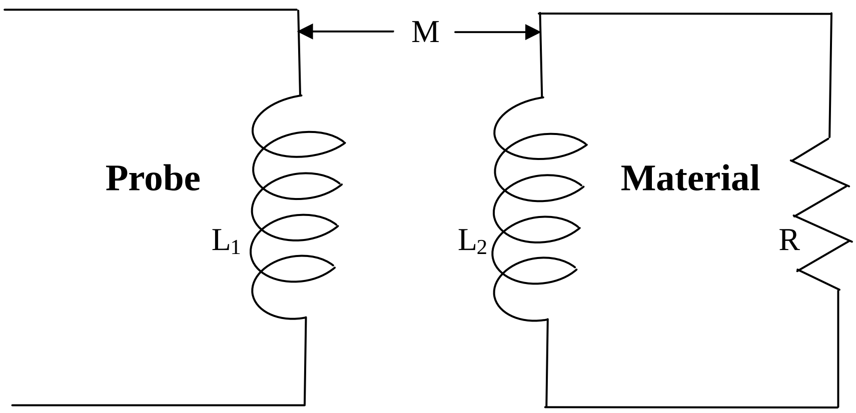

Figure 4.1 Circuit model for the eddy current probe and conductive material coupling

A simple electronic circuit can be used to describe the situation of eddy current measurement of a material. The two coupled coils in Figure 4.1 represent a simple two terminal eddy-current probe (sensor) with inductance L_1 and the current loop in the material with L_2 and resistance R respectively. The probe and the material are coupled by the mutual inductance M

$$M = k\sqrt{(L_1 L_2)} \tag{4.1}$$

where k is the coupling factor, which depends on the spacing between the probe and the material and on the design of the probe. Its value ranges from 0 to 1.

The impedance of the coil L_1 in the presence of a conductive, non-magnetic material is:

$$Z = Z_0 + \frac{(\omega M)^2}{Z_{22}} \tag{4.2}$$

$$Z_0 = j\omega L_1 \tag{4.3}$$

$$Z_{22} = R + j\omega L_2 \tag{4.4}$$

Where Z_0 is the impedance of the probe in air, and Z_{22} is the intrinsic impedance of material and ω is the angular frequency of exciting current. Thus, the normalized impedance of probe is:

$$\frac{Z}{Z_0} = 1 - \frac{k^2}{1 - jR/(\omega L_2)} \tag{4.5}$$

Figure 4.2 shows the locus of *Z/Zo* in the complex plane representation for several values of $R/\omega L_2$ and *k*. It shows that to observe variations in the resistivity of the material, good coupling and a proper selection of the measuring frequencies are prerequisites. Variations in the resistance are indicative of defects, such as cracks or delamination in material constructions. In a more rigorous treatment the diffusion of the magnetic field into the conducting material has to be taken into account.

From Figure 4.2 and equations (4.5), curves of the real and imaginary parts as a function of frequency can be obtained. Figure 4.3 shows the ideal response of the real and imaginary parts to frequency. A peak is also clearly shown in Figure 4.3 at which imaginary part is symmetric on both sides and the minimum value can be found while the real part is symmetric with regard to this maximum point.

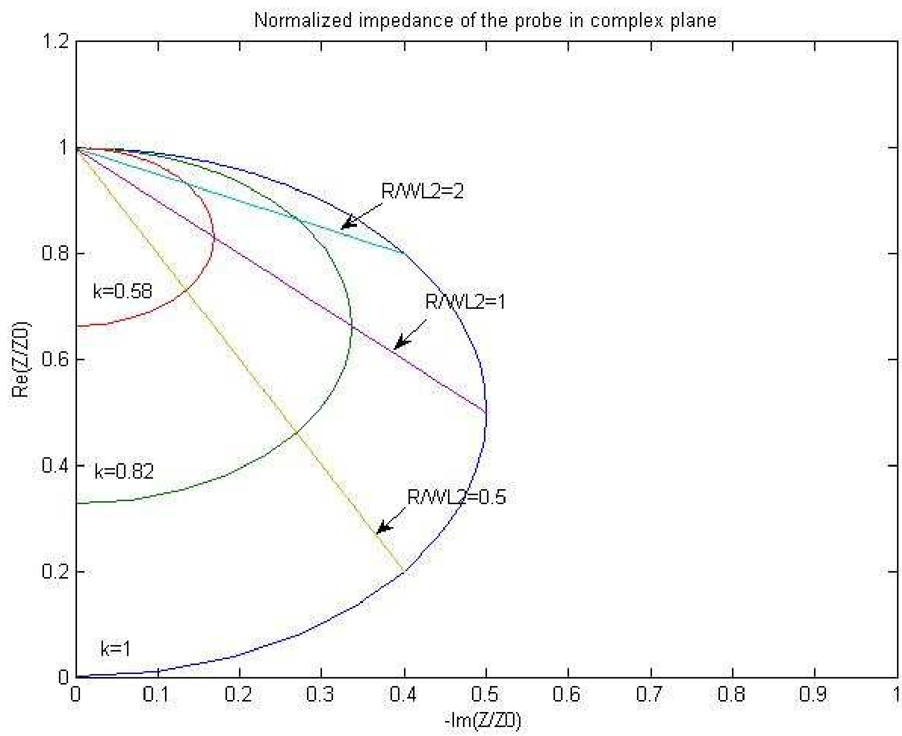

Figure 4.2 Normalized impedance of probe presented in the complex plane

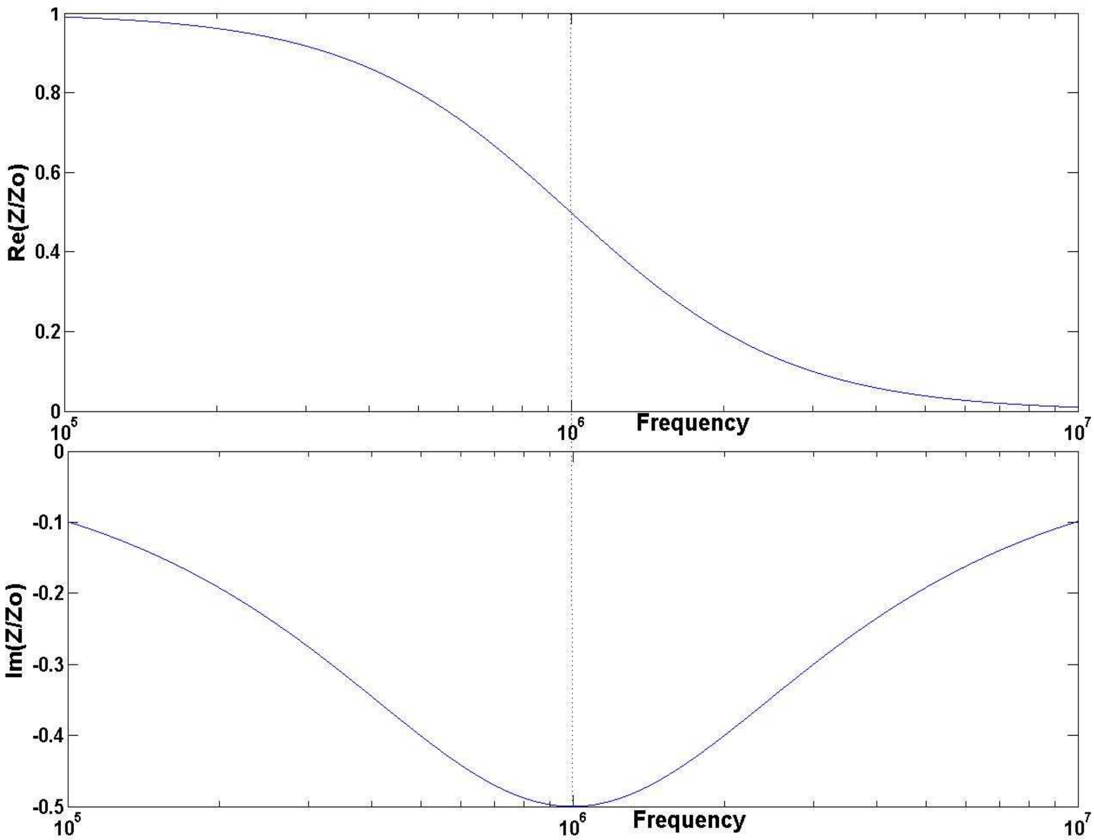

Figure 4.3 Simulated real and imaginary normalized impedance vs. frequency

4.2.2 The Dodd & Deeds' Formulation

Previous studies have shown that CFRP conductivity is related to fibre volume fraction, stacking sequence and fibre length etc [74]. This is a very important parameter of the inspected material. The intrinsic inhomogeneity of composites, due to variations in fibre-fibre contacts and in the fibre volume fraction, may cause difficulties in distinguishing acceptable variations from defects.

A more practical and detailed solution than the circuit equivalent model before can be obtained for a circular air-cored coil above a conductive plate, as showed in Figure 4.4 is [75]:

$$\Delta L(\omega) = K\int_0^\infty \frac{P^2(\alpha)}{\alpha^2} A(\alpha)\phi(\alpha)d\alpha \tag{4.6}$$

Where $$\phi(\alpha) = \frac{(\alpha_1+\alpha)(\alpha_1-\alpha)-(\alpha_1+\alpha)(\alpha_1-\alpha)e^{2\alpha_1 c}}{-(\alpha_1-\alpha)(\alpha_1-\alpha)+(\alpha_1+\alpha)(\alpha_1+\alpha)e^{2\alpha_1 c}} \tag{4.7}$$

$$\alpha_1 = \sqrt{\alpha^2 + j\omega\sigma\mu_0} \tag{4.8}$$

$$K = \frac{\pi\mu_0 N^2}{(h_1-h_2)^2(r_1-r_2)^2} \tag{4.9}$$

$$P(\alpha) = \int_{\alpha r_1}^{\alpha r_2} x J_1(x)dx \tag{4.10}$$

$$A(\alpha) = (e^{-\alpha h_1} - e^{-\alpha h_2})^2 \tag{4.11}$$

Where α -- integration variable;

α_1 -- a combination as shown in formulation (4.8);

ω-- angular frequency of excitation current;

μ-- the permeability of the conducting plate;

μ_0 -- the permeability of free space;

σ-- the conductivity of the conducting plate;

r_1 and r_2-- inner and outer radius of the probe;

h_1 and h_2-- height of the bottom and top of the probe;

c -- the thickness of the plate;

$J_1(x)$-- a first-order Bessel function of the first kind.

The conductivity of the CFRP plate under test is able to be obtained by fitting the results from equations (4.6) to (4.11) to experimental data. Alternatively, a much simpler method could be adopted which uses the features in multi-frequency response of the sensor to infer conductivity of the sample as in [76].

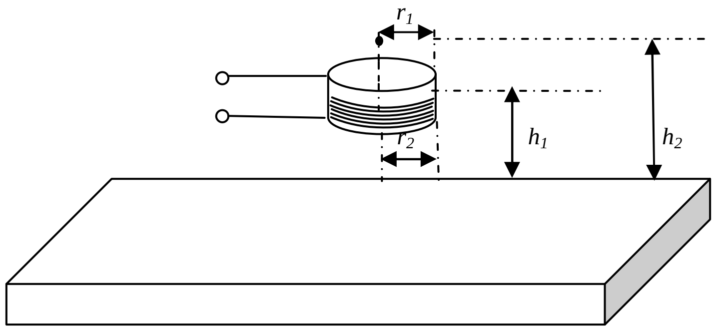

Figure 4.4 A circular probe above conducting plate

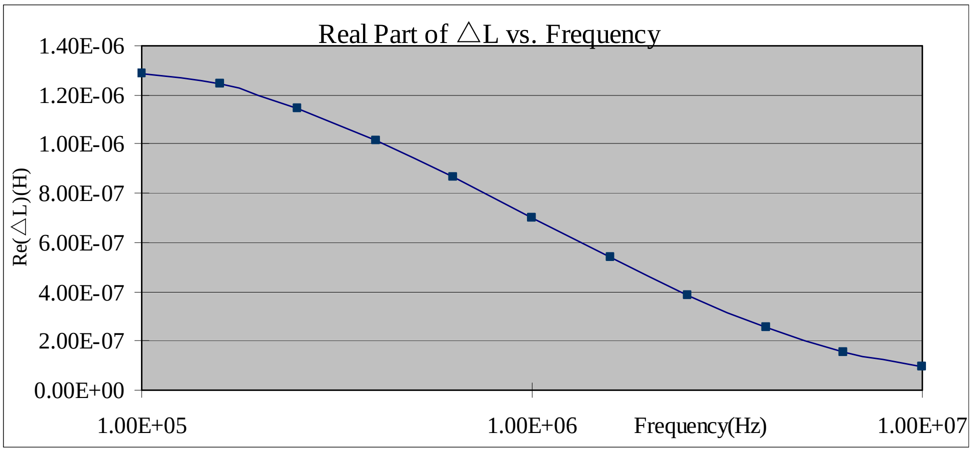

(a) Real part

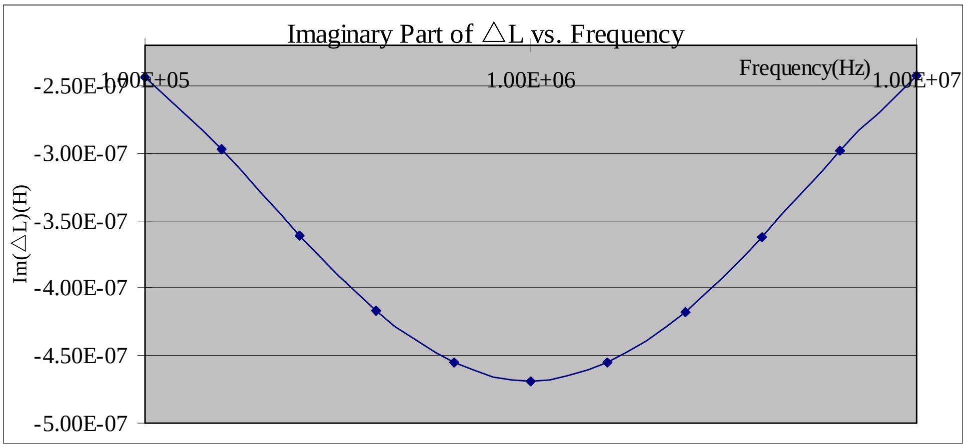

(b) Imaginary part

Figure 4.5 Normalized impedance of a circular coil above a conductive plate based on the Dodd and Deeds' solution.

Figure 4.4 presents a set of basic and most-used configuration for eddy current testing. In this specific experiment, h_1 and h_2 are set to 0.1 mm and 10.1 mm with r_1 and r_2 being 5 mm and 5.3 mm respectively. The test plate is made of CFRP with entire electrical conductivity of about 12 kS/m. The eddy current probe consists of copper coils wound on a plastic former and is a so called air-cored sensor. Alternatively, a ferrite core can be used for different inductance and effect. The curves in Figure 4.5 present the experiment results. Comparing them with Figure 4.3, it can be seen that in the frequency range from 100kHz to 10MHz, the curves for real part of the normalized impedance go by the same trend and they show same shape despite they are different on the magnitude, same as the imaginary parts. This agreement gives a strong support to Dodd and Deeds' solution.

The Dodd and Deeds' solution describes the relations between the parameters of the probe and material. Comparing with the results at different frequencies, we can verify the data of multi-frequency experiments. As shown in previous section, in the equation for the skin depth, the product $\omega\sigma$ has to be within a preferred range of values. A reduction in σ by a factor of 1000 or more requires an increase in the measuring frequency by the same factor to observe comparable eddy currents in composites and metals. With increasing frequency, the conductance between fibres should be considered, so the conductivity of CFRP perpendicular to the fibre axis will increase.

4.2.3 Fibre Direction Characterization

The large anisotropy in the electrical conductivity, in particular of unidirectional composites, suggests that eddy current methods may be suited to inspect the correct orientation of the fibres.

Rotating an eddy currents probe can be used to detected local fibres orientation, shown in Figure 4.6. Here, the probe is a ferrite-cored pair of rectangular coils with same dimensions and turns. The two coils are glued together to a base and used as transmitter and receiver separately.

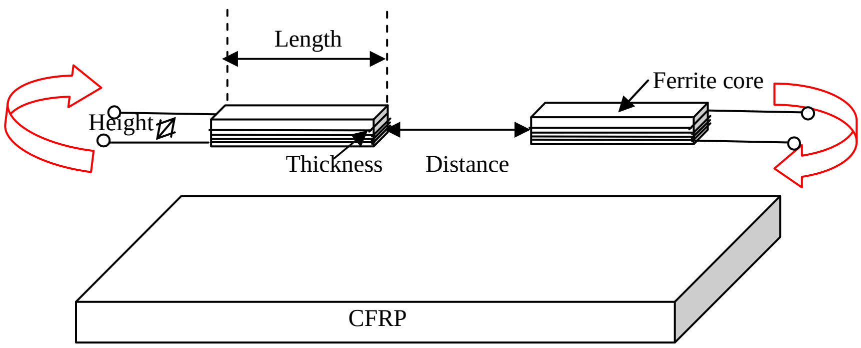

Figure 4.6 Fibre direction characterization with ferrite-cored pair probe

The effects of directionality will increase as either the coils thickness decreases and / or the transmitter-receiver distance increases. However, at the same time the signal-to-noise ratio decreased. Consequently, there is a compromise between these parameters. The directivity will also increase with increasing of the testing frequency. However, there are more factors that should be taken into consideration in choosing of the test frequency, such as:

- The directivity;
- The penetration depth of the eddy current;
- The signal-to-noise ratio;
- *The direction of lift-off and conductivity effects in the impedance plane.*

4.3 Measurement and Result Analysis

4.3.1 Measurement Setup

As can be seen from Figure 4.7, the measurement system is divided into three parts. This is the prerequisite setup for eddy current testing and more comprehensive equipment will be discussed in following sections. The probe is controlled by PC to perform different scanning tasks and its design varies for different measurements and requirements, and its position can be adjusted by individual devices or automation scanning equipment which can be instructed by computer. The eddy current signal device used here is an impedance analyzer, in this case, a Solatron 1260 (Figure 4.8). With wide measurement frequency range and providing alternating sine wave on the probe, it is usually working on two channels which are connected with probe's transmitter and receiver. Also, the analyzer is controlled and set by the computer through the interface software SMART (Figure 4.9). The computer is the core of the whole system with role including scanning control, device specification, data acquisition and processing, and material structure imaging.

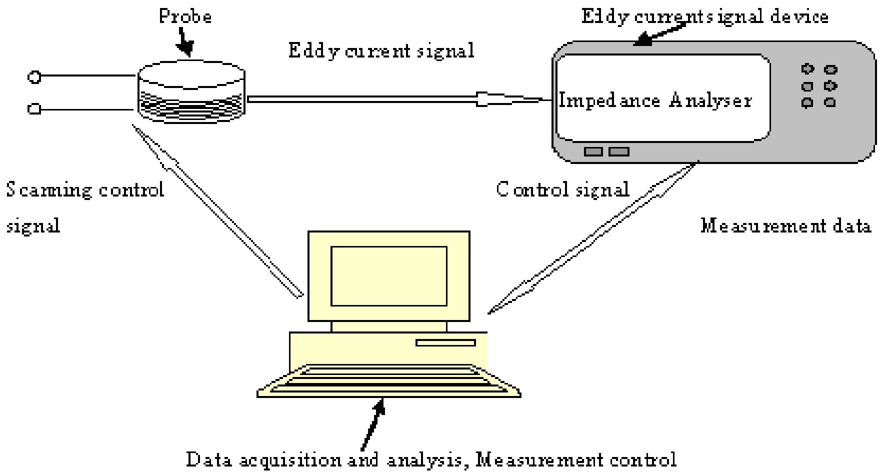

Figure 4.7 Diagram of eddy current testing system

Figure 4.8 Solatron 1260

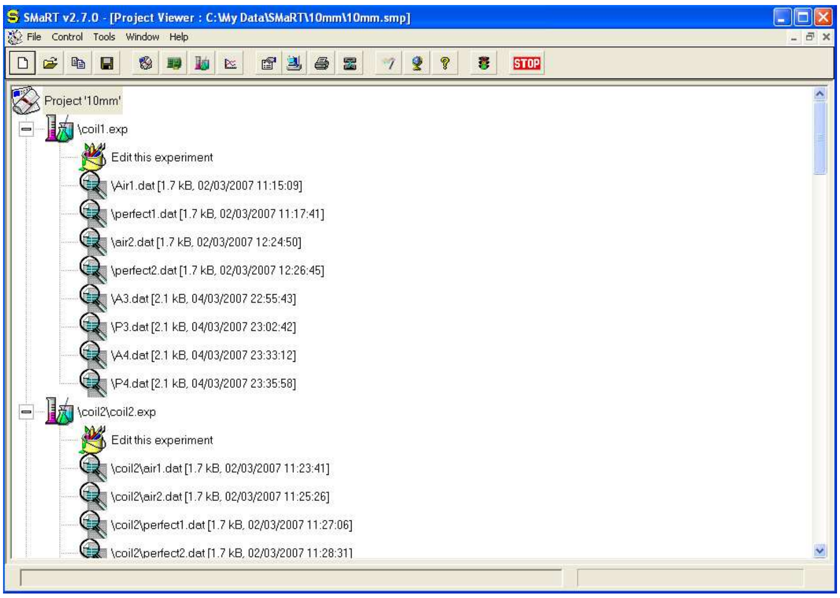

Figure 4.9 Snapshot of SMART

The Solatron 1260 Impedance/Gain-Phase Analyzer uses powerful microprocessor-controlled digital and analog techniques to provide a comprehensive range of impedance and frequency response measuring facilities. These include (from 1260 manual):

- Single sine drive and analysis of the system or component under test over the frequency range 10 MHz to 32MHz.
- Measurement integration, and auto-integration, of the analyzer input, for harmonic and noise rejection.
- Sweep facility, for any one of three measurement variables, frequency, amplitude, or bias.
- A comprehensive range of voltage and current transfer characteristics, each one available from the original base data.
- Plotter output, of immediate or filed data, to a digital plotter on the GPIB.
- Limit check and data reduction facility. Data output can be confined to those results that fall within, or outside, user-defined values.
- Output ports selectable from: RS 423, GPIB, and the History File.
- Result scaling that includes: a normalization facility that separates the desired results from confusing background data; and, for impedance measurements, a nulling facility that compensates for stray capacitance and inductance.
- Vernier facility, which allows the drive to be adjusted whilst measurements are being made.
- Learn program facility, which allows the instrument to learn a series of control settings and commands.
- Component sorting, manual or automatic.
- Self test facility.
- Local control from a simplified key panel or remote control from the GPIB.

The practical measurement setup is shown is Figure 4.10, which includes impedance analyzer, eddy current probe, CFRP sample, rotary tray for scanning and fixing device.

This may help give a direct view of how the measurement is carried out. Depending on the probe applied, this setup can be used to for various tasks.

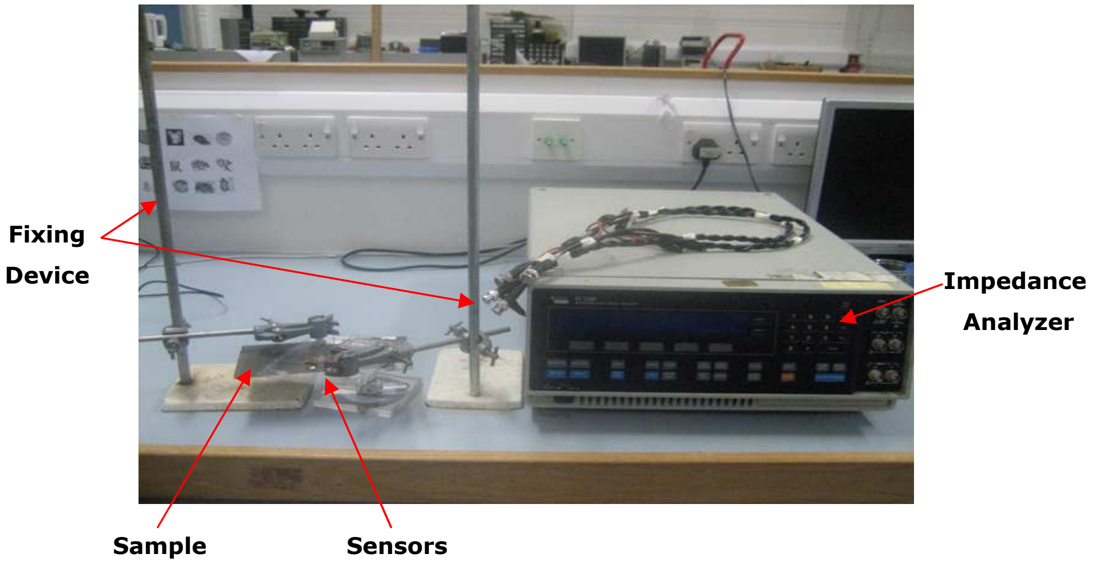

(a) Measurement setup

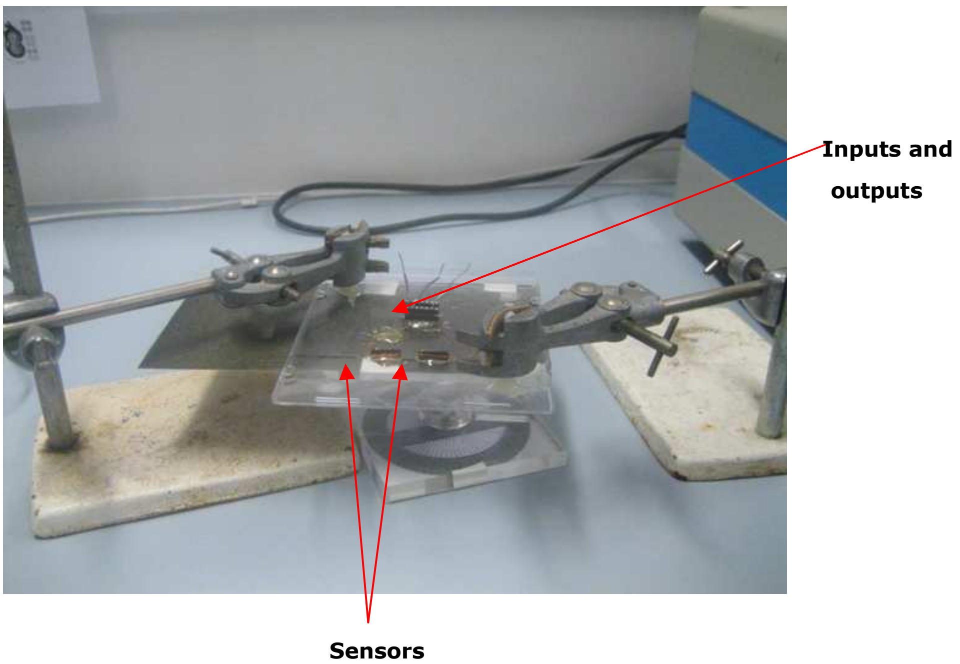

(b) A close view of probe setup

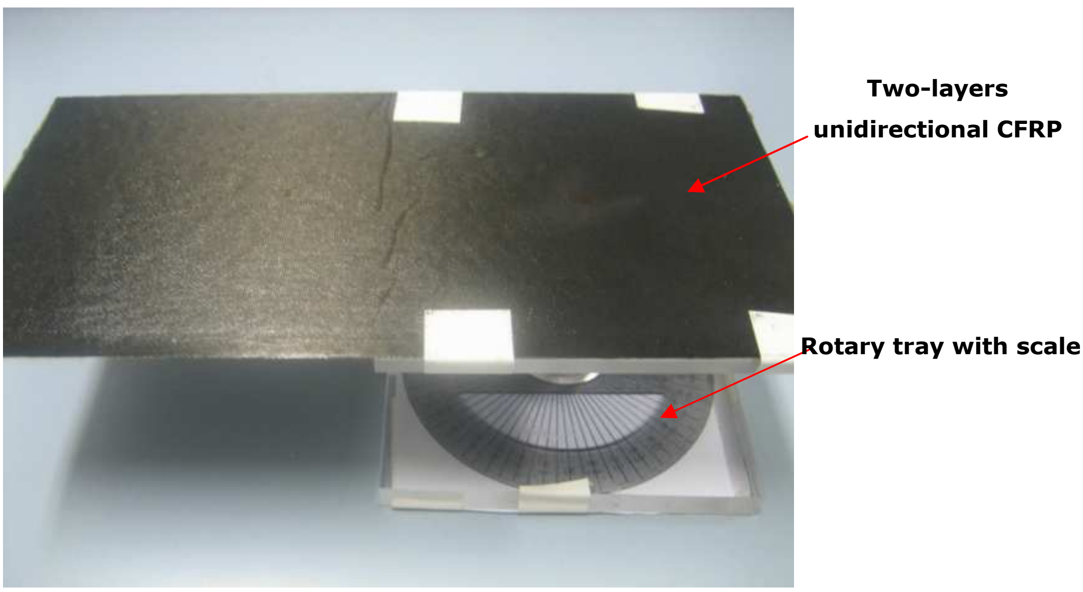

(c) Fixed CFRP sample

Figure 4.10 Practical eddy current testing system

The above figures show different views about how to carry on an eddy current testing for CFRP characterization. For the above example, it is to inspect the fibre direction, and it can also be used for other testing purpose. The inspected CFRP sample is fixed on a rotary tray with degree scale fixed on the bottom. The probe is controlled by a pair of clamps which can be used to adjust the probe's position. During one single testing, the probe is move to the required position and kept unchanged, then the sample is rotated by required degree which depends on the resolution. At every step, the transmitter of the probe is excited and produces eddy currents in the sample. Next, the receiver sends the signal back to the Solatron 1260 where the impedance is measured. At last, the data is passed to computer to record and analysis. The whole process is repeated within a degree range which may be 180 or 360 degree, etc.

This system can be working at a very wide frequency range which depends on the sample conductivity, inspection depth, coil specification, etc. However, cares must be taken on the measurement stability and electromagnetic interference at higher frequency, and the capacitance would not be ignored when the frequency increases. The causes come from the capacitance of the measurement cables, vibration during the testing, field interference by metal pieces in the system, and the capacitance in CFRP sample like inter-fibre capacitance and fibre-matrix capacitance.

4.3.2 Comprehensive Measurement System

4.3.2.1 Introduction

In practice, there have a few factors which limit the quality of eddy current testing results. It may introduce unexpected errors and reduce the system stability when inspector moves the probe and inspected sample manually to the desired position. In order to take inspection for materials with conductivity and thickness in a wider range, the impedance analyzer 1260 can not provide enough frequency bands. Also, there have only few options in 1260 for excitation wave configuration, signal processing and result analysis. Every time, the measurement result need to be extracted from Smart (program to communicate with 1260), transformed to correct format and sent to other program for signal processing and result analysis, which have high risk to bring in the error. For a task consisting of many individual measurements, it is subject to cause mistake if each measurement needs to be setup one by one. To overcome these shortcomings and get more accuracy, stability, automation and flexibility, a more comprehensive system is introduced and designed for eddy current testing. It is made up of computer, function generator, oscilloscope, automation equipment, improvement circuits and probe. The communication between instruments and computer are set up, therefore the computer gets control over them. Thus, the parameters of the measurement are configured by computer, and the results are also sent to computer for processing and analysis.

As can be seen in Figure 4.11, the excitation signal is generated by signal generator and flowing into the improvement circuit which has been introduced in the previous sections. After enhancing the quality of the signal and reducing noise, the excitation signal arrives at the transmitter coil of the probe. Then the inspection is carried out and the inspection signal from the receiver coil is sent to the improvement circuit for receiver coil. The improved signal is then fed into the oscilloscope for the calculation as well with result and waveform presentation. Finally, all the measurement signal and waveform data are extracted to computer for recording and analysis. Both the probe and the inspected CFRP sample are fixed to X-Y scanner, which can carry them to the required position accurately with high resolution. Every instrument is configured, controlled and monitored by the GUI interface program developed by MatLab on the computer. Also, all the signal processing and result analysis are carried out on the computer as well. Once fixing the probe and inspected sample onto the X-Y scanner, the inspector do not need to touch them any more until the inspection finishes. All the operations are performed by instruments which are controlled and monitored by computer in order to avoid the error caused by inspector. Therefore, this can enhance the system stability, flexibility and automation extensively.

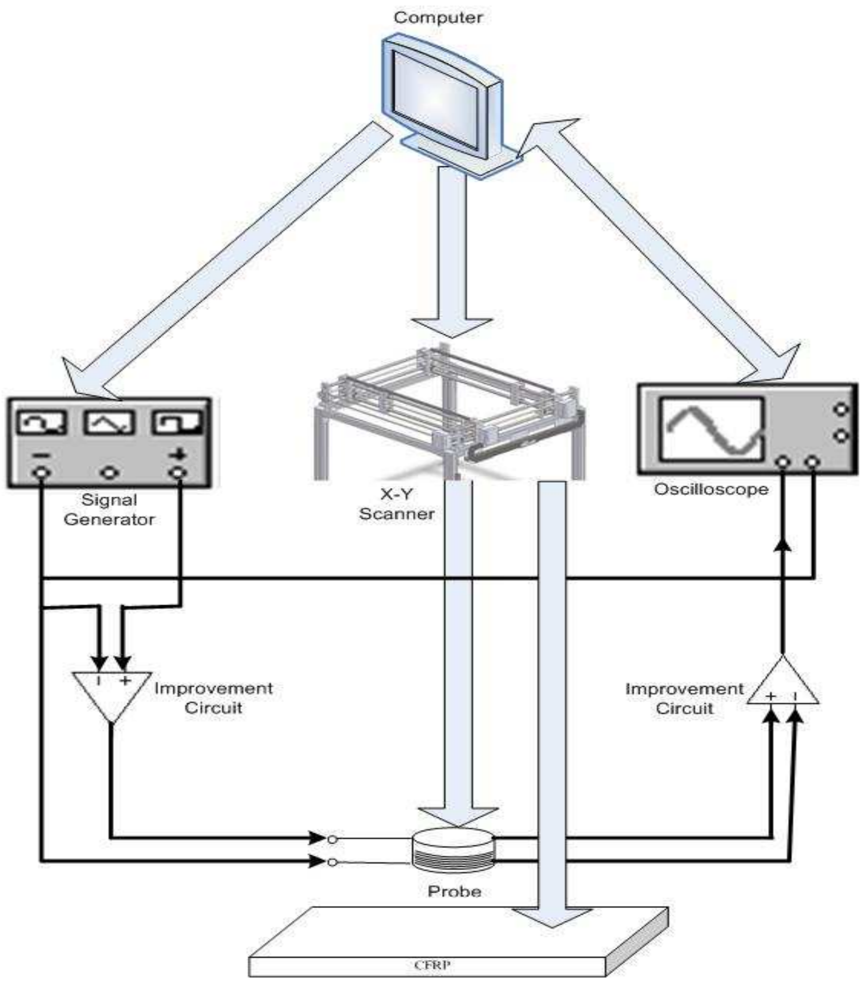

Figure 4.11 Comprehensive eddy current measurement system

4.3.2.2 Function Generator 33250A

The Agilent 33250A is a high-performance 80 MHz synthesized function generator with built-in arbitrary waveform and pulse capabilities. Its combination of bench-top and system features makes this function generator a versatile solution for the testing requirements. Compared with Solatron 1260, 33250A can generate arbitrary waveform in a wider frequency ranging up to 80MHz, which is much higher than 32MHz of 1260. And fully control on the excitation signal can be obtained through 33250A. Therefore, wider frequency sweep in eddy current testing can be achieved.

4.3.2.3 Oscilloscope 54615B

Using oscilloscope can better present the measurement result and offer more option to process the signal. The inspector is able to observe the result directly and immediately, also can plot the data on the screen using various methods. Full range of calculation for signal parameter can be obtained as well. Oscilloscope HP 54615B which is used in this system can deliver high level of digitizing performance for measurements.

4.3.2.4 X-Y Scanner

A commercial X-Y Scanner is utilized in the system (seen in Figure 4.12). It can provide high automation and accurate position for the probe and inspected sample. Shown in Figure 4.12, the X-Y scanner contains two carriages named by X-Y carriage and Z carriage. The first can be moving in two directions along X and Y axis, while the second can only move along Z axis. In the testing, the sample is fixed onto Z carriage and the probe is fixed onto X-Y carriage to take on a horizontal scan. The X, Y, Z axes are motor driven and the scanning parameters are controlled by the interface program. Therefore, the probe carried by X-Y carriage can be automatically positioned anywhere within a horizontal plane in the scanning area, and the sample carried by Z carriage can be automatically positioned anywhere along the Z axis. More details about the scanner are shown in Table 4.1.

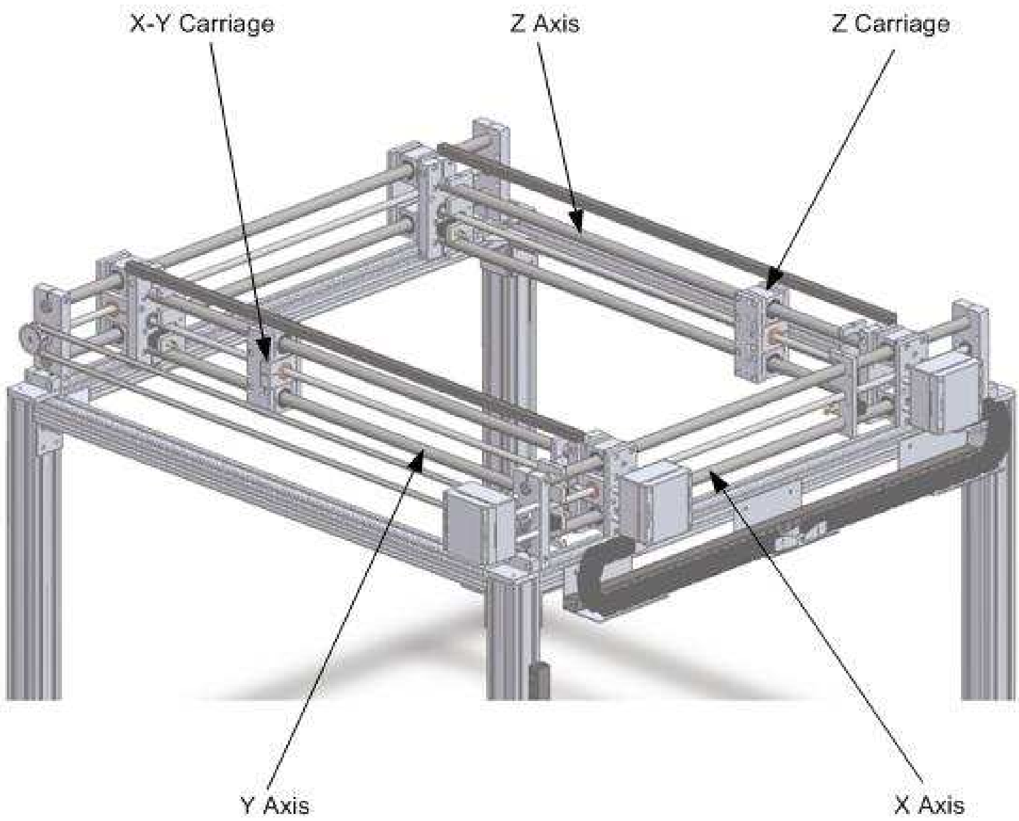

Figure 4.12 X-Y scanner

Axis	Maximum Axis Travel (mm)	Maximum Scanning Speed (mm/s)	Maximum Resolution (mm)	Accuracy (mm)
X	600	10	0.03	±0.05
Y	850	15	0.03	±0.05
Z	850	15	0.03	±0.05

Table 4.1 Properties of X-Y scanner

4.3.2.5 GUI Interface for Measurement System

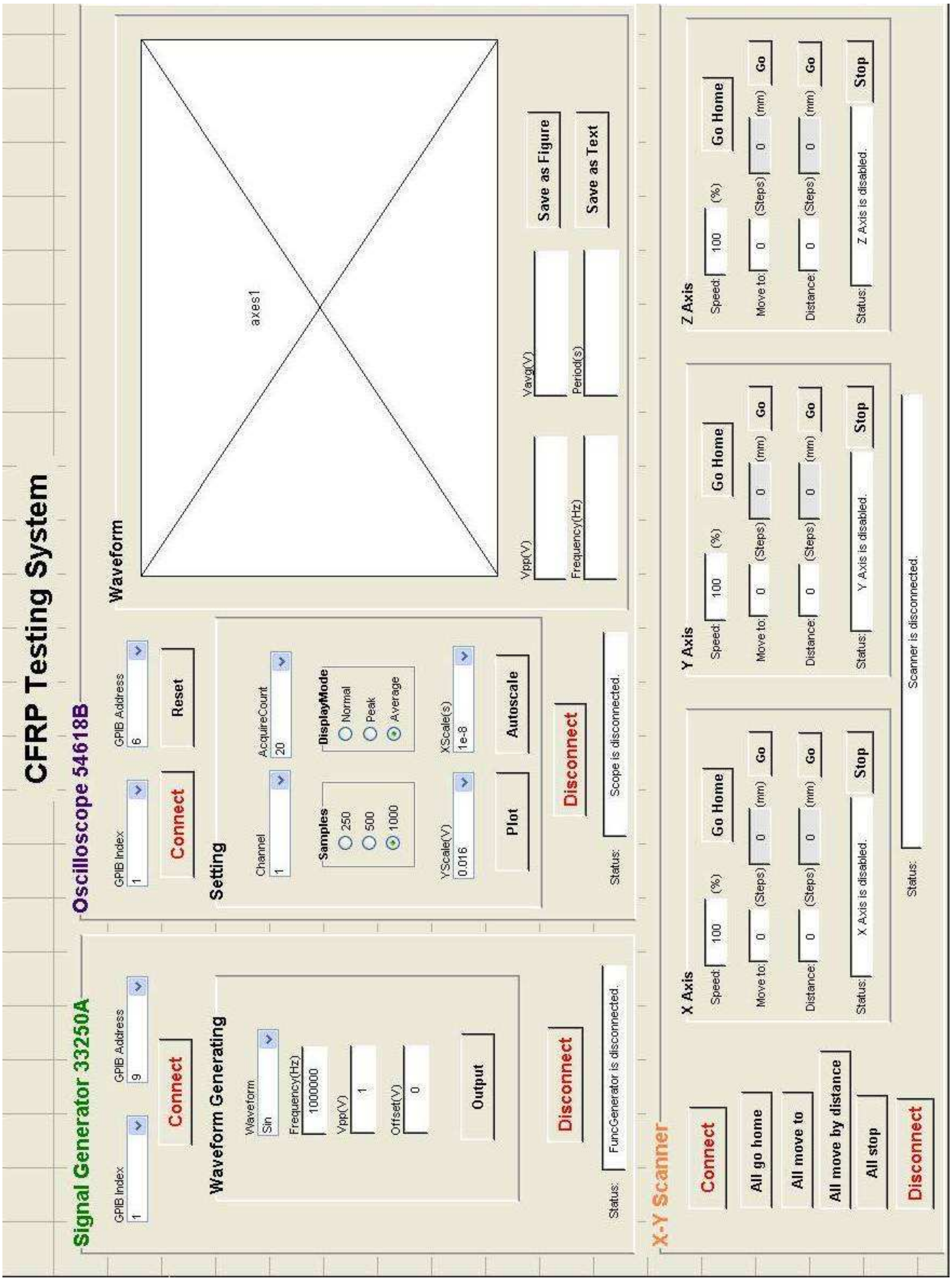

Figure 4.13 GUI interface for the measurement system

In the previous Figure 4.11, it presents that all the instruments and devices are connected to computer directly while the probe and sample are controlled by computer through X-Y Scanner. To incorporate all in one, a GUI interface for the whole measurement system has been developed basing on MatLab programming language as can been seen in Figure 4.13. This interface can perform instruments control, excitation generation, scanning setting, probe control, measurement signal acquisition, result processing and presentation. The signal generation 33250A and oscilloscope 54615B are linked to computer via one GPIB (General Purpose Interface Bus) connector, while the X-Y Scanner is connected via one serial communication port RS232. To drive the GPIB and RS232 connecters, it needs to install Instrument Control and Signal Processing toolboxes in MatLab. Before the measurement begins, the communication between instruments and computer needs to be set up. Then the MatLab can take the instructions from user and then send them to the connector from which the instruments get the controlling signal. At the same time, the MatLab can also ask the connector to receive the signal from instruments. To develop this interface, work including code programming of 2800 lines and GUI design has been involved.

It is can be observed from above figure that the interface has been divided into three main parts including Signal Generator 33250A, Oscilloscope 54615B, and X-Y Scanner. Each part is responsible for the performance of corresponding instrument. Next, it will be introduced in details.

Signal Generator 33250A

On the top of the block, the ‘GPIB Index’ and ‘GPIB Address’ pop-up menus are used to configure the instrument address on the computer, i.e. where or on which port the instrument is connected with the computer. The next sub-block contains the parameters of the excitation signal which can be set according to the inspection requirement and the ‘Output’ button by which the command is sent to 33250A to generate the signal with desired specification. The ‘Connect’ and ‘Disconnect’ buttons are used to setup and break the communication between 33250 and computer. The ‘Status’ bar indicates the instrument’s current situation which could be connected, busy or connected.

Oscilloscope 54615B

The address configuration, connection setup, and status indication are working as same as ones in 3320A part. In the ‘Setting’ sub-block, the parameters can be set for the measurement and presentation of the received signal. When press the ‘Plot’ button, the received signal will be plotted on the plotting area of ‘Waveform’ sub-block according to the setup, and the value of the signal’s properties including peak to peak voltage, average voltage, frequency, and period are presented on the four boxes on the bottom of the sub block. If the ‘Autoscale’ is chosen, the parameters will be setup to fit wave of two periods onto the plotting area. After the measurement, there have two options available to save the results. One of them is ‘Save as Figure’ button which means to store the waveform as a figure format file in the computer; another is ‘Save as Text’ button which is to save the measurement data of every point on the figure in a word format file. All of the result could be sent back to Matlab programming environment for analysis.

X-Y Scanner

It is as same as the previous parts that it needs to set up the connection between the scanner and computer firstly. On the left of the block is a column of instruction for both x-y carriage and z carriage. ‘All go home’ is a command to make all both carriages travel back to the default position, normally the starting point of each axis. ‘All move to’ can tell the carriages to go to the desired position according the configuration in individual axis sub-block, while ‘All move by distance’ will move the carriage by a specific distance which is also set in the sub-blocks. The right three sub-blocks are configuration for individual axis. ‘X Axis’ and ‘Y Axis’ are for x-y carriage which is travelling along x and y axis, while ‘Z Axis’ for z carriage which is only travelling along z axis. The speed box is used to decide how fast the carriage moves along the axis. The maximum or 100 percent speed is 10mm/s along x axis and 15mm/s for y, z axis. The ‘Move to’ and ‘Distance’ instructs carriage where and how much to move along the corresponding axis. They can be set by millimetre or a changeable step which can be set in Matlab. ‘Go Home’ and ‘Go’ are commands to start travelling along relevant axis. Not only does the scanner has a status bar showing the condition of the whole equipment on the bottom of the block, there also has individual status bar for every single axis which can be found on the foot of the each sub-block.

This comprehensive measurement system is able to bring many benefits to the operations and results as discussed in above sections. And it is also easy and flexible to add more functions or controls on instruments into the interface as required.

4.3.3 CFRP Samples

CFRP samples with different property and impact damage are inspected in the whole project. Here, they are numbered and listed in following table and figures. Sample No.1 is perfect orthogonal CRRP piece with straight fibre, while No.2 and No.3 are made by the AirBus which contains woven carbon fibre. No.4 is a very thin sheet of CFRP. It only contains one layer of straight carbon fibre, which was used to study the directionality behavior only.

CFRP Sample No.	Description	Size (mm)
1	Flat plate with straight fibre in two direction and without impact	152 by 110 by 2.5
2	6 square pieces with different impact damages (From AirBus)	50 by 50 by10(Approx.)
3	Flat plate with 7 dents of different impact energy (From AirBus)	250 by 152 by 2.5
4	Thin sheet with straight fibre in one direction and without impact	200 by 100 by 0.2

Table 4.2 Description of CFRP samples

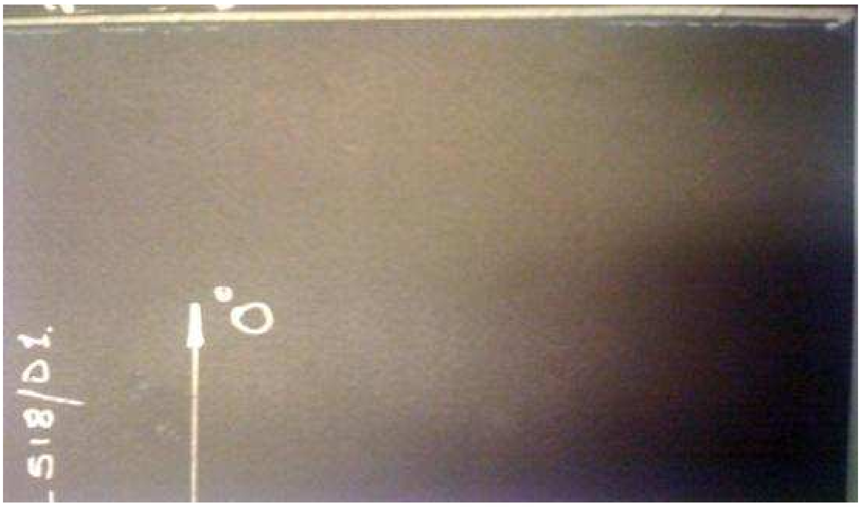

Figure 4.14 CFRP sample No.1

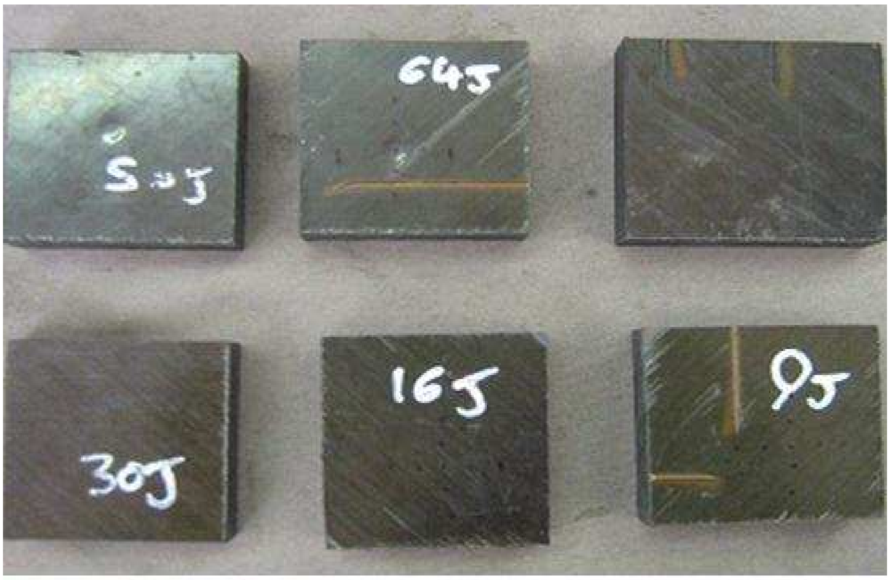

Figure 4.15 CFRP sample No.2

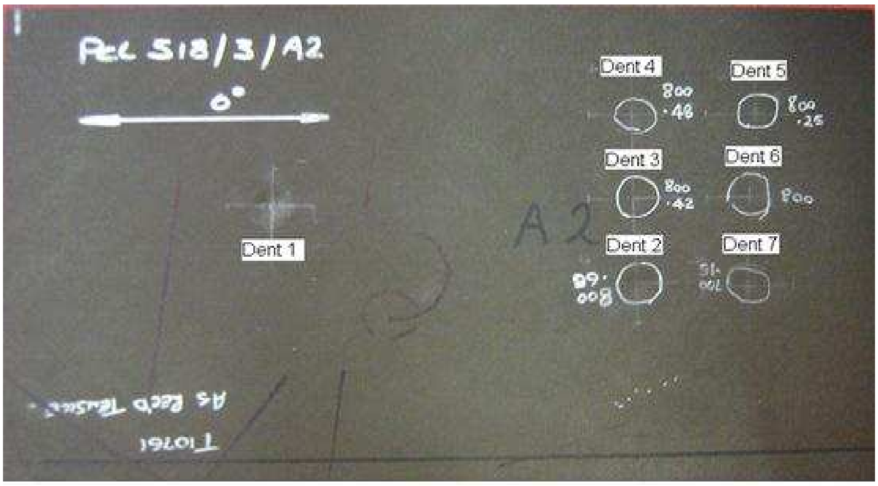

(a) Front side

(b) Back side

Figure 4.16 CFRP sample No.3

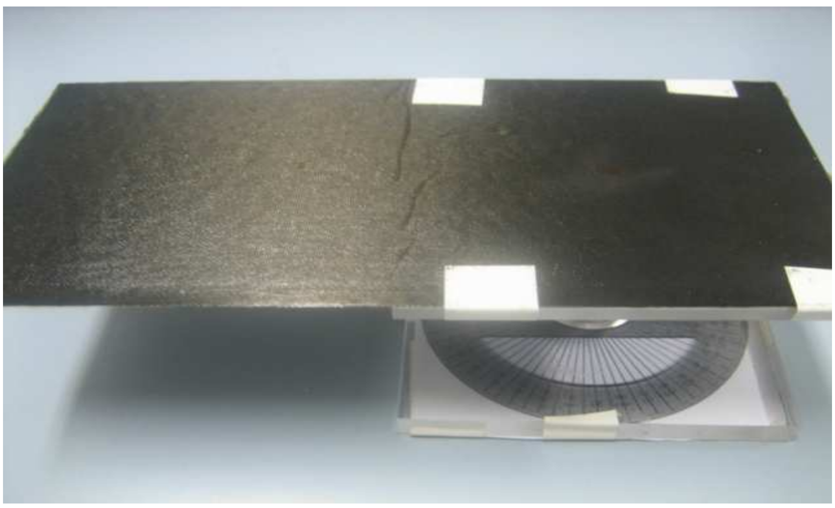

Figure 4.17 CFRP sample No.4

4.3.4 Conductivity and Damage Testing

4.3.4.1 Probe Specification

The conductivity of the composite is determined by the conductivity of individual fibres, the stacking sequence and the fibre volume fraction by the rule of mixture [93]. It has also been shown by experiments that the resistance of CFRP increases with the appearance of internal damage, such as fiber breakage and delamination [93]. These indicate that conductivity is closely related to other composite properties. To measure the bulk equivalent conductivity, a circular air-cored coil with specification in Table 4.3 was used above the composite to scan the inspected area, as depicted in Figure 4.18.

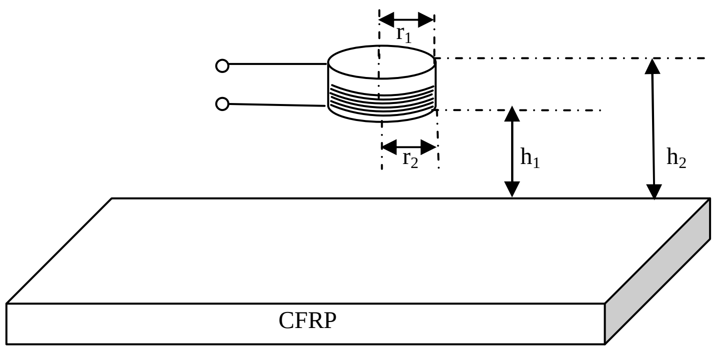

Figure 4.18 Conductivity testing probe

The sample No.1 is used for the experiments in which the system and probe configuration are optimized.

4.3.4.2 Impact Damage Inspection on Sample No.2

The impact damage results in fibre breaking, matrix cracks and delamination. In these inhomogeneities, only fibre breaking which interrupts the conduction current and delamination which influences the eddy signal by reducing the interlayer connection.

Increase in impact energy results in decreased eddy signal due to deformation in the structure. Delamination effectively reduces the electromagnetic depth of material which means there is an increase in eddy signal if compared with that sample which has not been damaged (delaminated/cracks) but has been impacted with same energy.

This experiment is carried out to inspect sample No.2 (the six thick square CFRP samples with different impact damage). In Figure 4.15, the combination of number and letter on the samples (9J, 16J, 30J, 53J, 64J) indicates how much impact energy is used to damage the samples in Joule. The only sample without number and letter is the perfect one without any damage. So, in Figure 4.19 to Figure 4.22 which show the measurement results, '0J' represents the perfect sample while '9J' represents the sample which gets impact damage of 9 Joule, and so on. The probe used is shown in the table 4.3.

Probe No.	Type	Turns	Inner diameter	Outer diameter
1	Circular air-cored	15	25mm	25.1mm

Table 4.3 Specification of probe No.1

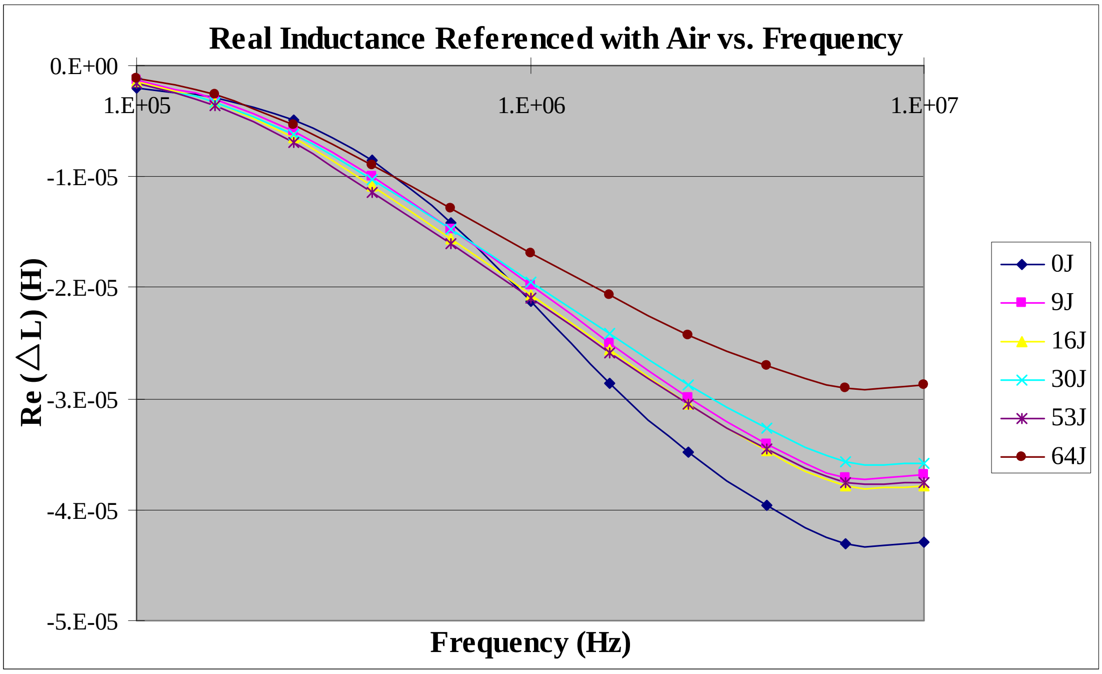

(a) Real part

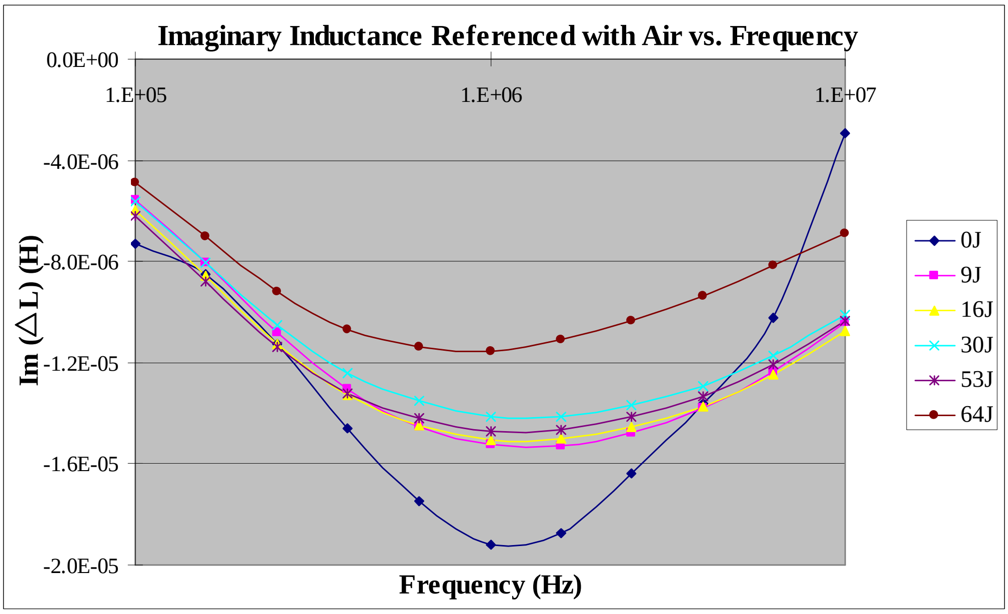

(b) Imaginary part

Figure 4.19 Normalized inductance referenced with air vs. frequency (experiments on Sample No.2)

* Measurement results are subject to machine error of ±5% from Solartron 1260.

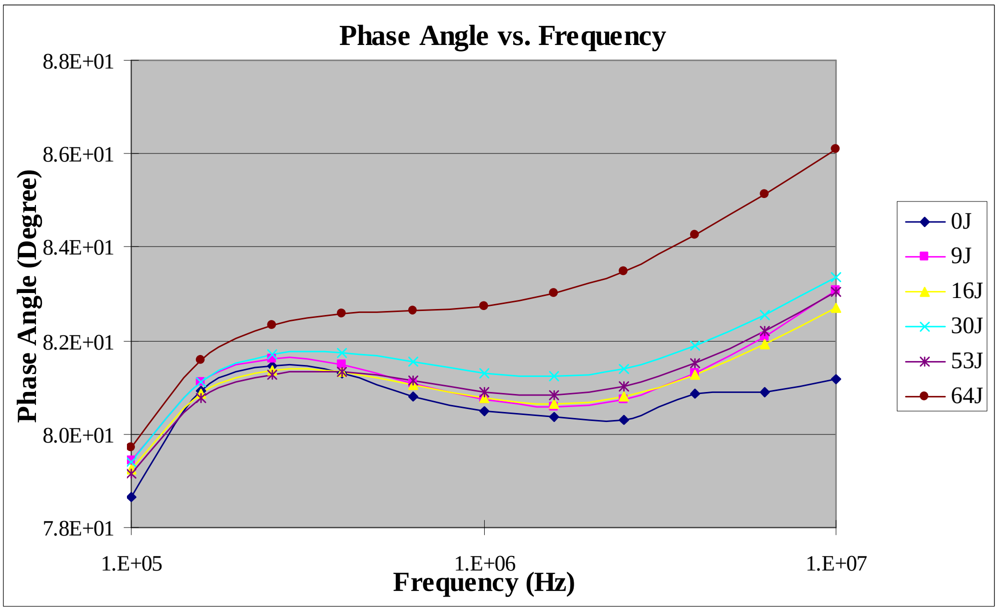

Figure 4.20 Phase angle vs. frequency (experiments on Sample No.2)

* Measurement results are subject to machine error of ±5% from Solartron 1260.

As it can be observed from Figure 4.19(a) and (b), the curve corresponding to 53 joule impact lies in between 16 and 30 joule impact curves, which indicates de-lamination in this sample. Phase angel in Figure 4.20 is also supporting the conclusion. Much better information is obtained when referenced with perfect sample data (Figure 4.21).

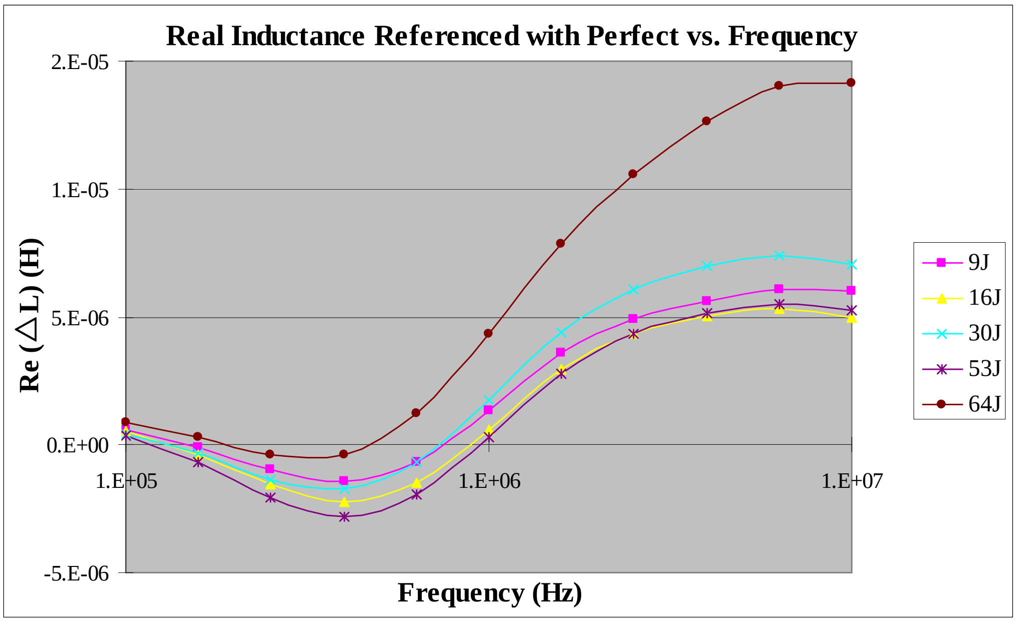

(a) Real part

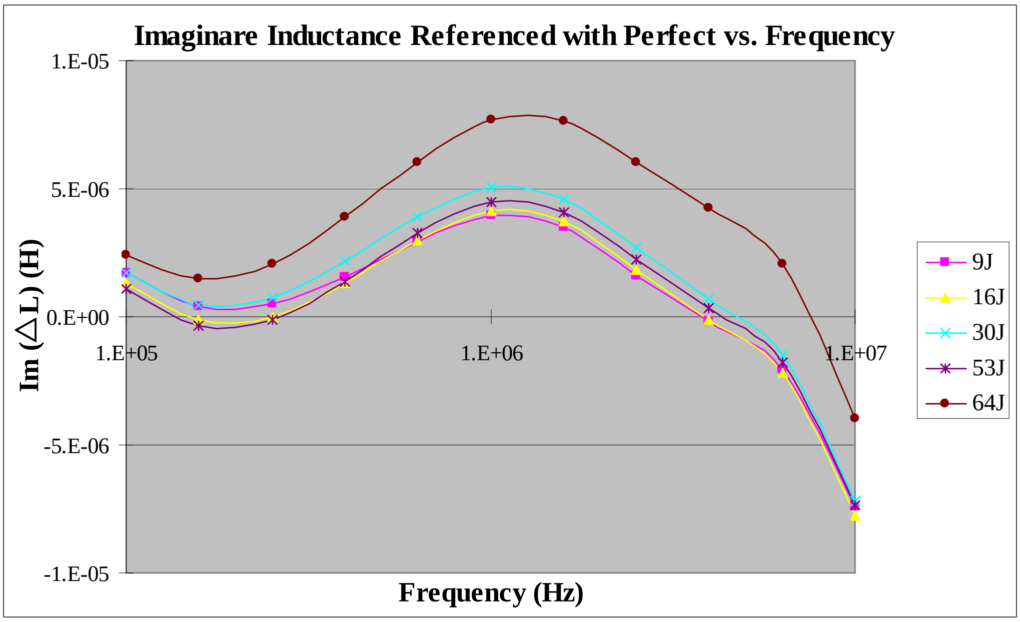

(b) Imaginary part

Figure 4.21 Normalized inductance referenced with prefect vs. frequency (experiments on Sample No.2)

* Measurement results are subject to machine error of ±5% from Solartron 1260.

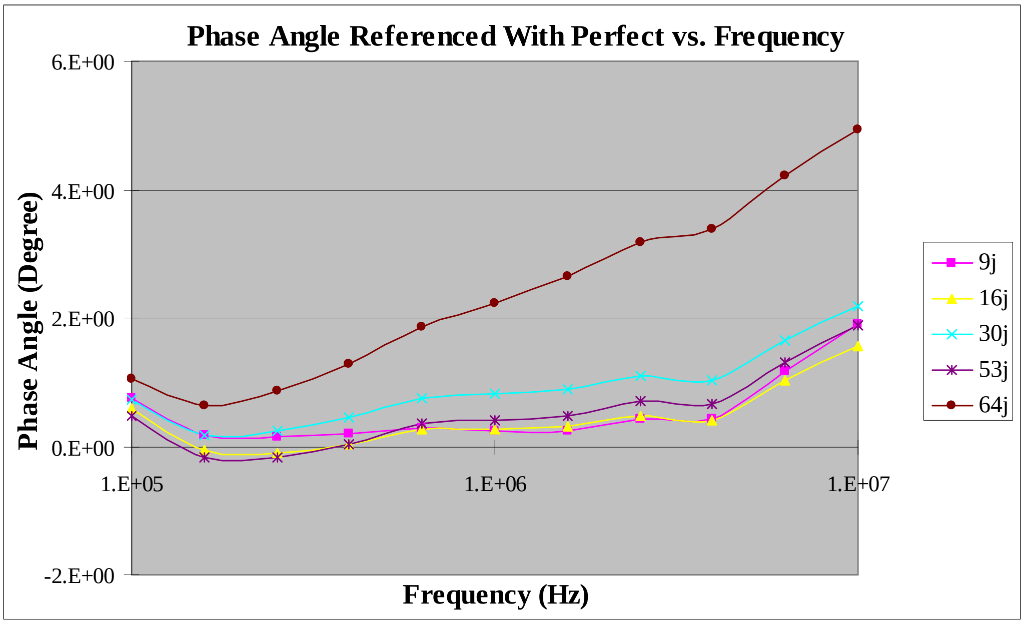

(a) Phase angle referenced with perfect sample

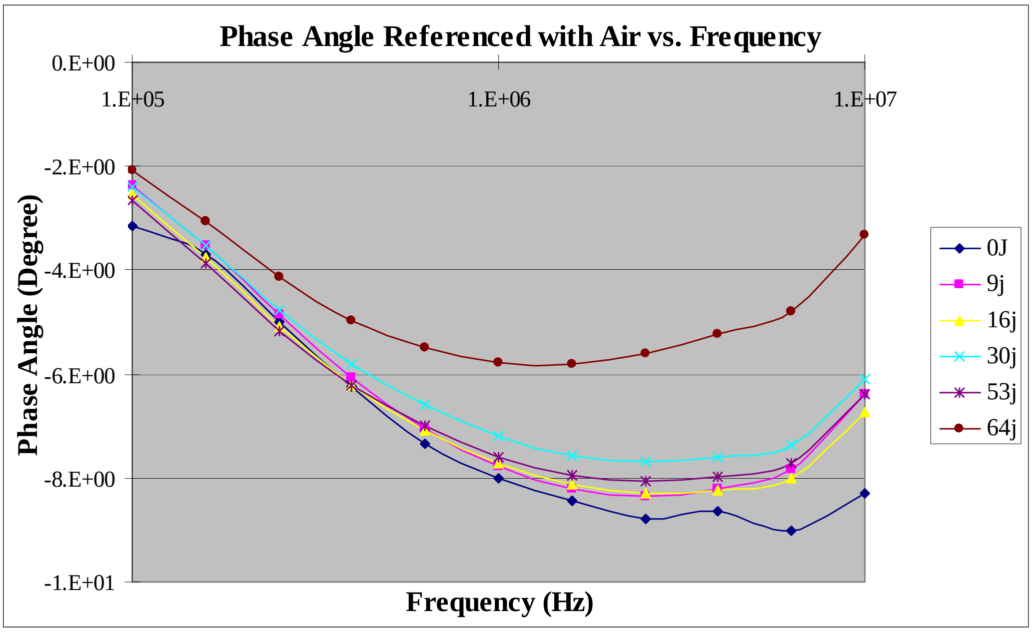

(b) Phase angle referenced with air

Figure 4.22 Normalized phase angle referenced with prefect and air vs. frequency (experiments on Sample No.2)

* Measurement results are subject to machine error of ±5% from Solartron 1260.

Figure 4.20 gives the coil's phase angle response against frequency while Figure 4.22

shows the normalized phase angle response referenced with air and perfect sample separately. It can be seen that the phase angel is shifted up when the sample gets bigger impact energy (more damaged), because the conductive part of coil's impedance is affected more by impact while inductive part is more dependent on geometry of the sensor. By indicating the change of coil's conductance and inductance, the phase angle may contain information such as CFRP's stacking and delamination.

4.3.4.3 Damage Depth Inspection on Sample No.3

The aim of this experiment is to study the signals obtained at impact sites with different damage depth. This inspection is also using the circular probe which is detailed in Table 4.3. Table 4.4 shows the depth of each dent on sample No.3 which is produced by impact damage of different energy. As previous section, the number 70050 indicates that the dent area suffers impact damage with 7.0050 Joule, thus the dent area is named as 70050 in the experiences and figures.

Dent No.	**Dent Depth (mm)**
70050	0.25
800	0.265
80025	0.3075
80048	0.4425
80060	0.665

Table 4.4 Dent size of sample No.3

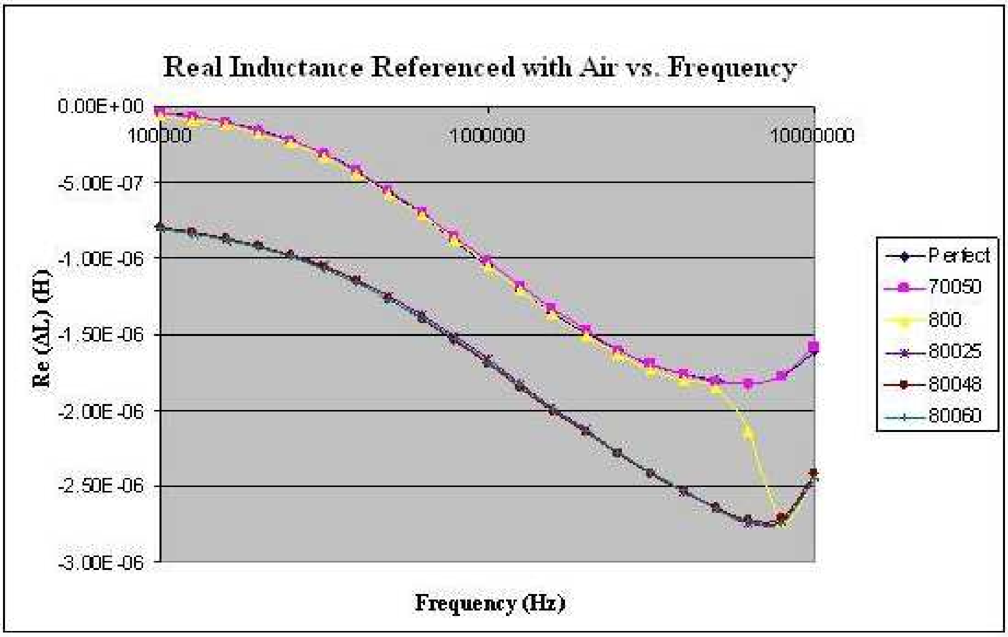

(a) Real part

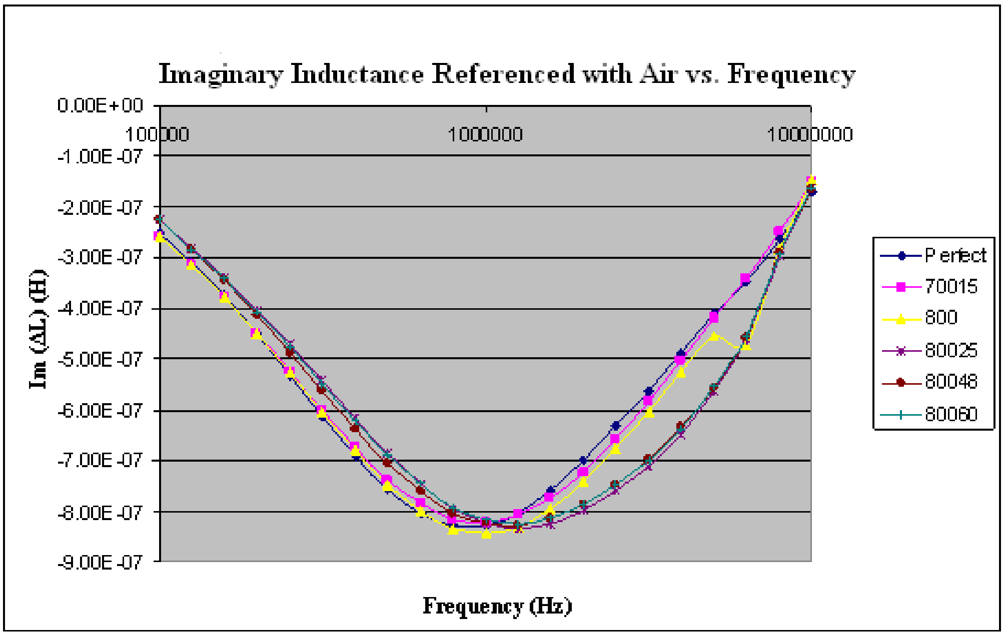

(b) Imaginary part

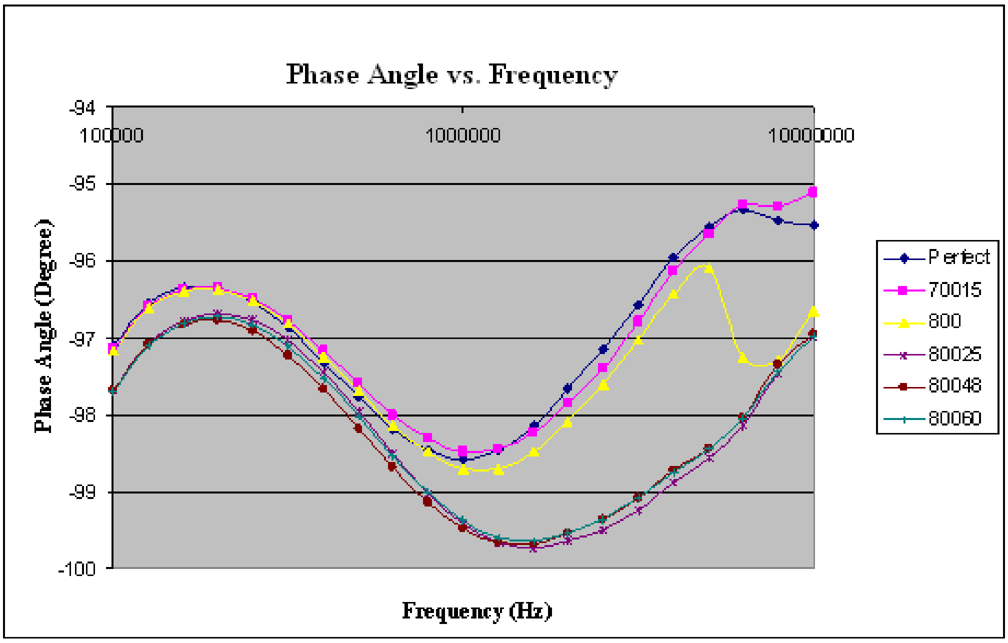

(c) Phase angle

Figure 4.23 Normalized inductance vs. frequency (experiments on Sample No.3)

* Measurement results are subject to machine error of ±5% from Solartron 1260.

From Figure 4.23, it is believed that the real and imaginary parts and the phase signature will relate to the size and features of the damages. We can see that increase in the impact energy results in the change in eddy current signal because of the inhomogeneities in CFRP structures. The order in which the signals from the damages are arranged contains the information about the damage magnitude as the smaller damage leads to the upper curve and vice versa. Figure 4.23(b) also gives information of the lift-off, as the bottom of the curves shift left or right as the damage varies. The way how to undo the effect of lift-off will be discussed in chapter 6.

4.3.5 Direction Characterization

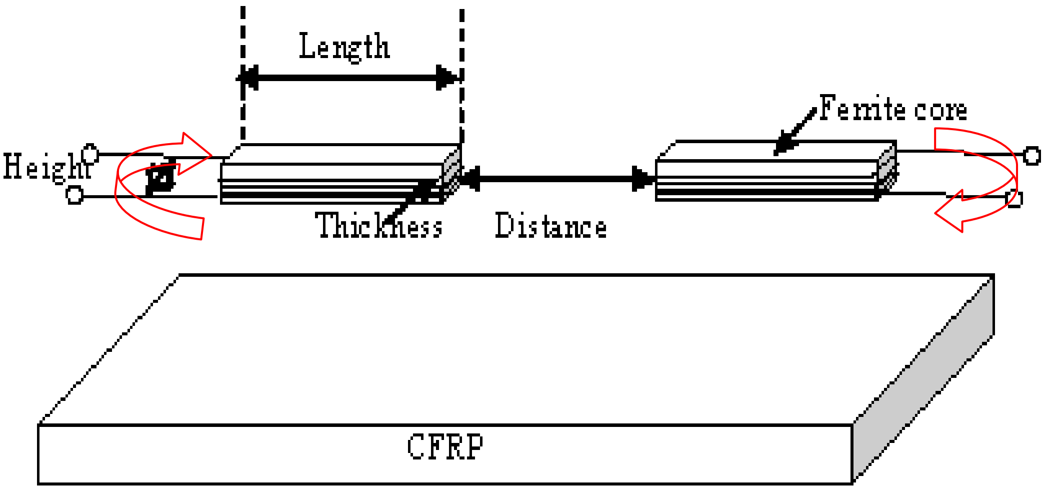

Figure 4.24 Fibre direction characterization with ferrite-cored pair probe

The anisotropy in conductivity, in particular of unidirectional composites, suggests that eddy current methods are ideally suitable to inspect the orientation of the fibres. Rotary eddy currents probes can be used to detect local fibres direction, shown in Figure 4.24. The inspected sample is No.4 which is a thin sheet with one fibre layer. The probe is a ferrite-cored pair of rectangular coils with same dimensions and turns (Table 4.5). The coils are glued together to a base and used as transmitter and receiver pair. The maximum conductivity can be observed along the fibre direction while the minimum conductivity occurring perpendicular to fibre direction. The experiments are performed by rotating the eddy-current probe at a required resolution (here, at 5 degrees per time) from 0 degree to 360 degree, where 0, 180, 360 degree indicate the direction following carbon fibre and 90, 270 degree indicate the direction perpendicular to fibre. It is supposed that the conductivity following the fibre direction is much higher that that perpendicular to fibre direction. The paired eddy current coil with specific dimension shows high directionality in measurements.

Probe No.	Type	Turns	Height	Length	Thickness	Distance
2	Ferrite-cored pair	5	5mm	10mm	1mm	10mm

Table 4.5 Specification of probe No.2

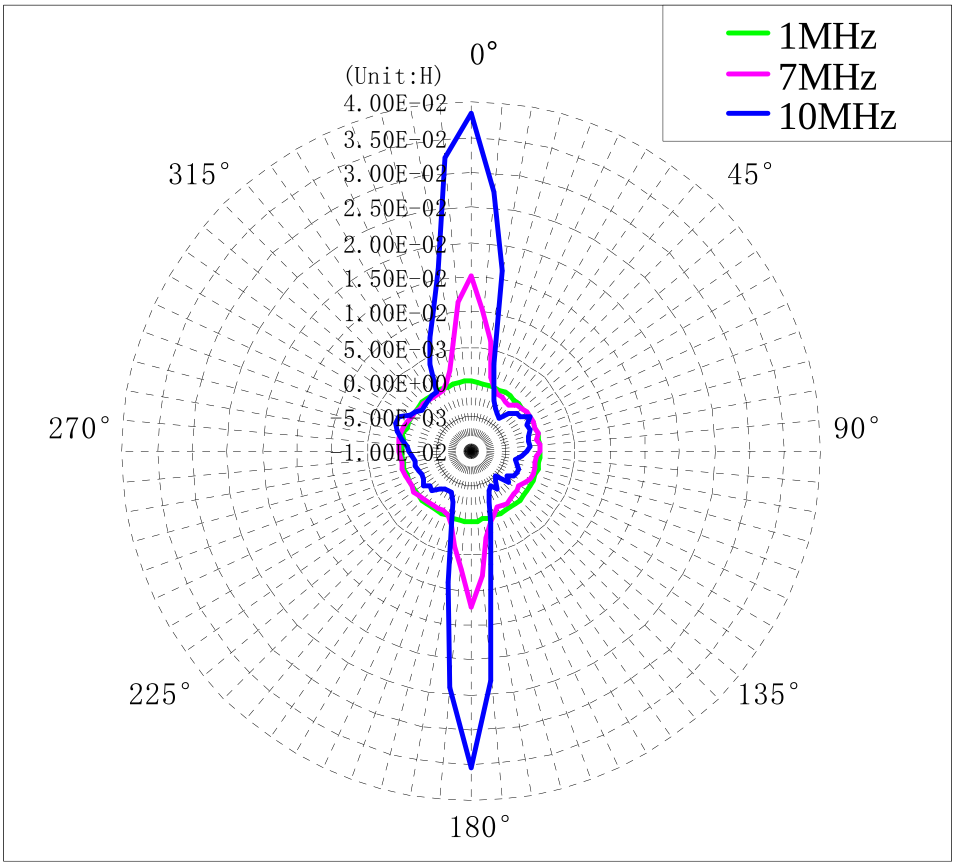

Figure 4.25 Experiment result of fibre direction characterization

* 1. Points on the curves have been removed for better clarity.

2. Measurement results are subject to machine error of ±5% from Solartron 1260.

The large lobes in the Figure 4.25 indicate the fibre direction and the small lobes are caused by the shape of the coils. The imbalance occurring in the figure may result from fibre contacts and electrical coupling between fibres and layers. From the result, it can also be seen that using higher frequency provides higher directionality, mainly due to that the eddy currents are distributed more over the sample surface and the capacitive reactance reduces as the frequency growing up. So, coils applying high frequency are more sensitive to this thin sheet and the high frequency curve has bigger peak value. However, the decision of the frequency is also dependent on the penetration depth and electrical coupling.

4.3.6 2D Eddy Current Scanning on CFRP

2D eddy current scanning has been performed on CFRP sample No.3 using the comprehensive eddy current measurement system. The results present the information about sample's surface condition and can suggest the optimal scanning frequency. The following sections are introducing the scanning results in detail.

4.3.6.1 Scanning on Whole Damaged Area

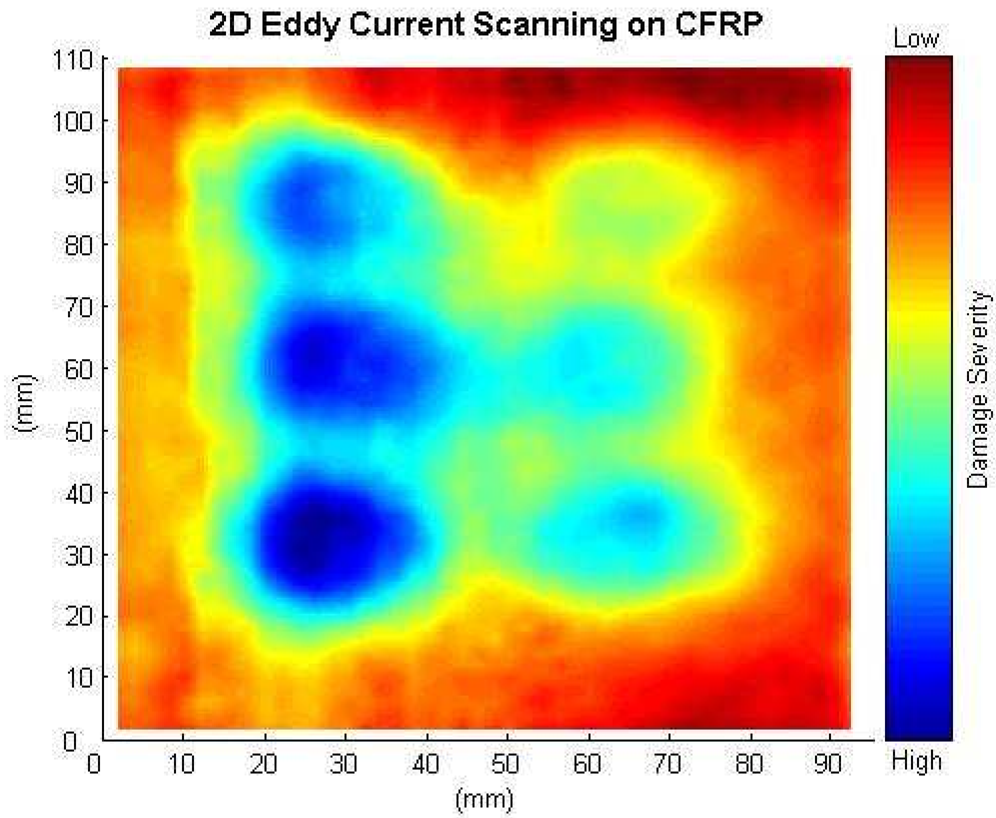

Figure 4.26 Eddy current scanning on whole damaged area of CFRP sample

* Measurement results are subject to machine error of ±5% from Solartron 1260.

Coil type	Coil former	Coil diameter	Coil turns	Sample	Scanning Resolution	Scanning Frequency	Scanning Area
Single ifferential	Air-cored round	10mm	15	No.3*	1.2 mm	1MHz	93×108 mm

* Details in section 4.3.3.

Table 4.6 Eddy current scanning configuration (whole area scanning)

This scanning is carried on to inspect the whole damaged area of CFRP sample. The scanning area is 93 by 108 mm. The scanning frequency is fixed at 1MHz and resolution is 1.2mm. The scanning result and configuration are shown in Figure 4.26 and Table 4.6. The figure can clearly inflect the surface condition of the inspected area where six damages with different severity can be observed. The mapping color indicates how much damage severity is, where the blue area represents the bigger damage and red area means smaller damage.

4.3.6.2 Multi-Frequency Scanning on Single Defect

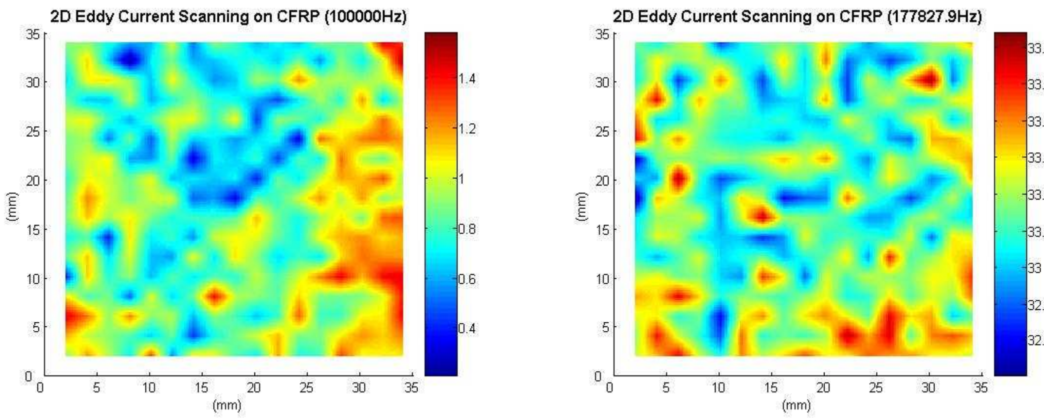

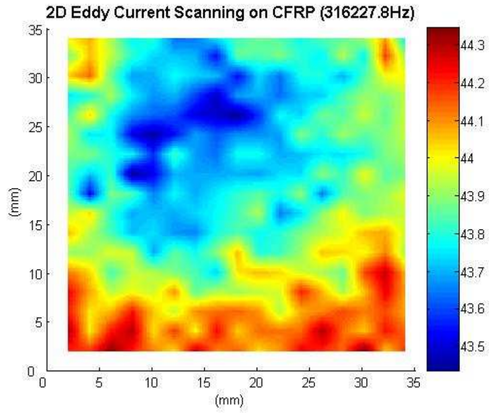
2D Eddy Current Scanning on CFRP (316227.8Hz)
(mm)
(mm)

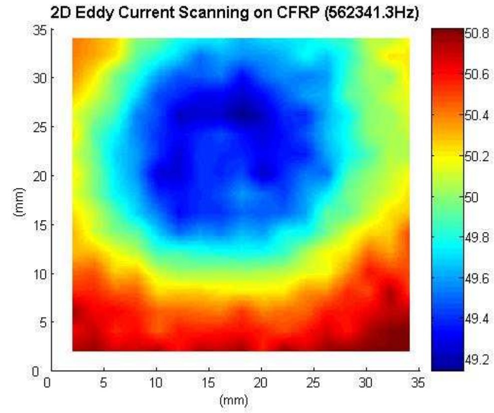
2D Eddy Current Scanning on CFRP (562341.3Hz)
(mm)
(mm)

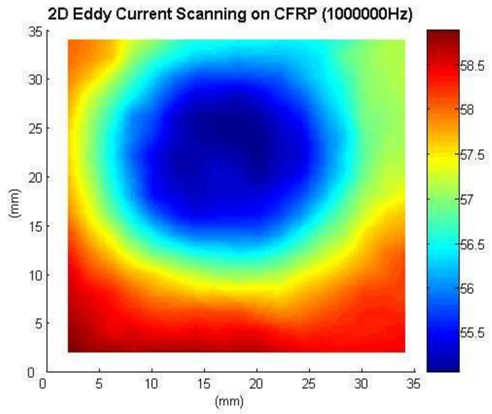
2D Eddy Current Scanning on CFRP (1000000Hz)
(mm)
(mm)

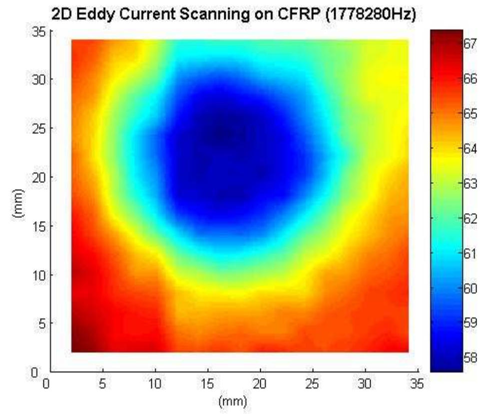
2D Eddy Current Scanning on CFRP (1778280Hz)
(mm)
(mm)

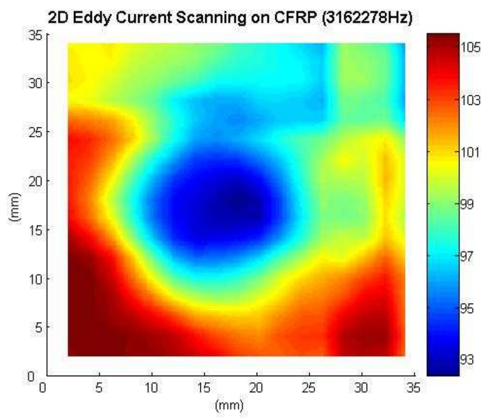
2D Eddy Current Scanning on CFRP (3162278Hz)
(mm)
(mm)

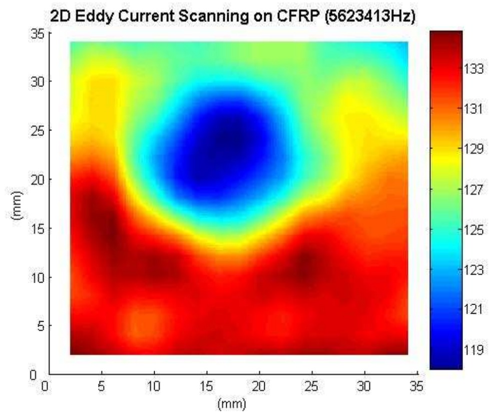
2D Eddy Current Scanning on CFRP (5623413Hz)
(mm)
(mm)

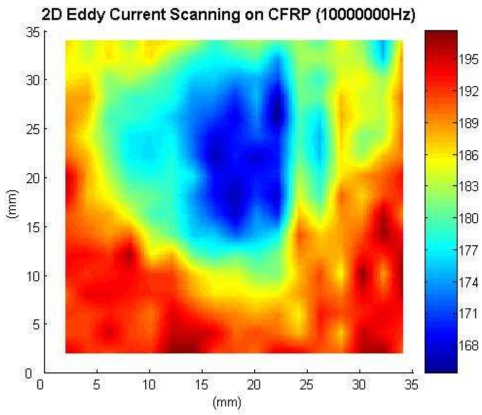

Figure 4.27 Multi-frequency eddy current scanning on single defect

(Colour bar indicates the normalized coil impedance change. Unit: Ω)

* Measurement results are subject to machine error of ±5% from Solartron 1260.

Coil type	Coil former	Coil diameter	Coil turns	Sample	Scanning Resolution	Scanning Frequency	Scanning Area
Single ifferential	Air-cored round	10mm	15	No.3*	1.2 mm	100k-10MHz	34×34 mm

* Details in section 4.3.3.

Table 4.7 Eddy current scanning configuration (Multi-frequency scanning)

Multi-frequency eddy current scanning has been performed on one single defect of the CFRP sample. The scanning result and configuration are shown in Figure 4.27 and Table 4.7. The scanning frequencies are set from 100kHz to 10MHz in 9 steps. From the results shown in Figure 4.27, it can be found that as increasing the frequency, the clearer and sharper result can be obtained. Also, the change of coil impedance increases with the frequency, which may present better measurement signal. However, when the frequency goes too high, the penetration depth of eddy current into the sample becomes smaller according to skin depth effect, thus makes the scanning result worse. By comparing the above images in Figure 4.27, it can be observed that the optimal scanning frequency for the inspected CFRP sample is 5623413Hz though it is not the highest frequency, because the corresponding image is clearest and most focused.

4.4 Conclusion

This chapter is discussing in details about the eddy current technology for the characterization of CFRP, some of which has been published in [93]. A practical and detailed solution for a circular air-cored coil above a conductive plate is based on Dodd and Deeds' formulas. This solution considers most of the measurement parameters in the calculation and offers a set of fundamental equations. Special probes are required to make use of the electrical anisotropy of this material. It is proved that rotary probes are capable to detect fibre orientation while circular air-cored coils are more suitable for the conductivity estimation. Both the specification of the probes such as shape, number of turns and dimension, and the work frequency can influence the measurement result and the testing accuracy. The basic measurement system to carry on eddy current testing consists of eddy current probe, impedance analyzer Solatron 1260 and computer plus devices used to fix and position probe and inspected sample. Four sets of CFRP samples are available for the measurement experiments, some of which are commercially used and other are produces for laboratory. They are being used in different experiments for specified purpose. Both Theoretical and experimental results can prove that eddy current method is a useful tool to characterise CFRP non-destructively.

However, the quality of the measurement results is very likely to be negatively influenced by temperature change, electromagnetic noise and instrument inherent instability. And in measurements, there have some possible causes which result in the reduction of the accuracy of eddy current testing results. So, a more advanced and comprehensive measurement system has been developed for more accuracy, stability, automation and flexibility. It consists of computer, function generator, oscilloscope, automation equipment, improvement circuits and eddy current probe. And a GUI interface for the whole measurement system has been developed basing on MatLab programming language and taking use of the Instrument Control and Signal

Processing toolboxes through which the measurement is carried out. Using this system, 2D scanning results have been obtained which can present sample's surface condition and defect information.

In sum, it is believed that eddy-current techniques, as a more feasible and efficient measurement method, are able to contribute to the development and maintenance of light weight CFRP composites.

Chapter 5. Modeling Techniques and Simulation

5.1 Introduction

The finite element method (FEM), amongst the various numerical methods, has emerged as a suitable technique for electrical design, performance evaluation, and device optimization in a range of applications. Over the last two decades, several variants of the finite element method have been developed and these have successfully been applied to rotating electric machines, transformers, permanent magnet motors, power generation and transmission equipment, and instrumentation application including non-destructive testing.

Maxwell 3D, developed by Ansoft, was the FEM software used in this project to solve Maxwell's differential equations for electromagnetic fields. In essence, the finite element method finds the solution to any engineering problem that can be described by a finite set of spatial partial derivative equations with appropriate boundary and initial conditions. It is used to solve problems for an extremely wide variety of static, steady state, and transient engineering applications from diverse markets such as automotive, aerospace, nuclear, biomedical, etc.

The finite element method has a solid theoretical foundation. It is based on mathematical theorems that guarantee an asymptotic increase of the accuracy of the field calculation towards the exact solution as the size of the finite elements used in the solution process decreases. For time domain solutions the spatial discretization of the problem must be refined in a manner coordinated with the time steps of the calculation according to estimated time constants of the solution (such as magnetic diffusion time constant).

Maxwell solves the electromagnetic field problems by solving Maxwell's equations in a finite region of space with appropriate boundary conditions with user-specified initial conditions in order to obtain a solution with guaranteed uniqueness. In order to obtain the set of algebraic equations to be solved, the geometry of the problem is discretized automatically into tetrahedral elements. All the model solids are meshed automatically by the mesher. The assembly of all tetrahedra is referred to as the finite element mesh of the model or simply the mesh. Inside each tetrahedron, the unknowns characteristic for the field being calculated are represented as polynomials of second order. Thus, in regions with rapid spatial field variation, the mesh density needs to be increased for good solution accuracy.

In the following sections, the modeling work carried on for the CFRP characterization system is described. The simulation experiments start from the convergence test to get the optimal configuration for the tetrahedral. Then, models have been developed for analytical solutions based on the Dodd and Deeds formulation for electrical conductive sample and then moves on to consider the application of FEM for CFRP models.

5.2 Interface Programming

The following Figure 5.1 shows the screen shot of the 3D modeler user interface, which is part of the Ansoft Maxwell 3D software. The user interface is working as an eddy current simulation for characterization of CFRP's fibre direction using a pair of ferrite-cored probes. The window looks quite like other common Engineering Design and Analysis (EDA) software with menus, tool bar, project window, simulation history window, and working space. Also, it can be linked with other tools as MatLab, Excel and Visual Basic which provide an open working environment.

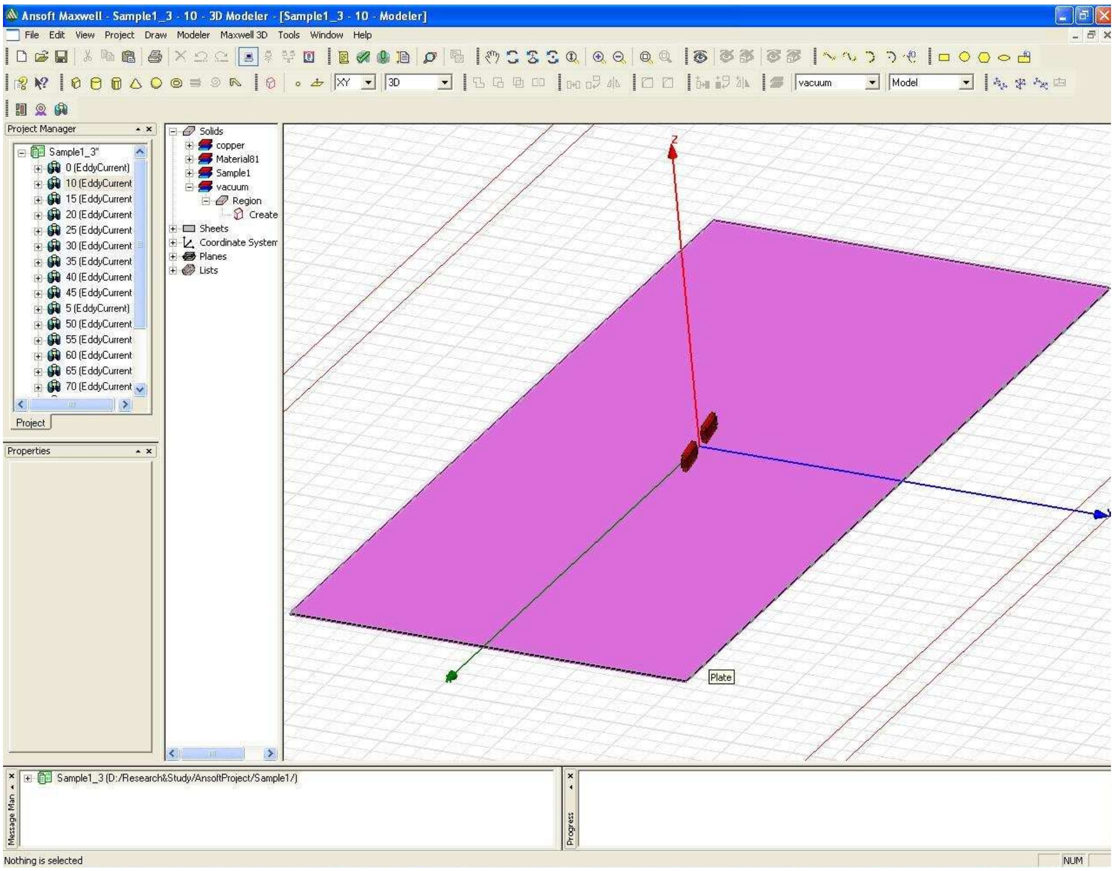

Figure 5.1 Screen shot of Ansoft Maxwell 3D

On the middle left is the 'Project Manager' which displays the open project's structure and is referred to as the project tree. The project tree is located in the 'Project Manager' window and contains details about all open Maxwell projects. The top node listed in the project tree is the project name. Expanding the project icon can view the project's Maxwell design information and material definitions. In the middle is the 'History Tree Window' which contains the description of each component and relevant operation. The right part is the '3D Modeler Window' indicating the geometry of current working model. The function of other parts such as toolbars, menus, and status bars are similar to those of other software.

Later on in this thesis, measurement data will be compared with the model results. This involved processing a large amount of data and measurement files. Consequently, it is important to build up efficient communication and link between the simulation software, the measurement instrument (e.g. Solartron 1260), and the computer. The communication between the measurement system and computer has been introduced in chapter 4. The similar link needs to be set up between simulation tool and computer as well.

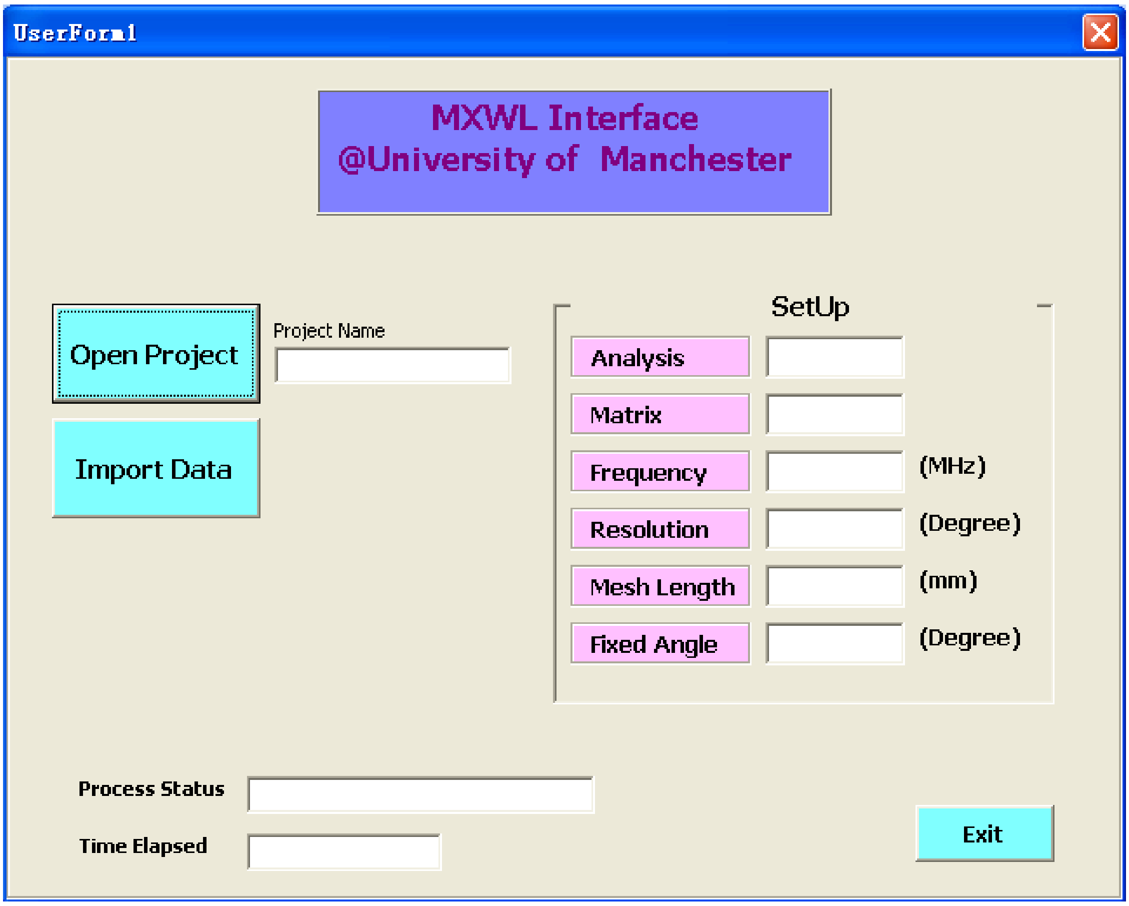

Figure 5.2 MXWL-PC interface

In chapter 4, an interface was introduced that has been developed in MatLab to integrate all the measurement parts and signal processing. Similarly, to achieve the communication between simulation software and computers, an interface based on Visual Basic Script (VBScript) program was developed. The reason to utilize VBScript is that Ansoft is only compatible with this programming language. Figure

5.2 shows the user interface panel used for communication between the simulation software (Ansoft MXML) and other computer programs. It can perform the tasks including simulation setup, control and data analysis etc. This panel is able to shorten the simulation time by setting up all the models at the same time, automatically outputting simulation data and graphing. By using VBScript code, this program can be run at any computer installed with Microsoft Excel.

5.3 Three Dimensional Modeling of CFRP Characterization

5.3.1 Convergence Test

In Maxwell 3D, the collection of tetrahedra is referred to as the finite element mesh or more simply, the mesh. A mesh can be generated automatically for each model prior to computing a field solution or be generated according to specific requirement. The accuracy of the solution depends on the size of each of the individual elements (tetrahedra). The Figure 5.3 gives detail about the mesh setup applied to the CFRP model. The figure 5.3 (a) shows a whole view of the mesh configuration, while figure 5.3 (b) focuses on the area below the probe which indicates that a finer mesh is allocated on the area with stronger changes in electromagnetic field, and the mesh becomes sparser away from the central area. Generally speaking, solutions based on meshes using thousands of elements are more accurate than solutions based on coarse meshes using relatively few elements. To obtain a precise description of the field, the system can size each tetrahedron so that it is small enough for the field to be adequately interpolated from the nodal values.

However, for meshes with a large number of elements, a significant amount of computing power and memory are required. Basically, there is a tradeoff between the size of the mesh and the desired level of accuracy. So, the first simulation prior to all the inspection experiment is a convergence test which is to find the optimal configuration for accuracy and mesh size.

The Figures 5.4 shows the results of the convergence test. The factors which are considered here include mesh size, number of tetrahedra, working memory, running time on computer (core 2 Duo CPU @ 2.99 and 3.00 GHz, 12 GB of RAM) , and simulation result. Comparing the response to the change of mesh size from 2 mm to 10 mm, it can be found that the best result occurs when the mesh size is set to 2 mm; however the benefit to simulation result by setting the mesh size to 2 mm is very slight (seen in Figure 5.4) with much more cost on the computing resource and running time. So, considering all these factors, the mesh size was chosen to be 3 mm.

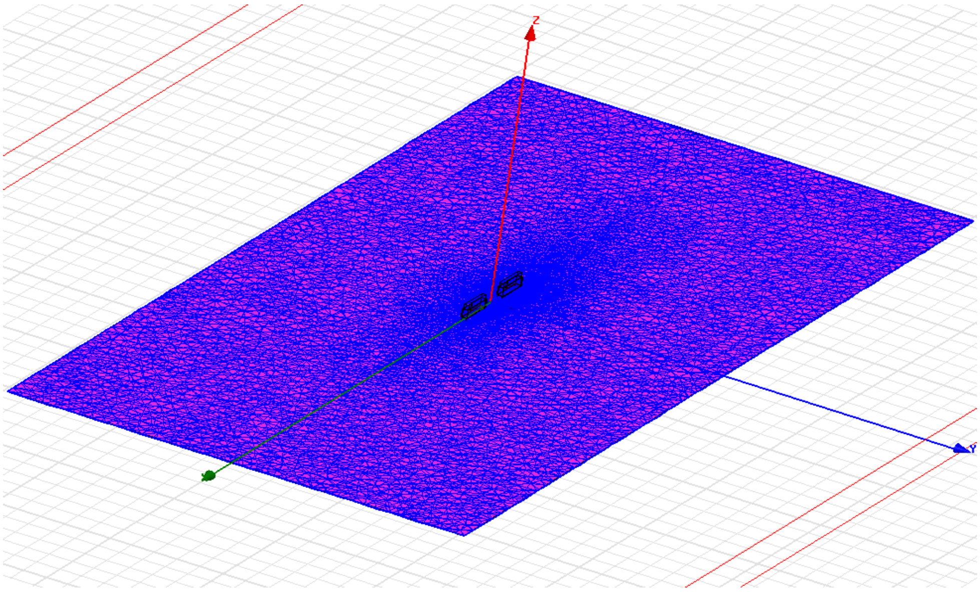

(a)

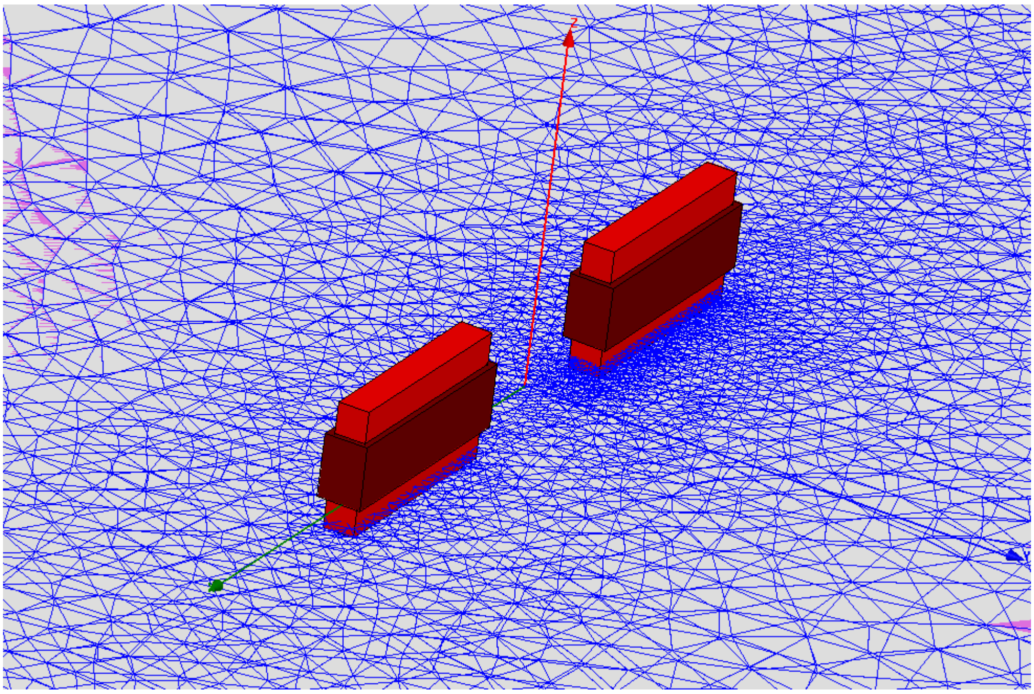

(b)

Figure 5.3 Mesh plotting on CFRP model: (a) Whole view of the mesh configuration; (b)Mesh on the centre area.

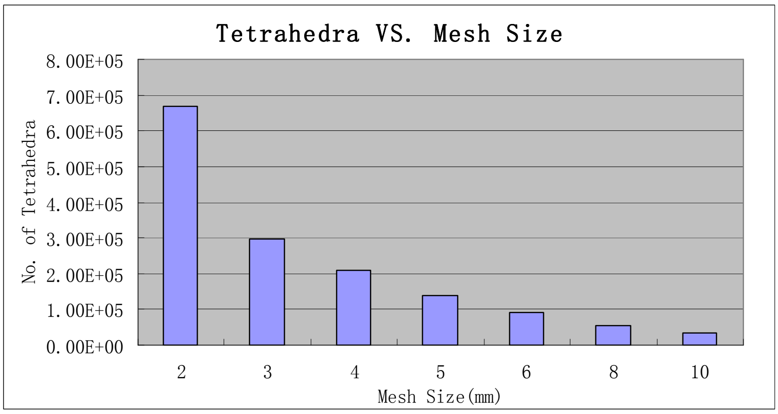

(a)

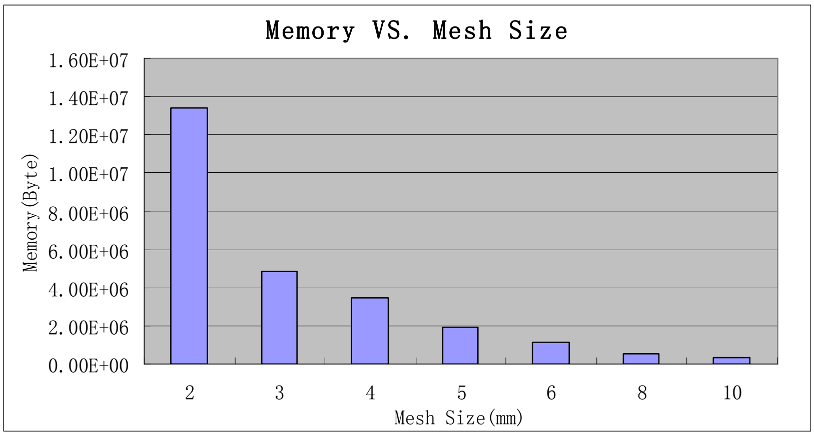

(b)

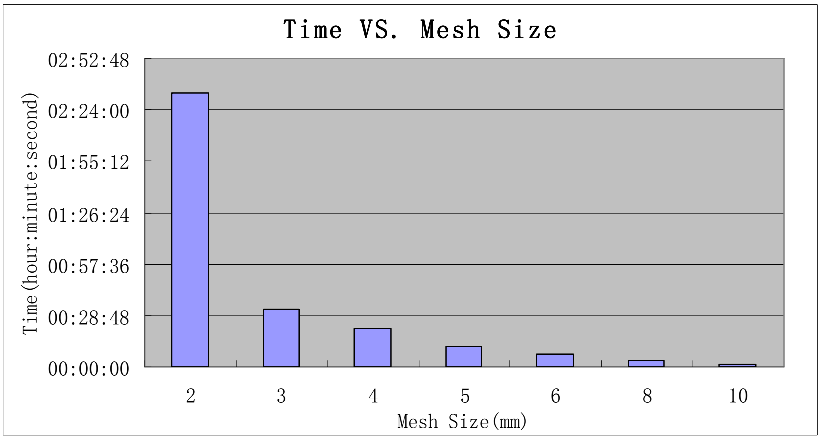

(c)

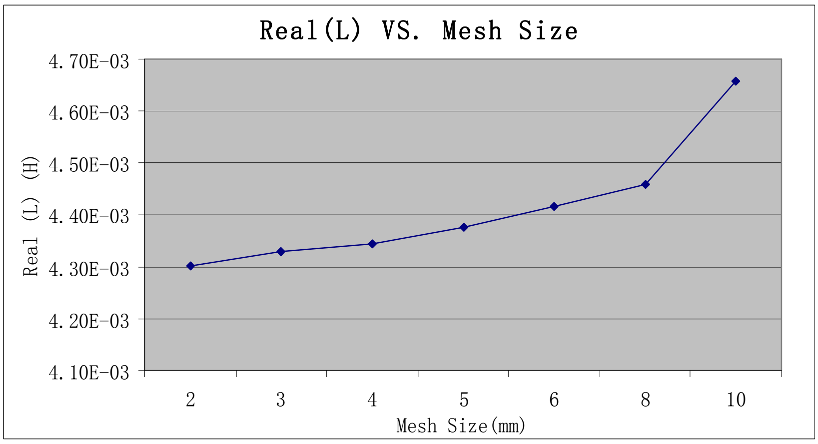

(d)

Figure 5.4 Convergence test results: (a) Tetrahedra number versus mesh size; (b) Working memory versus mesh size; (c) Running time versus mesh size; (d) Result change versus mesh size

5.3.2 Conductive Plate Modeling

The first stage of this section begins with the modeling of the single air-cored probe and the CFRP plate in Maxwell 3D. This work also supports the Deeds and Dodd’s solution for the conductive plate and to find how the parameters such as plate thickness and fibre conductivity affect the results. Following the first stage work, the modeling of the fibre directionality testing begins with single layer CFRP and multi-layers CFRP.

A simulation experiment is performed to validate the FEM models against the Dodd and Deeds analytic solution which is reported in chapter 4. Identical geometries and material properties were used in both case and initially the material is assumed to be isotropic. In this experiment, we design models of inspected samples with the same dimension as the AB (Air Bus) sample except for the thickness. The detailed parameters of the coil and samples are shown in Table 5.1. The lift-off is fixed at 0.1 mm.

Coil Type	Diameter	Height	Material	Excitation
Single air-cored	25 mm	13 mm	Copper	1 A

(a) Coil parameters

Sample No.	Type	Length	Width	Thickness	Conductivity
Sample_1	Entire plate without fibre	255 mm	153 mm	2.2 mm	50 kS/m
Sample_2		255 mm	153 mm	0.8 mm	50 kS/m
Sample_3		255 mm	153 mm	0.6 mm	50 kS/m
Sample_4		255 mm	153 mm	0.5 mm	50 kS/m

(b) Samples parameters

Table 5.1 Models parameters (conductive plate modeling)

The most important parameters for the simulation results and their values are presented in Table 5.2. Mesh operation and adaptive mesh setup have a great effect on the accuracy of the result, while the frequency sweep is determined by many factors.

Mesh operation	Method	Type	Maximum Number of Elements
	Inside plate	Length based	5000
Frequency sweep	**Scope**		**Count**
	100 kHz-10 MHz		19
Adaptive setup	**Maximum Number of passes**		**Percent error**
	10		1

Table 5.2 Analysis setup (conductive plate modeling)

The 3-dimensional model of the experiment is shown in Figure 5.5. Figure 5.6 gives the distribution of eddy currents on the samples. We can clearly see the loops of induced eddy currents on the surface of the plate which is expected. The magnitude of currents is decreasing from the core of the plate to the edges which can indicate the testing area of the specific coil.

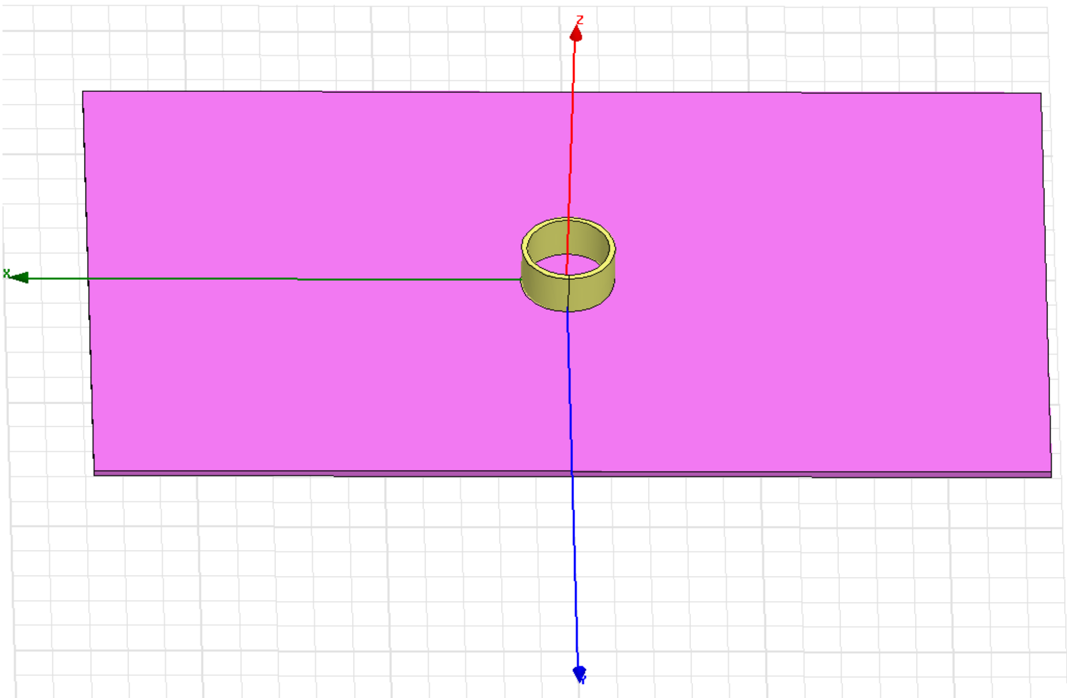

Figure 5.5 Model of conductive plate inspection in 3D Maxwell

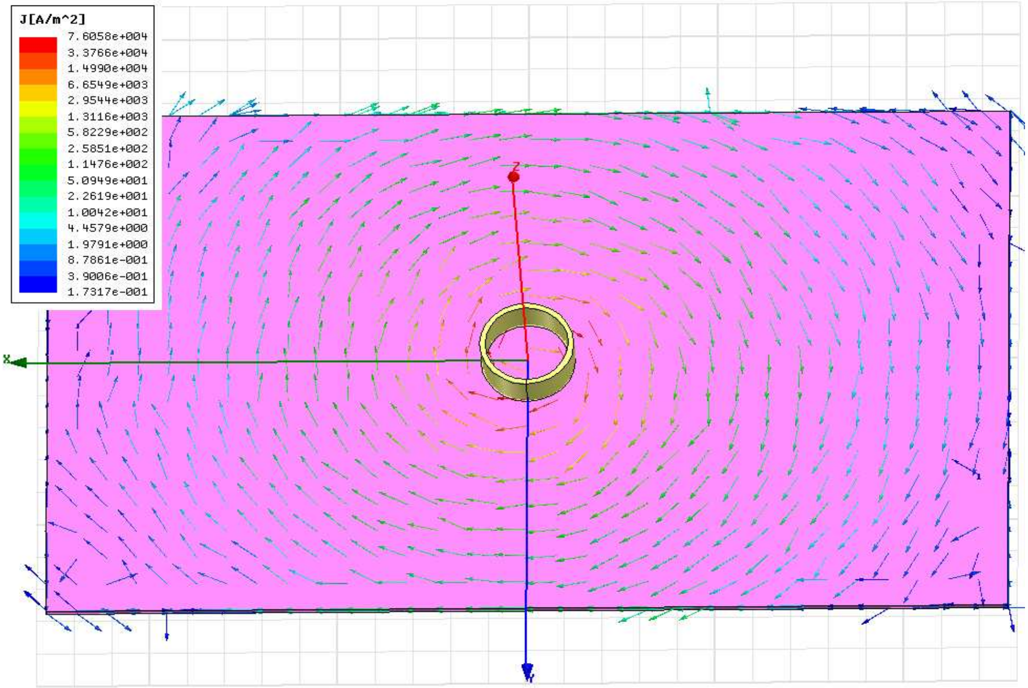

Figure 5.6 Eddy current distributions

The results in Figure 5.7 show a good agreement with Deeds and Dodd's analytic solution presented in chapter 4. What's more, we can see clearly how the change of thickness of the plate affects the inductance of the coil. By decreasing the thickness of the plate, there has a decrease on the conductivity of the plate, thus a higher excitation frequency is needed.

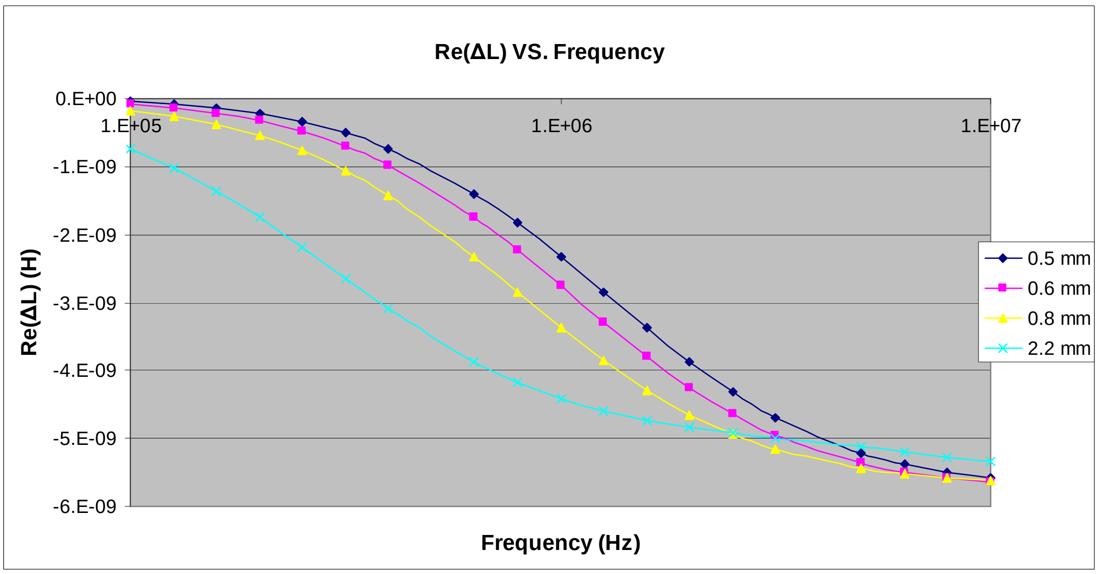

(a) Real part

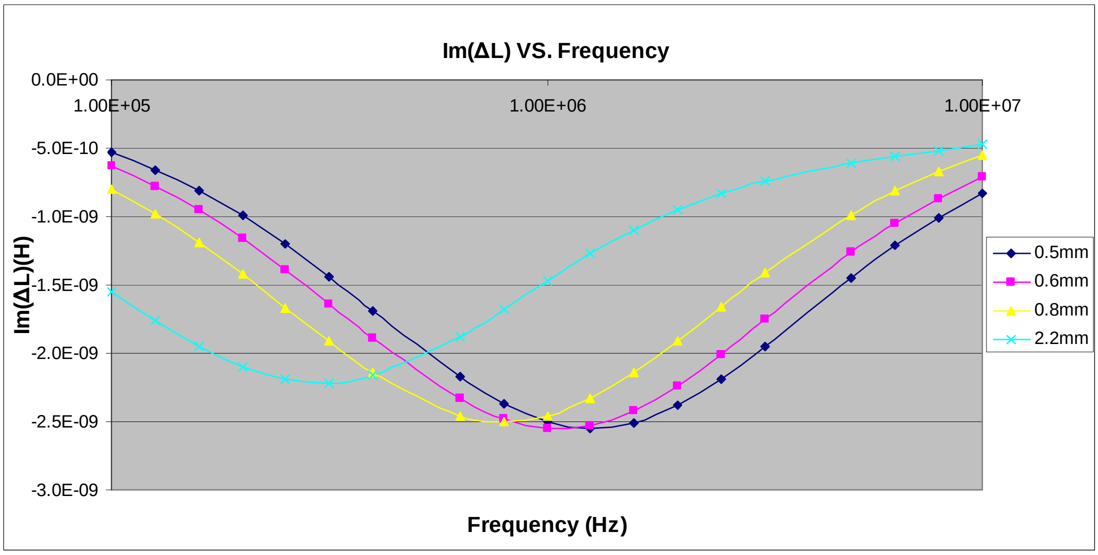

(b) Imaginary part

Figure 5.7 Calculated inductance of coil above plates with different thickness

FEM simulation results have a good agreement with previous Dodd and Deeds' experiment and prove to be a very strong and powerful tool for eddy current analysis.

5.3.3 CFRP Modeling

Based on the previous experiments of Dodd and Deeds' solution, CFRP modeling is built using 3D FEM simulation. Because CFRP is made of composite material which contains both conductors (carbon fibre) and insulators (plastic matrix), its electrical property is influenced by various factors such as fibre volume, layers, the distance between fibres etc. So, the analysis becomes more complicated. Here, CFRP models with various fibre conductivities are produced and simulated.

The first set of CFRP experiments is performed to inspect a single layer CFRP plate. Bulk conductivity is one of the most important parameter of the CFRP as it has direct relations to many other parameter and factors such as thickness, fibre volume, fibre contact, layers number, imperfect and so on. Here, various values of conductivity have been selected to simulate its effect on the inspection. As with the previous section, the test equipment configuration and analysis setup are listed in Table 5.3 and Table 5.4. As before, the lift-off is also fixed at 0.1 mm.

Coil type	Diameter	Height	Material	Excitation
Single air-cored	25 mm	13 mm	Copper	1 A

(a) Coil parameters

Type	Length	Width	Thickness	Material	Conductivity
Plate with fibres	50 mm	50 mm	2.2 mm	Epoxy	0

(b) Plate parameters

Fibre No.	Type	Length	Width	Thickness	Conductivity	Number	Distance	Volume
Fibre 1	4-sectioned Polyhedron	50 mm	3.3 mm	1.35 mm	1000 kS/m	15	0.03 mm	61%
Fibre 2		50 mm	3.3 mm	1.35 mm	700 kS/m	15	0.03 mm	61%
Fibre 3		50 mm	3.3 mm	1.35 mm	600 kS/m	15	0.03 mm	61%
Fibre 4		50 mm	3.3 mm	1.35 mm	50 kS/m	15	0.03 mm	61%

(c) Fibres parameters

Table 5.3 Models parameters (CFRP modeling)

Mesh operation	**Method**	**Type**	**Maximum Number of Elements**
	Inside fibres	Length based	2000
Frequency sweep	**Scope**		**Count**
	100 kHz-10 MHz		19
Adaptive setup	**Maximum Number of passes**		**Percent error**
	10		1

Table 5.4 Analysis setup (CFRP modeling)

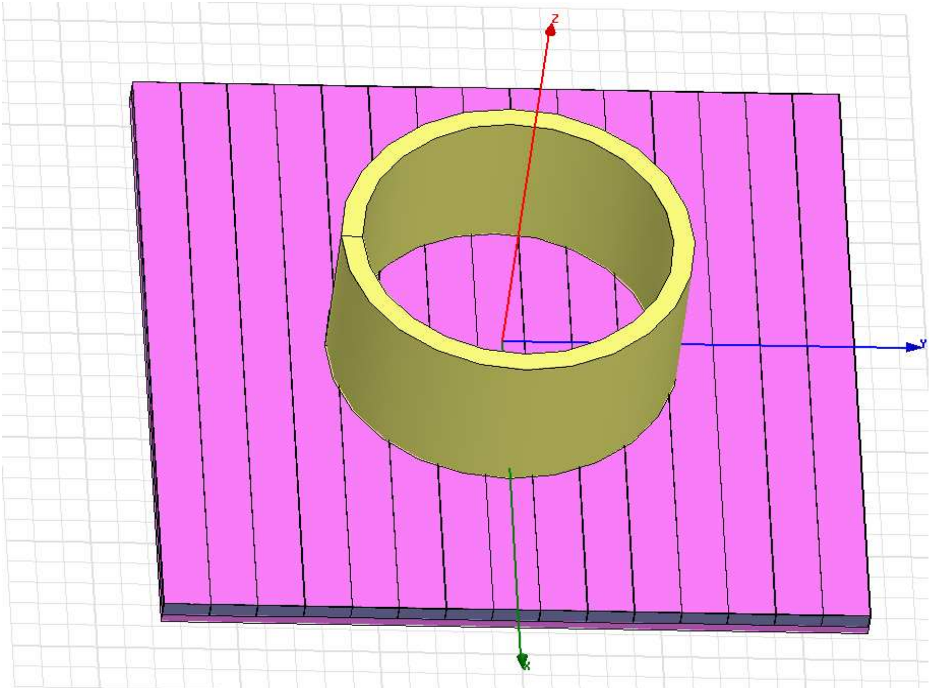

Figure 5.8 Model of CFRP plate inspection in 3D Maxwell

In the model (Figure 5.8), fibres are designed as non-connected bars ideally, which is also similar to reality as fibres in CFRP material are often in bundles. At the same time, it is not possible to model the exact fibre number, fibre shape and connection condition because of the limitation of computer resource and the information about the sample's inner structure. Figure 5.9 shows the eddy currents flowing on the CFRP model.

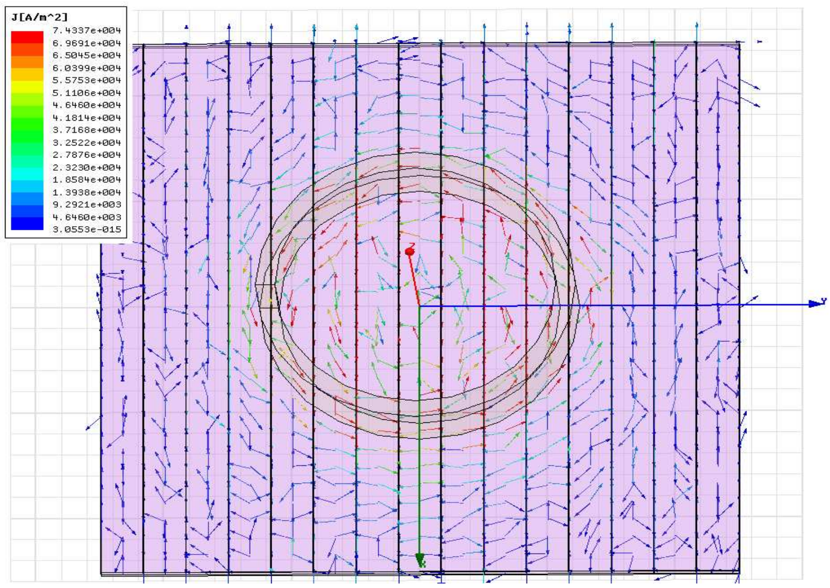

Figure 5.9 Eddy current distributions

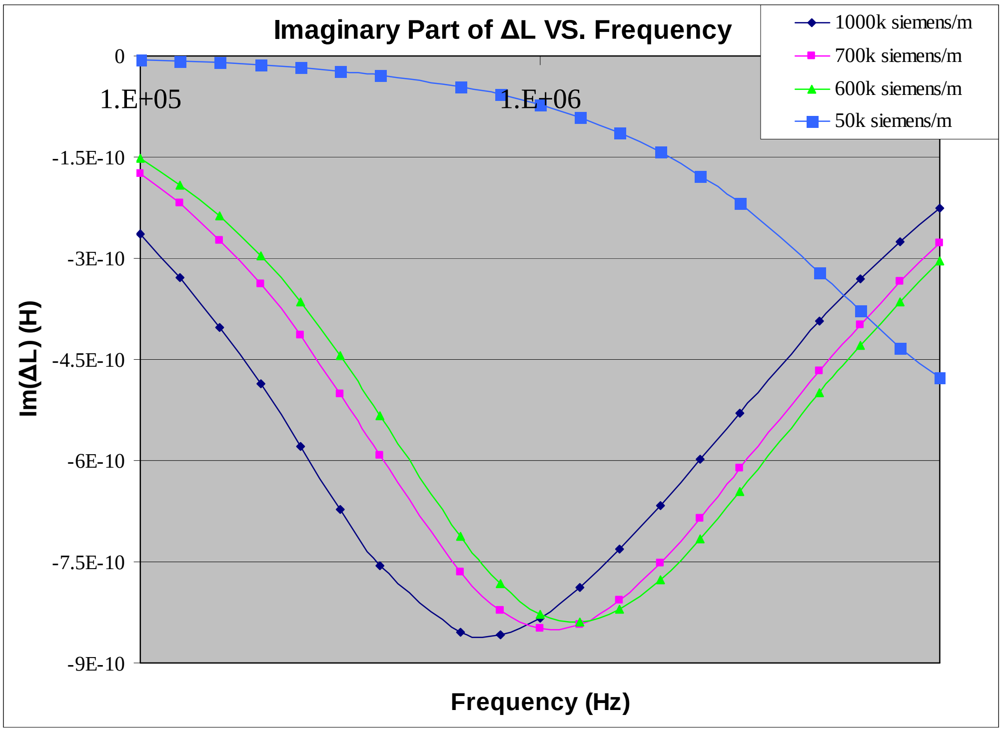

(a) Real part

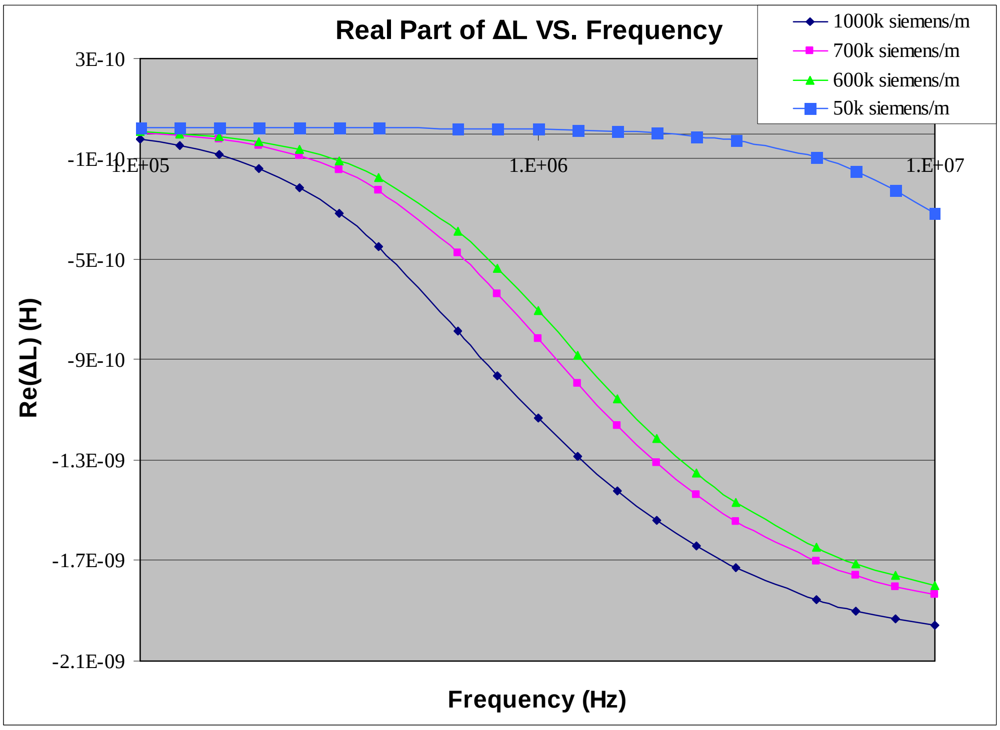

(b) Imaginary part

Figure 5.10 Simulation results of coil above plates with different fibre conductivity

The simulation results (seen in Figure 5.10) prove that the Deeds and Dodd solution can be applied for the CFRP thanks to the carbon fibre's conductivity, and show the possibility to test the material conductivity. However, the conductivity of the material without any damage is not only determined by the fibre conductivity but also by the distance between fibres, layers number, fibres volume and fibres contacting conditions, etc. So, next work will be carried on the multi-layers CFRP and damaged CFRP with fibre fracture for example.

5.3.4 Lift-off Simulation

The lift-off simulation is also performed to prove the effect of lift-off on the measurement result. In this simulation, the probe is moved from the 0.1 mm to 5 mm. In Figure 5.11, responding to the change of lift-off, the magnitude of the simulation result decreases with increasing the lift-off and the curve shifts toward left at the same time. This does also agree with the measurement result. To study the lift-off effect, it is easier in simulation to setup lift-off and get an exact distance between probe and inspected sample.

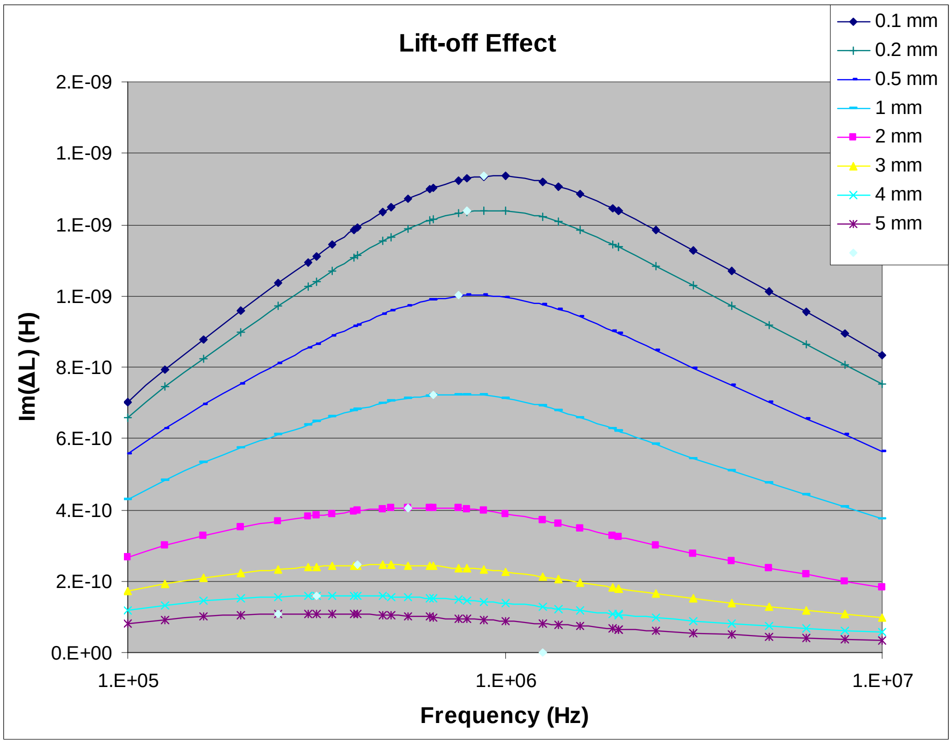

Figure 5.11 Simulation result of lift-off effect

5.3.5 Direction Characterization

Models have been made to simulate the fibre direction characterization. The probe is a pair of regular ferrite-cored coils, while the CFRP modes include one-layer plate and two-layer plate samples. The probe is fixed above the sample with certain lift-off and rotates around the centre from 0 degree to 360 degree in 5 degree steps, which is similar to the measurement process. The detailed simulation setup is shown in the following tables.

Type	**Diameter**	**Height**	**Material**	**Excitation**
Ferrite Pair	25 mm	13 mm	Copper	1 A

(a) Probe parameters

Sample	**Type**	**Length**	**Width**	**Thickness**	**Conductivity**	**Freqency**
No.1	Unidirectional	255 mm	153 mm	2.2mm	50 kS/m	10 MHz
No.2	Unidirectional	255 mm	153 mm	0.8mm	50 kS/m	10 MHz
No.3	Unidirectional	255 mm	153 mm	0.6mm	50 kS/m	10 MHz

(b) Parameters for samples of different thickness

Sample	**Type**	**Length**	**Width**	**Thickness**	**Conductivity**	**Frequecy**
No.1	Unidirectional	255 mm	153 mm	2.2 mm	50 kS/m	5,7,10MHz

(c) Parameters for samples of different frequencies

Sample	**Type**	**Length**	**Width**	**Thickness**	**Conductivity**	**Frequecy**
No.1	Two-layers(0,90)	255 mm	15 mm	2.2 mm	50 Ks/m	10 MHz

(d) Parameters for samples of two layers

Table 5.5 Models parameters (Direction characterization)

<table>
<tr><td rowspan="2">Mesh operation</td><td>Method</td><td>Type</td><td>Maximum Length</td></tr>
<tr><td>Inside fibres</td><td>Length based</td><td>5 mm</td></tr>
<tr><td rowspan="2">Frequency sweep</td><td colspan="2">Fixed</td><td></td></tr>
<tr><td colspan="2">10 MHz (1MHz, 7MHz)</td><td></td></tr>
<tr><td rowspan="2">Adaptive setup</td><td colspan="2">Maximum Number of passes</td><td>Percent error</td></tr>
<tr><td colspan="2">10</td><td>1</td></tr>
</table>

Table 5.6 Analysis setup (Direction characterization)

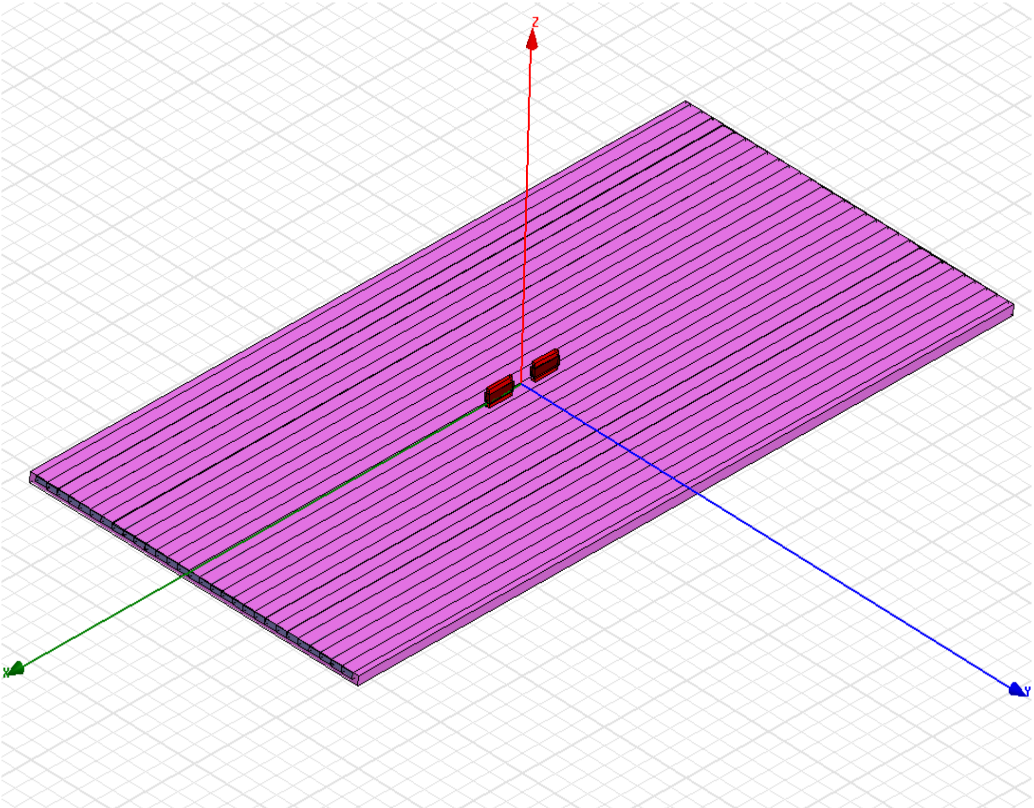

Figure 5.12 Model of fibre direction characterization

The simulation model for fibre direction characterization in Ansoft Maxwell is shown in Figure 5.12 which is designed according to real measurement probes and tested sample. Also, the fibres are modelled as bundle bars as explained in section 5.3.3. The probe could be rotated automatically by running the macro script, which can be opened and modified by users.

The simulation results (Figure 5.13, 5.14 and 5.15) clearly show that this kind of probe not only can effectively characterize the direction of fibre bundles in CFRP, but also is sensitive to other parameters of the material condition and measurement environment such as sample's thickness, measurement frequency and sample's stacking sequence. Figure 5.13 shows how the result changes with the sample thickness. Three CFRP models have been tested in simulation and the results been compared together, in which it shows that the thicker model produces bigger lobes resulting from the increased equivalent conductivity when the probe aligns with the direction of the fibres. Figure 5.14 presents how the stimulating frequency affects the characterization results. The change on the size of lobes proves that higher excitation frequency can bring higher sensitivity to the probe. However, by comparing Figure 5.13 and Figure 5.14, it can be found that although the lobes size would change by the modification on both model thickness and the working frequency, the way it changes is different. The change on the thickness only can result in the change on the size of vertical lobes, while change on the frequency can produce changes on both the vertical and the horizontal lobes. This phenomenon may be helpful in complicated measurement environment where uncertain factors cause the change of measurement signal. Figure 5.15 shows the result of layer detection which can find out how many layers in the sample, and in which order they are stacked where larger lobes indicate the upper layer. From the figure, it can be seen that this sample has two layers of carbon fibre, and the top layer's fibre is on 0 degree direction while the bottom's is on 90 degree direction by comparing the size of individual lobes.

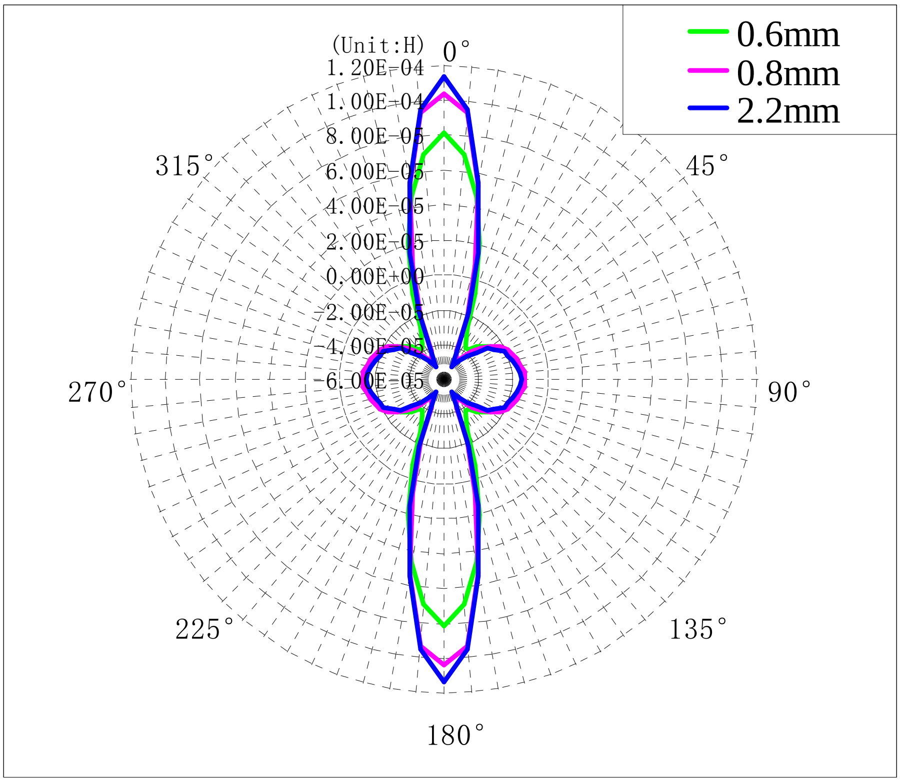

Figure 5.13 Simulation result of direction characterization for different thickness

* Points on the curves have been removed for better clarity.

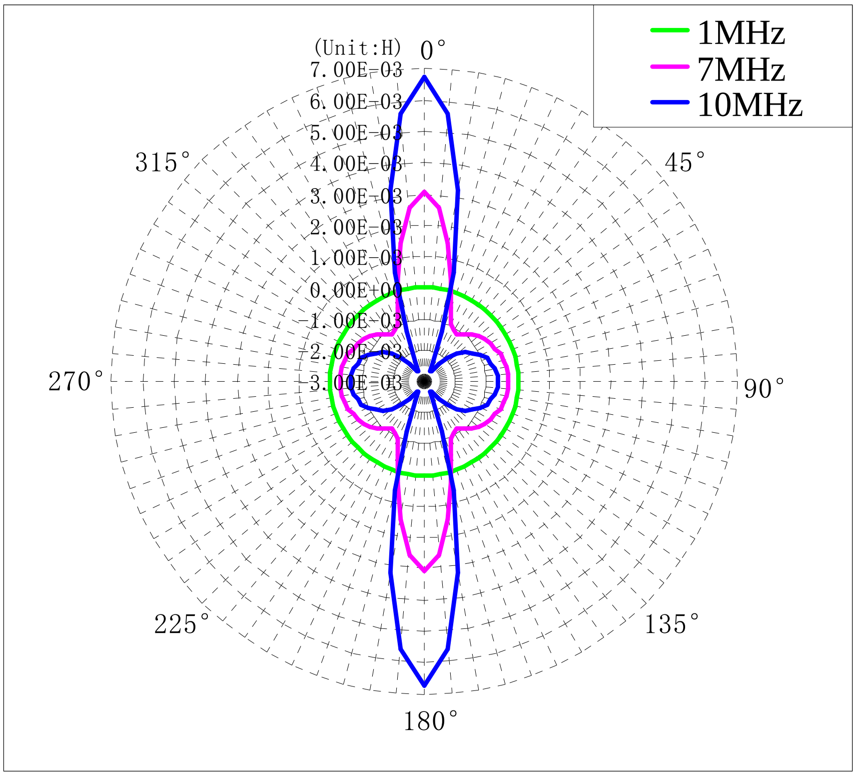

Figure 5.14 Simulation result of direction characterization for different frequency

* Points on the curves have been removed for better clarity.

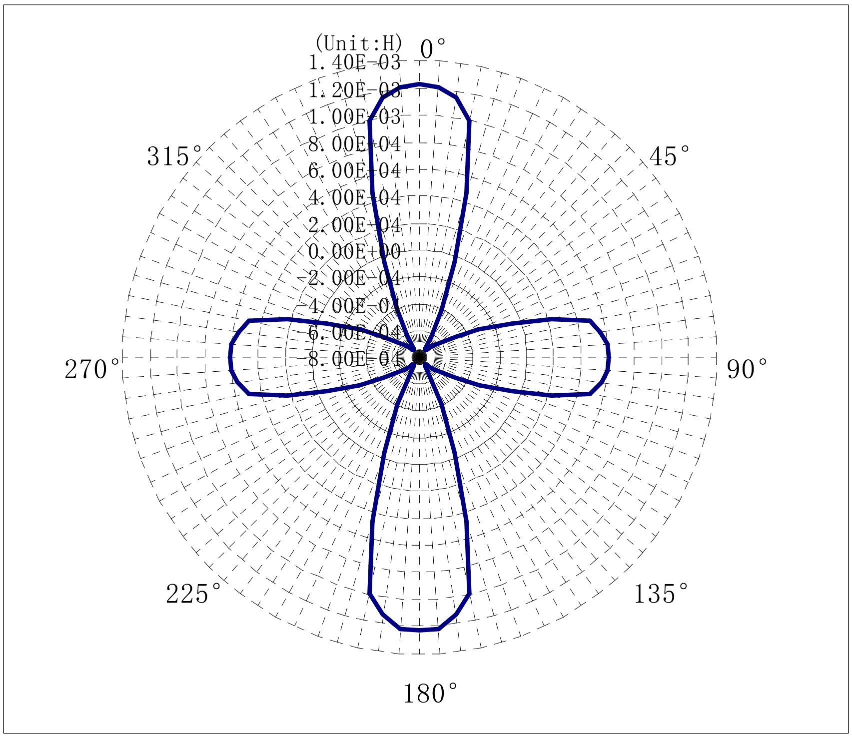

Figure 5.15 Simulation result of direction characterization for two layers

* Points on the curves have been removed for better clarity.

5.4 Conclusion

3D FEM simulation gives a strong support to Dodd and Deeds' solution which was discussed in previous chapters. Both eddy current probes and CFRP samples can be modelled in the software. The simulation results have a good agreement with analytic and measurement results, which further proves that the eddy current testing is an effective method for CFRP characterization. Electrical conductivity and fibre direction are two basic and important properties of CFRP, and in the simulation experiments, they can be characterized and well tested. Also, eddy current probe is sensitive to conductivity change, lift-off effect and multi-layers which means this method has a potential to be widely used in the inspection of CFRP material.

Chapter 6. Non-destructive Characterization of Hybrid Aluminium / CFRP Sheets by Eddy Current Techniques

6.1 Introduction

It has been widely recognized that the outstanding mechanical properties of CFRP, especially its high strength-to-weight ratio has made it an increasingly popular material in the aerospace and automotive industries. In particular, hybrid materials (such as CFRP/aluminum) which have been shown to possess excellent fatigue, impact and residual strength characteristics have now been used in the fuselage and more recently in wing boxes and nacelles of aircrafts. In the automotive industry, high-pressure vessels composed of an aluminum liner covered by CFRP can be made to stores compressed gaseous hydrogen in fuel cell vehicles (FCV)s.

Therefore, the development of non-destructive methods for the characterization of such material is in strong demand for many practical applications. Various methods based on acoustic emission, optical fiber and microwave techniques and methods exploiting DC or AC conductivity of carbon fibers as the detection principle have been studied for CFRP. However, there are very few results on the characterization of CFRP/aluminum hybrid materials, possibly due to their more complex structures. Eddy current methods has been proved an effective method to inspect CFRP materials in previous reports and an initial study of the hybrid Aluminum / CFRP material was also published.

In this chapter, the characterization of hybrid aluminium / CFRP sheets using multi-frequency eddy current sensors is presented. Both air-cored circular sensors and highly directional ferrite-cored sensors are designed for bulk conductivity measurements and directionality characterization of hybrid Aluminum/CFRP samples. An analytical model treating the hybrid samples as two layers homogenous and isotropic material has been developed to provide an explanation for the response of the sensor to sample bulk conductivity. Finite element (FE) models describing the interaction of the ferrite-cored eddy current sensor with the hybrid Aluminum/CFRP plate samples are also developed to provide an explanation of, and physical insights into, the directionality of the sample. It is shown that an anisotropic model (tensor expression for conductivity) is appropriate for the CFRP materials under investigation. A formula to link the bulk conductivity with the conductivity tensor is proposed and verified for selected cases.

6.2 Experiment Setup

6.2.1 Probe Configuration

As the previous experiments discussed in chapter 4, two types of sensors were designed to characterize the hybrid CFRP samples. The first sensor (shown again in Figure 6.1 (a)) is a circular air-cored coil with an outer diameter of 25.1 mm and an inner diameter of 25 mm. Its height is 0.2 mm and the number of turns is eight. It is referred as Coil A. Coil A is mainly used for estimating the bulk conductivity of the samples. Coil B (shown in Figure 6.1 (b)) is made of a ferrite-cored coil pair, one being a transmitter and the other a receiver. The number of turns for both the transmitter and the receiver is three; the height, length and thickness of the ferrite cores are 5 mm, 10 mm and 1 mm respectively. The two ferrite cores are glued to a perplex base, giving a lift-off of about 1 mm. The separation between the two ferrite-cored coils is 10 mm. The dimensions of this sensor are chosen for its high directionality. All measurements are conducted using a commercial impedance analyzer (Solatron 1260) fitted with the sensors, working in a frequency-swept mode covering a frequency range of 10^2 to 10^7 Hz.

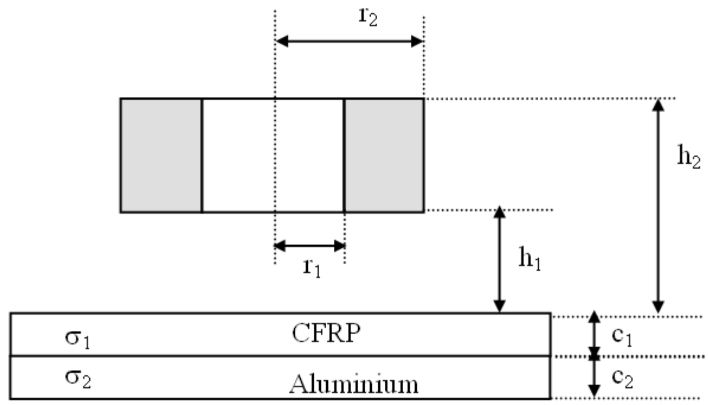

(a) Sensor A for conductivity testing

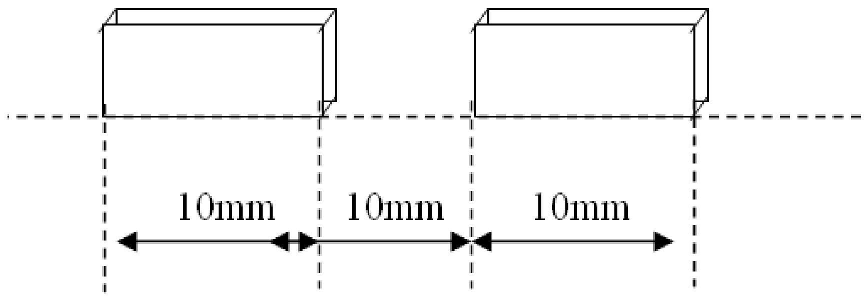

(b) Sensor B for direction characterization

Figure 6.1 The diagrams of the eddy current sensors

6.2.2 Hybrid Aluminum/CFRP Sample

The samples with aluminum plates of different thicknesses pressed against a CFRP plate are produced to simulate hybrid structures. As can be seen in Figure 6.2, the top layer is an unidirectional CFRP sample; the thickness of the aluminum plates are 1 mm, 2 mm, 3 mm, 4 mm and 5 mm respectively.

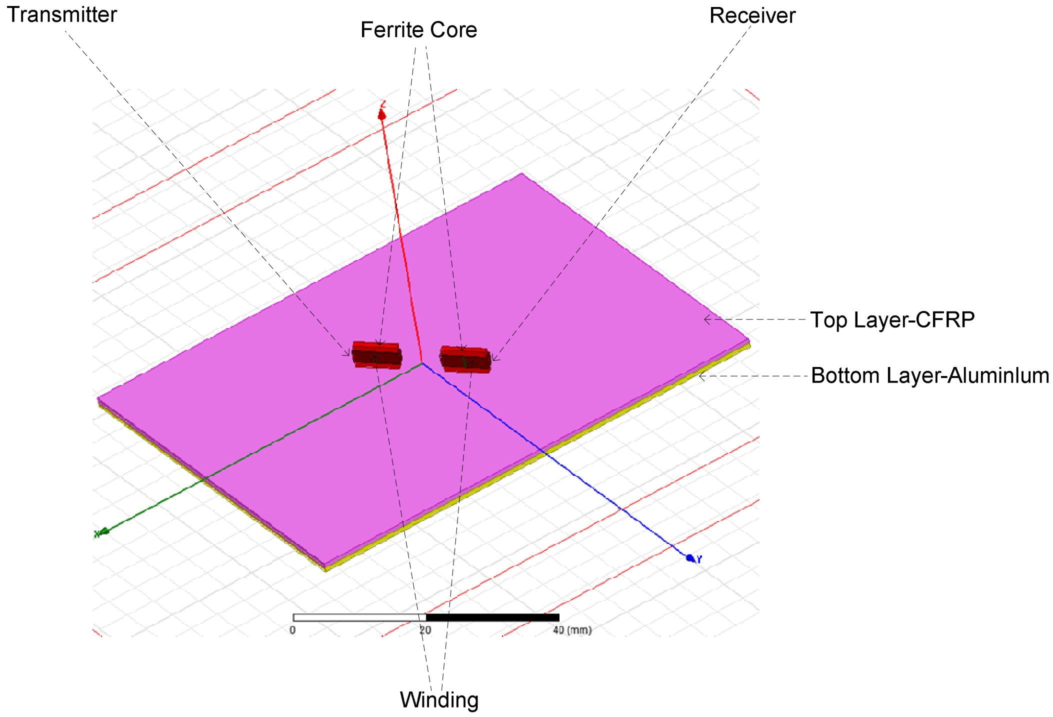

Figure 6.2 3D model of sensor B testing a hybrid plate.

During measurements, the sensors are pressed against the sample under investigation and measurements are conducted on one unidirectional CFRP sample with aluminium sheets of different thicknesses.

Simulations were conducted using an electromagnetic formulation that describes a circular coil above a layered conducting plate of any conductivity at different frequencies. These simulations were performed to estimate the bulk conductivity of the hybrid material and to gain an insight into the expected sensor response under different test situations. Noting that the sample has a complex structure with anisotropic and inhomogeneous properties, treating it as a simple conducting plate can not account for its directionality. Therefore, finite element models are also setup to describe the directionality of the eddy current sensor and the plates under test.

6.3 Result Analysis

6.3.1 Bulk Conductivity Estimation

The first test was conducted to evaluate the bulk conductivity of the CFRP layer for a hybrid sample using sensor A. Previous results had indicated that electrical conduction occurs both along the fiber and transverse to the fiber direction due to fiber to fiber contacts. Some studies have shown that longitudinal conductivity is linearly related to fiber volume fraction, and transverse conductivity is related to other factors such as stacking sequence, fiber length, etc. Conductivity thus provides important insights into composite architecture.

The analytical solution of a circular air-cored coil above a layered conducting plate is given by Dodd and Deeds. Figure 6.1(a) shows the schematic diagram of the model. The base of the coil is at a height of h_1 above the surface and the top of the coil is at h_2. The coil parameters of importance are number of turns N, inner and outer radii r_1 and r_2 and coil length $L= h_2- h_1$.

$$\Delta L(\omega) = K\int_0^{\infty} \frac{P^2(\alpha)}{\alpha^6} A(\alpha)\frac{U_{12}}{U_{22}}\, d\alpha \tag{6.1}$$

$$\text{where, } U = H_2 \cdot H_1 \cdot H_0 \tag{6.2}$$

$$H_k = \frac{1}{2}\begin{bmatrix} (1+\frac{\alpha_k}{\alpha_{k+1}})e^{(\alpha_{k+1}-\alpha_k)\cdot z_k}, & (1-\frac{\alpha_k}{\alpha_{k+1}})e^{(\alpha_{k+1}+\alpha_k)\cdot z_k} \\ (1-\frac{\alpha_k}{\alpha_{k+1}})e^{(-\alpha_{k+1}-\alpha_k)\cdot z_k}, & (1+\frac{\alpha_k}{\alpha_{k+1}})e^{(\alpha_k-\alpha_{k+1})\cdot z_k} \end{bmatrix} \tag{6.3}$$

$$A(\alpha) = (e^{-\alpha h_1} - e^{-\alpha h_2})^2 \tag{6.4}$$

$$P(\alpha) = \int_{\alpha r_1}^{\alpha r_2} x J_1(x) dx \tag{6.5}$$

$$K = \frac{\pi \mu_0 N^2}{(h_1 - h_2)^2 (r_1 - r_2)^2} \tag{6.6}$$

$$\alpha_k = \sqrt{\alpha^2 + j\omega\sigma_k \mu_k} \tag{6.7}$$

where α -- spatial frequency variable;

ω -- the angular frequency of excitation;

r_1 and r_2-- inner and outer radius of the probe;

h_1 and h_2-- height of the bottom and top of the probe;

U and H -- transfer matrices;

K-- pre-factor;

J_1(x)--first-order Bessel function of the first kind.

The interface between layers *k* and *k+1* occurs at a depth z_k. σ_k denotes the conductivity of layer *k*.

Coil A was placed next to the hybrid CFRP/aluminum (1 mm thickness) plate with a lift-off of 0.1 mm. By fitting the results from Equations (6.1) to (6.6) to the experimental data, it is possible to obtain the conductivity of the CFRP plate under test. Alternatively, a much simpler method can be adopted which uses the features in multi-frequency response of the sensor to infer conductivity of the sample.

Thanks to the co-work from the research group, Figure 6.3 shows the real and imaginary inductance of the coil obtained by experiment compared with the analytical solution. Good agreement can be observed between these two data sets and the bulk equivalent conductivity of the CFRP layer is inferred to be 12.6 kS/m. This is comparable with data reported in literature and previous work. At the lower frequency end (from 100 Hz to 10 kHz), the real inductance decreases and then reaches a plateau, which corresponds to the situation that the incident magnetic flux penetrates though the CFRP, but is increasingly excluded from the aluminium plate. At the higher frequency end (from 10 kHz to 10 MHz), the real inductance again decreases from the plateau, however, this is caused by the CFRP. Two negative peaks in the imaginary inductance plots correspond to the effect of the aluminium and the CFRP respectively.

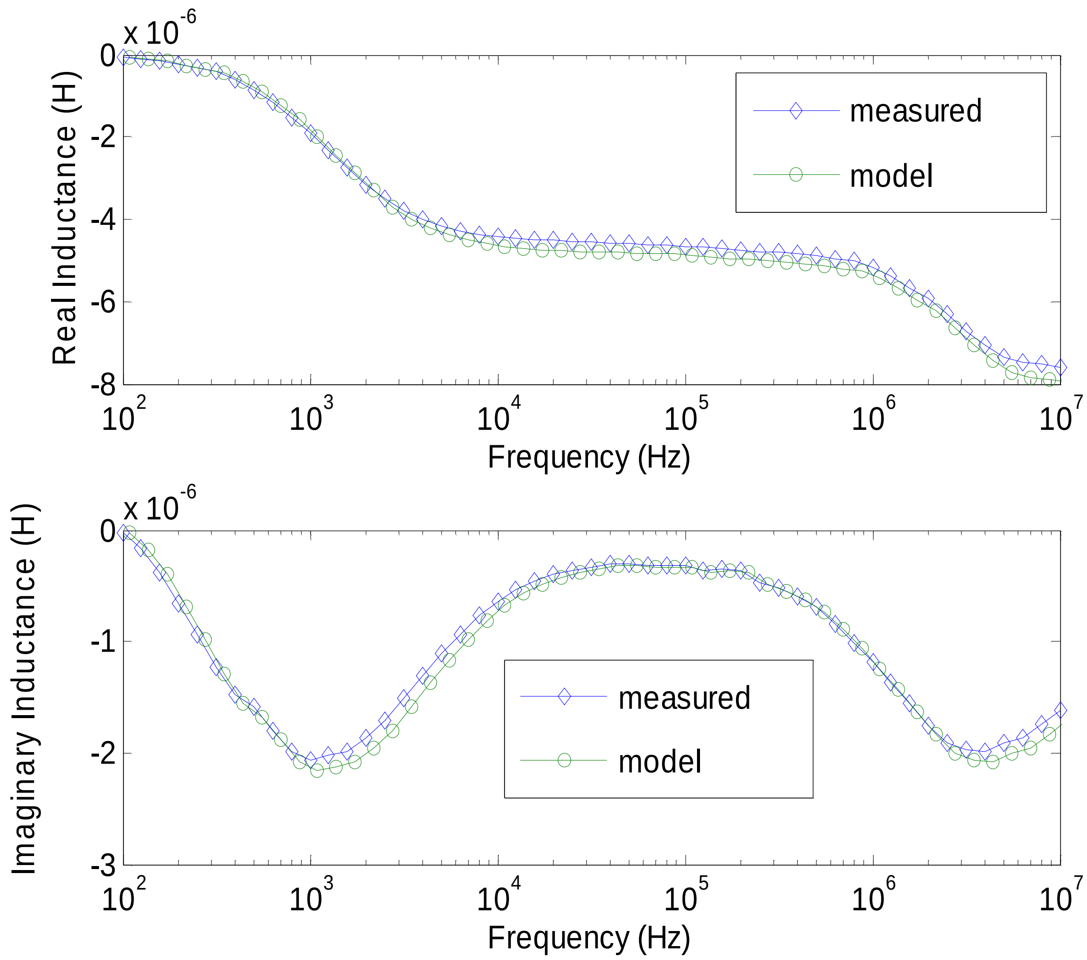

Figure 6.3 Experimental and simulation inductance of Coil A when placed next to the hybrid Aluminum/CFRP plate (Thickness of aluminum layer is 1mm).

* Measurement results are subject to machine error of ±5% from Solartron 1260.

This physical insight is clearly verified when the inductances of coil A placed next to hybrid plates with aluminium layer of different thicknesses (i.e. 1 mm, 2 mm, 3 mm, 4 mm, 5 mm) are compared (shown in Figure 6.4). At the lower frequency end, the real inductance reaches a plateau at different frequencies. However, at the higher frequency end (from 10 kHz to 10 MHz), the real inductance curves overlap as this part of the curve is controlled by the CFRP. There are still two negative peaks in the imaginary inductance plots; the first one shifts to the left as we increase the aluminium plate thickness, but the second one remains the same for all cases as this part is due to the contribution from the CFRP. The fact that the higher frequency part remains constant proves that the estimation of the conductivity of the CFRP plate will not be influenced by the variation in the thickness of the aluminium plate. The fact that the lower frequency part shifts to the lower end as increasing the thickness of the aluminium plate verifies the first order approximation theory in the previous work [94].

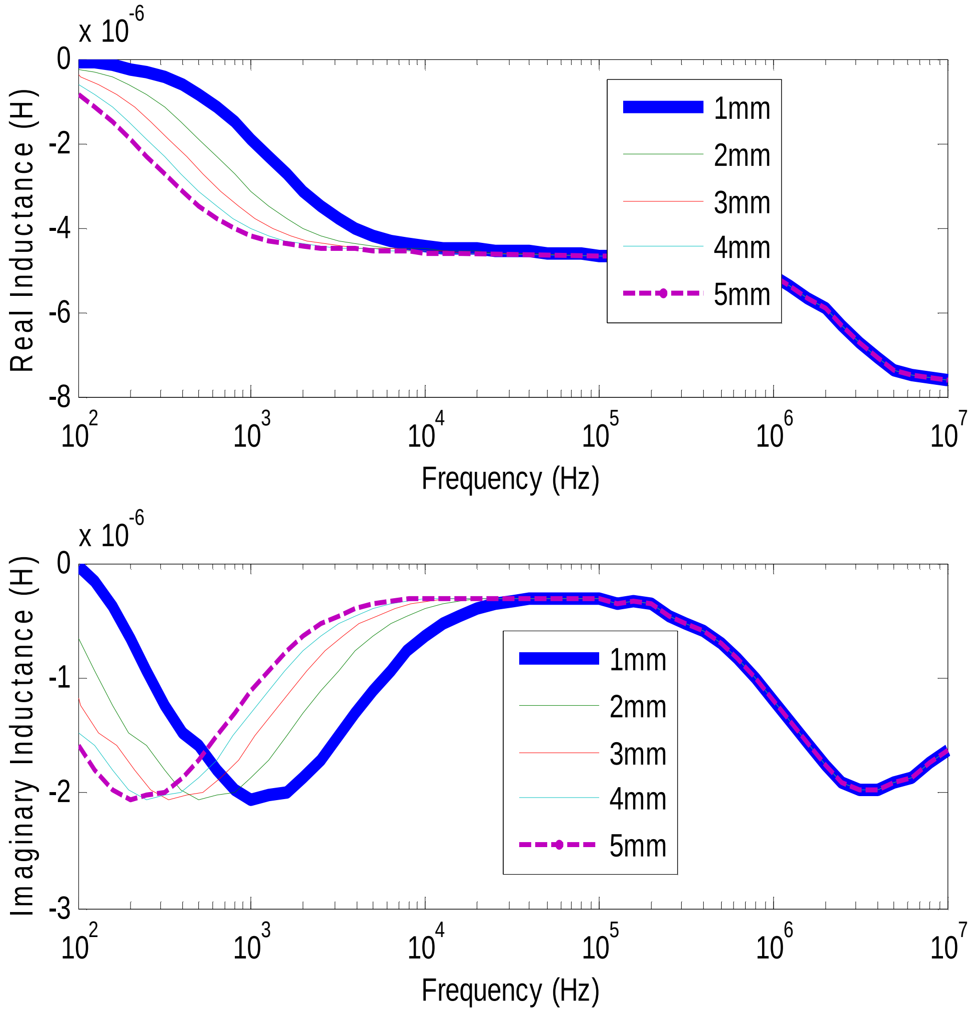

Figure 6.4 Experimental inductance of Coil A when placed next to the hybrid Aluminum/CFRP plate (aluminum layer = 1mm, 2mm, 3mm, 4mm, 5mm).

* Measurement results are subject to machine error of ±5% from Solartron 1260.

It is worth pointing out that the formulae of Dodd and Deeds are based on the assumption that the conductor placed next to the coil is homogenous and isotropic, but hybrid aluminium/CFRP is neither homogenous nor isotropic. Therefore, the conductivity obtained here is an effective conductivity in an averaged sense (also called the bulk conductivity), similar to the concept used in effective media theory. It is actually not the true anisotropic conductivity.

6.3.2 Characterization of Directionality

CFRP is highly anisotropic, but aluminium is uniform and isotropic. At lower frequencies (<100 kHz), the effect of the CFRP layer on the inductance signal from eddy current sensor is negligible due to the very weak eddy currents, therefore directionality is not detectable. At higher frequencies, the effect of the aluminium layer becomes increasingly weaker compared to the CFRP layer as the magnetic field decays quickly and only small portions of the field can reach the aluminium layer, and the effect of the CFRP becomes more pronounced. Therefore, it is expected that at the higher frequency end, the directionality of the CFRP in the hybrid material is still detectable.

This section is concerned with characterizing anisotropy using Coil B for one of the hybrid samples (CFRP + 1 mm Aluminium plate). During the measurements, the samples were fixed, while the sensor was attached to a mechanical rotor, which was rotated from 0 to 360º in steps of 5 º. The lift-off was 1 mm.

Figure 6.5 shows the polar diagram of the impedance measurements obtained for the hybrid sample (unidirectional composite). It can be seen that the fiber direction was 0º, giving rise to the large lobes due to the higher conductivity in this direction. This is a high frequency phenomenon and the measured curve in Figure 6.5 corresponds to data measured for a frequency of 5 MHz. As reducing the frequency, the effect of aluminium becomes more predominate; therefore, the polar diagram shows less directionality (shown in Figure 6.6). At medium frequencies, the diagram reflects the effects of both the CFRP and aluminium, resulting in a response between these two extreme cases. Note that in Figure 6.6, inductance values instead of impedance values are plotted to make the lower frequency plots visible on the same scale.

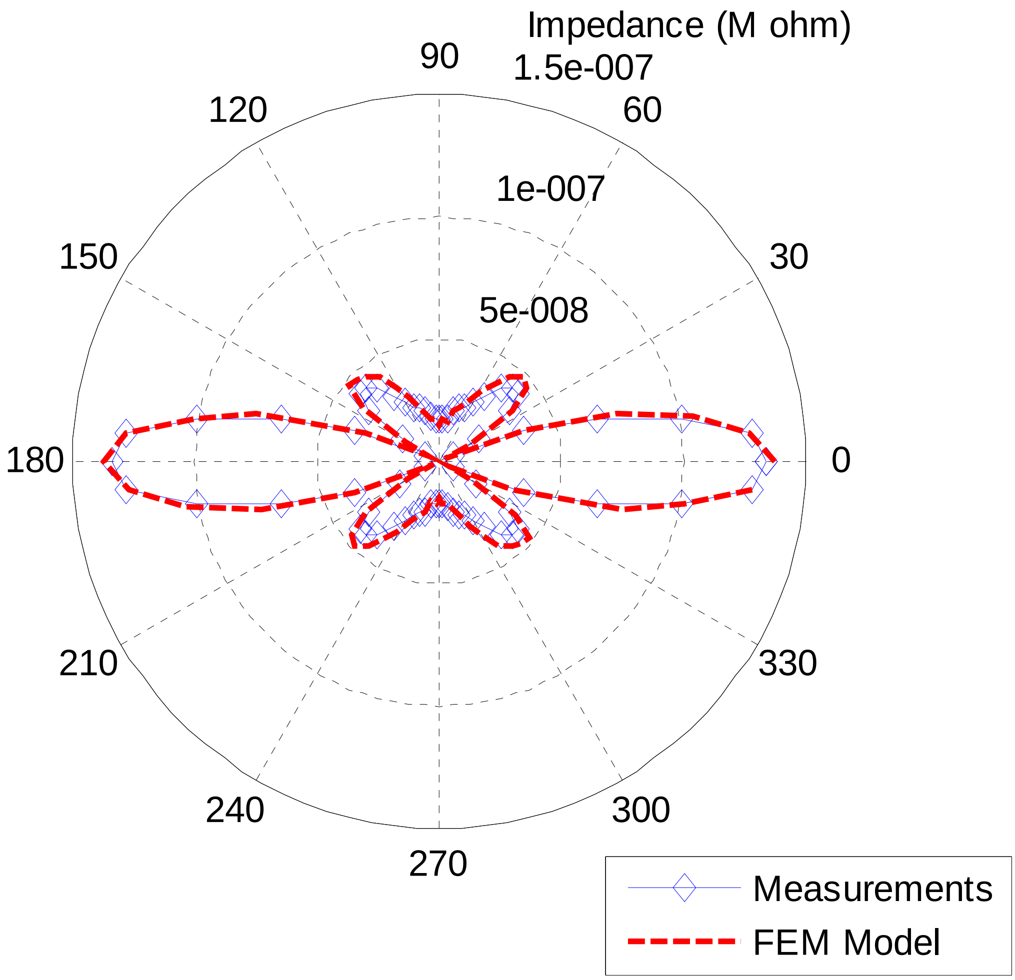

Figure 6.5 Directional measurements of impedance for the hybrid CFRP/aluminium plate

* 1. Simulation results have been normalized with measurement results for better comparison.

2.Measurement results are subject to machine error of ±5% from Solartron 1260.

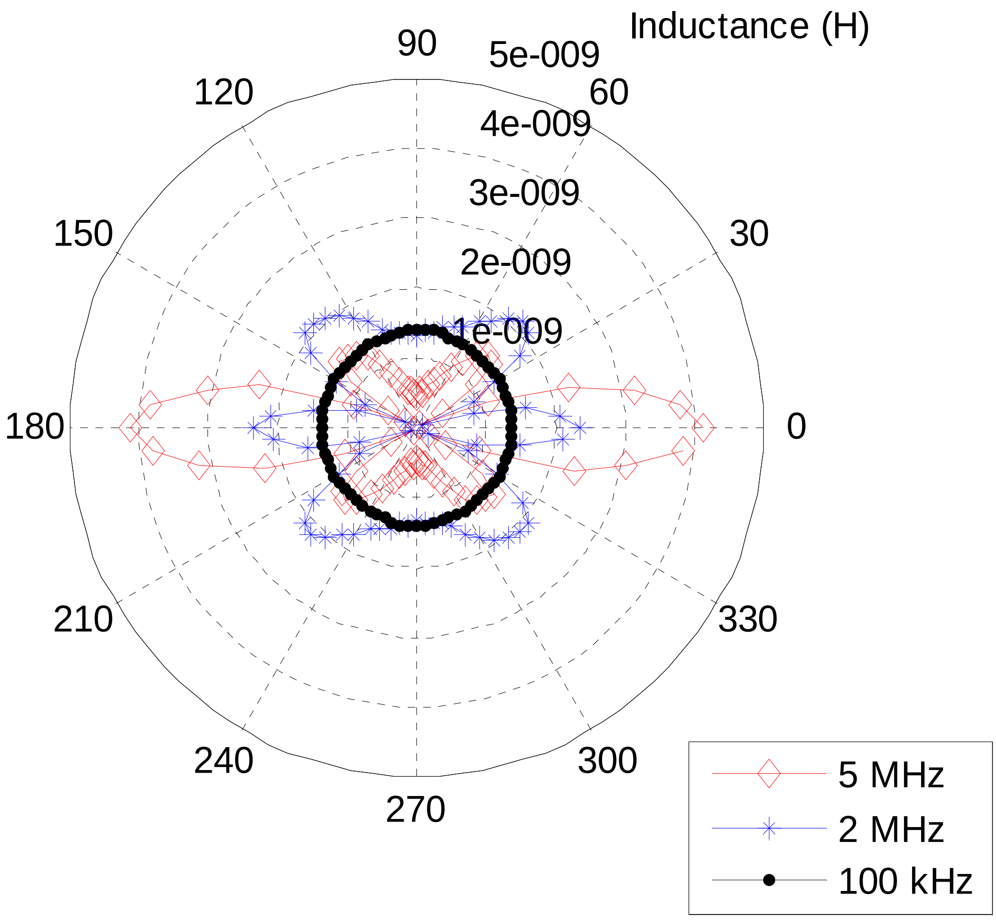

Figure 6.6 Polar diagrams for the hybrid CFRP/aluminium plate at three frequencies

* Measurement results are subject to machine error of ±5% from Solartron 1260.

6.4 Finite Element Modeling of Materials with Anisotropic Conductivity

Since the analytical model in section 6.3.1 is not capable of accounting for and predicting the anisotropic phenomena of the CFRP/Aluminium material, Finite element models were set up to simulate the sensor responses for the unidirectional sample. There are two possible approaches to carry out the simulation. The first one is to simulate the detailed structures of the CFRP, e.g. to simulate each of the many individual fibers. This is not computationally feasible due to the geometrical complexity of the composite and our computing capabilities. The second approach is to treat the CFRP as an anisotropic material and apply anisotropic conductivity property to it, which is computationally possible. In this case, the anisotropic conductivity of the CFRP needs to be represented by a tensor.

In Cartesian coordinate system, the anisotropic conductivity can be expressed as:

$$\hat{\sigma} = \begin{vmatrix} \sigma_x & 0 & 0 \\ 0 & \sigma_y & 0 \\ 0 & 0 & \sigma_z \end{vmatrix} \tag{6.8}$$

$$J = \hat{\sigma} \cdot E \tag{6.9}$$

Where $\hat{\sigma}$ is the conductivity tensor, σ_x, σ_y and σ_z are the conductivities in each direction respectively; J is the current density and E the electric field. The FEM formulation stays the same.

During the simulations, the hybrid samples are kept to be stationary, while the sensor is rotated from 0 to 360^o at step of 5^o. The probe geometry in the simulations is set to correspond to sensor B. The size of the samples is taken to be 40 by 40 by 1 mm (length, width and depth). The simulated frequency is 5 MHz. In order to determine appropriate anisotropic conductivity values for the sample, different ratios between the conductivities along and perpendicular to the fiber direction is simulated. The results are given in Figure 6.7. When the ratio is 1, i.e. the isotropic case with conductivity of 6×10^3 S/m, the pattern is nearly circular as expected; as the ratio increases, anisotropic patterns gradually appear; when the ratio reaches 10/1, the simulated pattern is close to the measured pattern. Here, σ_x, σ_y and σ_z are set to be [6×10^4, 6×10^3 and 6×10^3] S/m respectively, i.e. the conductivity tensor is

$$\hat{\sigma} = \begin{vmatrix} 6\times10^4 & 0 & 0 \\ 0 & 6\times10^3 & 0 \\ 0 & 0 & 6\times10^3 \end{vmatrix} \tag{6.9}$$

In this setup, as can be seen in Figure 6.7 the model correctly predicts the measured anisotropy in the signal patterns.

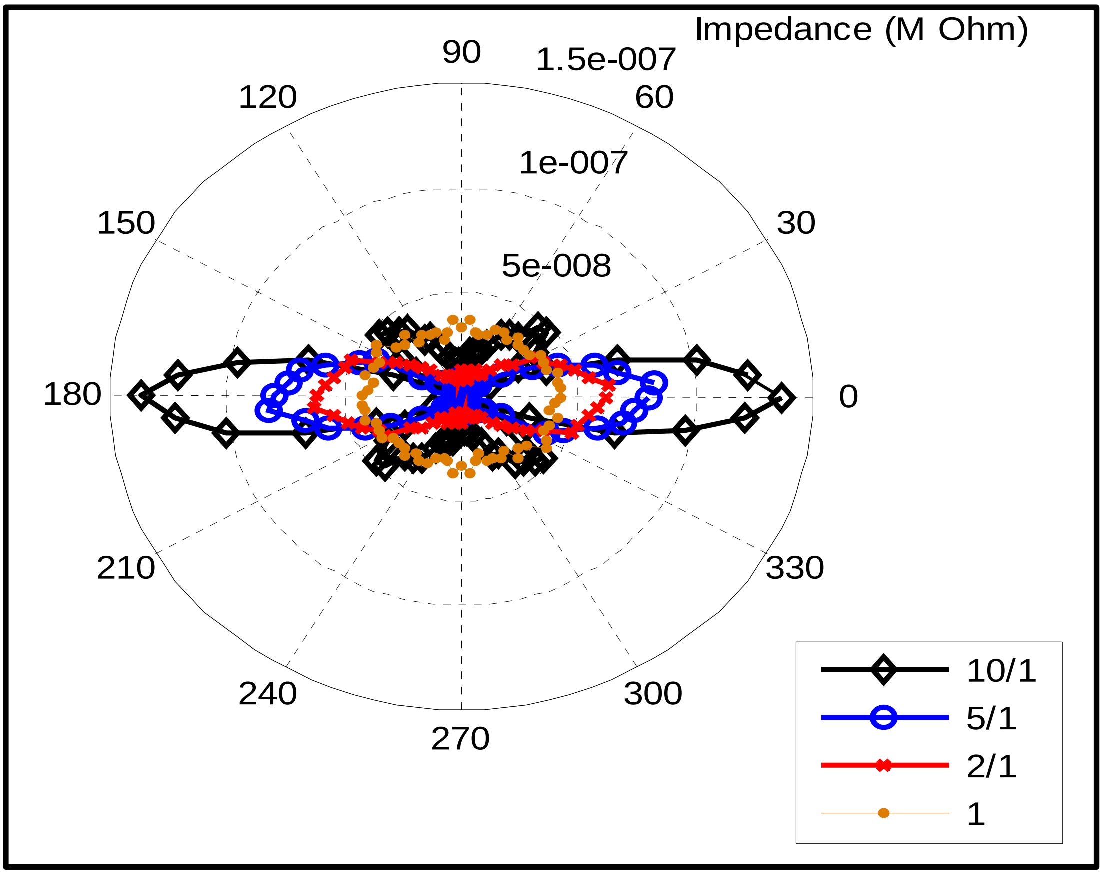

Figure 6.7 Simulation results for different ratios between the conductivities along and perpendicular to the fiber direction

Considering the bulk conductivity (or equivalent conductivity) was 12.6 k S/m according to the results from the air-cored sensor, a formula can be proposed to link the equivalent conductivity σ_e with σ_x, σ_y and σ_z, i.e.

$$\sigma_e \approx \sqrt[3]{\sigma_x \times \sigma_y \times \sigma_z} \qquad (6.10)$$

This formula has been verified using different simulated conductivities.

6.5 Lift-off Effect Consideration

In practical situations, it is difficult to totally avoid lift-off variations. This section is to evaluate the effects of lift-off using experimental data. Different lift-offs are used in measuring the hybrid samples. Figure 6.8 (a) presents one set of results. It can be seen from the graph that as increasing the lift-off, the signal amplitude decreases, which is as expected. It is also noted that the peak frequencies also shift toward the low frequency end with the increase of the lift-off. Since the peak frequency is one of the most important features that can be used to infer conductivity, a compensation method is proposed using the following equation:

$$f_{corr} = f \,/\, amplitude^{0.25} \tag{6.11}$$

Where 0.25 is an empirical parameter obtained through trials and the *amplitude* is unit of μH . Figure 6.8 (b) shows the results after correction. The peak frequency is shown to remain constant and therefore can be used reliably to infer conductivity.

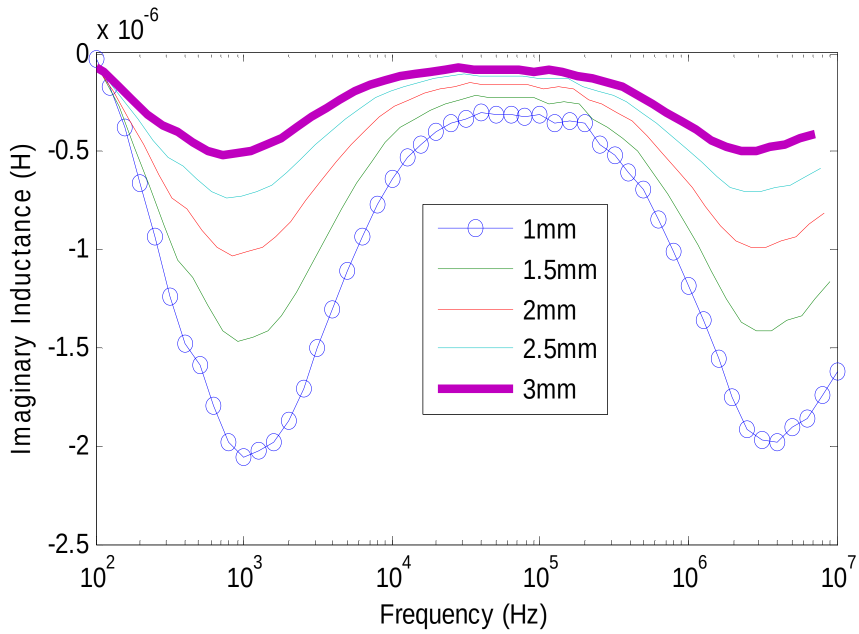

(a)

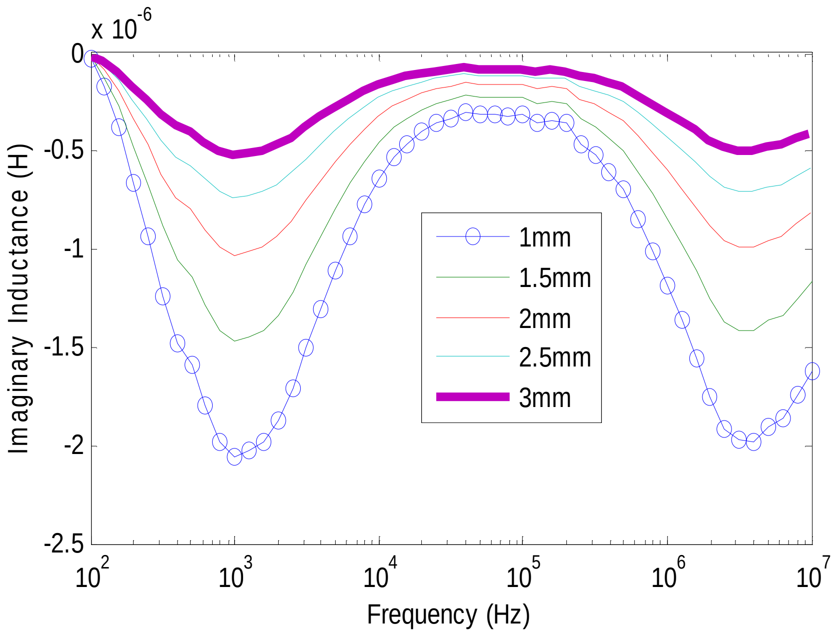

(b)

Figure 6.8 Lift-off effect: (a) before and (b) after peak shift correction

* Measurement results are subject to machine error of ±5% from Solartron 1260.

6.6 Conclusion

This chapter introduces an application of eddy current testing for non-destructive inspection of hybrid aluminium/CFRP material, which has been published in [95, 96]. Two eddy current sensors have been designed for the characterization of hybrid samples. The bulk conductivity of the CFRP layer is inferred from impedance measurements by best fitting, while the directionality is characterized by impedance patterns. Both simple analytical and finite element (FE) models are developed to describe the sensor responses with good agreement to the experimental results. It has been shown that for the cases considered, an anisotropic model (tensor expression for conductivity) is appropriate for the CFRP materials under investigation. A formula to link the bulk conductivity with the conductivity tensor is proposed and verified. The lift-off effect is also discussed. Based on the measured results and simulations, it is believed that an instrument can be made based on eddy current principles for the characterization of hybrid aluminium/CFRP samples. This will be the topic of future work.

Chapter 7. Conclusions and Future Work

7.1 Conclusions

The applications of eddy current testing techniques for non-destructive characterization of CFRP materials have been described in this thesis. The work combines a fundamental theory study on non-destructive testing using the eddy current method and CFRP, real sample measurements, FEM simulations, hardware and system design, and interface programming.

Theoretical analysis, experimental and 3D simulation results show that the eddy-current method can be used to characterise CFRP non-destructively. Special probes are required to make use of the electrical anisotropy of the material in order to monitor specific properties such as bulk conductivity, fibre direction, layer sequence and lift-off. It has been demonstrated that a rotary probe is capable of detecting fibre orientation of different layers and defects associated with fibre direction, while circular air-cored coils are more suitable for the estimation of the bulk effective electrical conductivity. Both the specification of the probes such as shape, number of turns and dimensions, and the operation frequency can influence the measurement result and the testing accuracy. CFRP material is more likely to suffer defects which are produced by different mechanisms than conventional metallic engineering materials. CFRP is also likely to show different characteristics which have different negative effects on material. To detect and distinguish various defects on or in CFRP material, specific probes and methods have been designed and applied. The results presented in this thesis show that eddy current probes are more sensitive to defects perpendicular to carbon fibre than defects parallel with carbon fibre. Although certain information about the CFRP properties, inner and outer structure and work condition can be obtained from the experiment results, further analysis should be carried on to extract more information about the material’s structural details such as fibre percentage, delamination characterization, impact damage level, location of fibre cracks, depth of fibre layer and so on.

As introduced in Chapter 4, an electronic eddy current testing system has been developed based on eddy current probes, computer, Solatron 1260 and accessories. This arrangement has been used to obtain most of the experiment result presented in this thesis. However the accuracy of the results is subject to distortion and noise particularly at higher frequency as the Solatron 1260 reaches the limits of its operating range and the effects of parasite impedances in the connecting cables become important. Also introduced in this chapter, to overcome the deficiency of the Solatron 1260 and in particular to increase the operation frequency range above 10 MHz, a new measurement system has been built up. This system consists of a computer, function generator, oscilloscope, automation equipment, improvement circuits and eddy current probe. All the devices are configured and controlled through a GUI interface which is developed based on the MatLab programming language. Also, the whole measurement is set up and controlled by an interface, where the parameters of the measurement are configured by computer, and the results are also sent to computer for processing and analysis. As a whole, this comprehensive eddy current testing system integrates every piece of the device and measurement task together so as to provide a prototype for the system used in the laboratory.

Three dimensional computer simulation has been used extensively during this project with Ansoft Maxwell models of the probe and CFRP, which are discussed in chapter 5. The simulation of conductivity testing has been carried out for CFRP models with various thickness and conductivity. The results prove that Deed and Dodd's analysis about plane conductive materials can also be applied to anisotropic CFRP composite to determine the bulk equal electrical conductivity. Meanwhile, the simulation for fibre characterization has successfully provided the information about the fibre direction, layer number, the stacking sequence and lift-off. In addition, mesh convergence tests have been undertaken to find the optimal compromise between accuracy and mesh size. To set up an efficient communication link between the simulation software, the measurement instrument (e.g. Solartron 1260), and the computer, an interface based on VBScript program has been developed so that the computer working as a controller part is able to have full access to other parts and the experiment data. Thank to VBScript code, this program can be run at any computer installed with Microsoft Excel.

In chapter 6, an application of eddy current testing for non-destructive inspection of hybrid aluminum/CFRP material has been introduced. Both the bulk conductivity of the CFRP layer is derived from impedance measurements by fitting and the directionality is characterized by impedance patterns. The results from simple analytical and finite element (FE) models which are developed to describe the sensor responses show good agreement to the experimental values. Based on the results, a mathematical formula is proposed to relate the bulk conductivity with the conductivity tensor. In turn, this formula is proved by experimental results to be able to estimate the sample's conductivity.

As a whole, the outcome of this PhD project provides information about how to build up a system for eddy current non-destructive characterization of CFRP samples. The results of mathematic analysis, laboratory experiments and 3D FEM simulation have good agreement and all can support this proposed method. Also, a set of measurement system has been built up to improve the operation and result.

7.2 Future Work

It is recommended that further research following this project should be focused on three directions. The first is concentrated on improving the measurement on CFRP samples. The second puts its emphasis on probe configuration and design for more applications and higher accuracy, and the third is aimed at improving simulation of CFRP samples and testing systems. Besides these three major technical aspects, image reconstructing, signal processing, experiments with other NDT methods, literature review and economic evaluation would be valuable. Details of the further research within the three areas are listed below respectively.

7.2.1 CFRP Testing and System Improvement

Although testing results have been obtained to support the basic theory of eddy current characterization for CFRP, stability, sensitivity, reliability, efficiency and signal to noise ratio of the testing system are always the issue to be considered. Although some work has been done to facilitate a better experimental system, even further improvement may be achieved by use of a customized data acquisition system, more advanced measurement devices and automated equipment, and application of high level signal processing. What is more, the scanning mechanism should be able to works on a larger area as the components made of CFRP material are usually very big such as airplane body parts.

Meanwhile, further analysis should be carried out to extract more information about the material’s structural details such as fibre volume, layer depth, coating, thickness and so on. Another important task is to inspect flaws in the material. As a promising NDT method, eddy current testing has already showed its potential in detection of damage, particularly delamination, impact damage and fibre crack. But, it is difficult to distinguish between the three types of defect. However, it is believed that these limitations can be overcome by developing specifically designed apparatus for composite evaluation.

7.2.2 Probe Design

Both the specification of the probes such as type, number of coils, shape, number of turns and dimension, and the work frequency can influence the measurement result and the testing accuracy. Thus, optimization of the probe design for specific inspection is required, and the use of coil arrays is expected to be important. A balance between the parameters of probes including coil number, coil position, shape, size and form is still being studied to obtain the better result. More applications of this method will be proposed as well. What is more, commercial evaluation should be taken into consideration in the drives for practical applications.

7.2.3 Modeling of CFRP and System

The future simulation work will focus on the modeling of more detailed internal structure of various CFRP samples. This bottom-up task will be divided into three main steps: fibre modeling, layer modeling and laminate modeling. Secondly, more types of defects will be modeled in or on the samples for analysis. Modeling work also includes optimum design of probes. Besides 3D FEM modeling, electrical and mathematical modeling will be still carried on in order to improve the accuracy of the results.

References

[1] Emmanuel P. Papadakis, *"Quality degradation due to shipment of nonconforming product under statistical process control in the absence of quarantining"*, Materials Evaluation, Vol. 51(11), pp. 1274–1278, 1993.

[2] FM Burdekin, *"NDT in perspective"*, British Journal of NDT, Vol. 32(11), pp. 563-567, 1990.

[3] N N Peters, *"Standardisation of NDT in aerospace"*, Insight, Vol. 37(2), pp. 115-116, 1995.

[4] P J James, *"The role of non-destructive testing in the control of boiler tube failures"*, Insight, Vol. 37(2), pp. 179-183, 1995.

[5] C B Scruby and R Colbrook, *"Novel application of NDT to the monitoring of manufacturing process"*, British Journal of NDT, Vol.34(3), pp. 109-115, 1992.

[6] Drexel P and Scott L, *"Return on Investment from NDE and Maintenance Expenses — A Case History"*, Materials Evaluation, Vol. 52(11), pp. 1279–1281, 1994.

[7] Barry Hull and Vernon John, *"Non-destructive Testing"*, Basingstoke: Macmillan Education, 1988, ISBN-0333357884.

[8] Ronald Halmshaw, *"Non-destructive testing-2nd Ed"*, Edward Arnold, 1991, ISSN: 09638695.

[9] J. F. Hinsley, *"Non destructive Testing"*, Macdonald & Evans, 1959.

[10] Don E. Bray, *"Non-destructive evaluation: a tool for design, manufacturing, and service"*, McGraw-Hill, 1989, ISBN-10**:** 0849326559.

[11] Chuck Hellier, *"Handbook of Non-destructive evaluation"*, McGraw-Hill Professional, 2001, ISBN0-07-028121-1; ISBN0-07-139947-X.

[12] Herschel B. Smartt and John A. Johnson, *"Role of Intelligent Systems in Weld Process Control"*, Materials Evaluation, Vol. 51(10), pp. 1166–1173, 1993.

[13] I. Grabec, Wolfgang Sachse and D. Grabec, *"Intelligent Processing of Ultrasonic Signals for Process Control Applications"*, Materials Evaluation, Vol. 51(10), pp. 1174–1182, 1993.

[14] K. N. Hitchcock, *"Design evaluation through improved non-destructive testing technology"*, British Journal of NDT, Vol. 33(4), pp. 167-171, 1991.

[15] G Prince and M Shortland, *"Condition monitoring: the automated manufacturing perspective"*, British Journal of NDT, Vol. 29(2), pp. 94-95, 1987.

[16] Helmut Thielsh and Florence Cone, *"Using modern non-destructive testing techniques for plant reliability: part 1"*, Material Evaluation, Vol. 52(4), pp. 457-461, 1994.

[17] Helmut Thielsch and Nancy Knarr, *"Back to Basics: Fitness-for-Purpose Evaluation of a Deaerator with Cracking"*, Materials evaluation, Vol. 50(5), pp. 561–564, 1992.

[18] W. L. Mercer, *"NDT-A vital force in engineering"*, British Journal of NDT, Vol.

29(1), pp. 11-14, 1987.

[19] Wenk, S.A. and R.C. McMaster, *"Choosing NDT: Applications, Costs and Benefits of Non-destructive Testing in Your Quality Assurance Progra"*, Columbus, OH, American Society for Non-destructive Testing, 1987.

[20] McMaster, R.C. and S.A. Wenk, *"A Basic Guide for Management's Choice of Non-destructive Tests"*, Special Technical Publication No. 112, Philadelphia, PA, American Society for Testing and Materials, 1951.

[21] R. J. Ditchburn, S. K. Burke and C. M. Scala, *"NDT of welds: state of the art"*, NDT&E International, Vol. 29(2), pp. 111-117, 1996.

[22] James R. Dickens and Don E. Bray, *"Human performance considerations in non-destructive testing"*, Material Evaluation, Vol. 52(9), pp. 1033-1041, 1994.

[23] P.J. Heffernan, *"Fatigue behaviour of reinforced concrete beams strengthened with CFRP laminates"*, PhD thesis, Royal Military College of Canada, 1997.

[24] J. Waller, *"Carbon fibre cement composites"*, Civil Engineering and Public Works Review 67, 789, pp. 357—361, 1972.

[25] M. P. De Goeje and K. E. D. Wapenaar, *"Non-destructive inspection of carbon fibre-reinforced plastics using eddy current methods"*, Composites, Vol. 23(3), pp. 147-157, 1992.

[26] X. E. Gros, K. Ogi and K. Takahashi, *"Eddy current, ultrasonic C-scan and scanning acoustic microscopy testing of delaminated quasi-isotropic CFRP materials: a case study"*, Journal of Reinforced Plastics and Composites, Vol. 17(5), pp. 389-405, 1998.

[27] Barret R, *"All-moving active aerodynamic surface"*, Research in Smart Materials and Structures, Vol. 4, pp. 65-71, 1995.

[28] Hanselka H, *"Realization of smart structures by using fiber composite materials"*, Smart Mechanical Systems-Adaptronics, pp. 1-10, Dusseldorf, 1997.

[29] A. Mahoon, *"The role of non-destructive testing in the airworthiness certification of civil aircraft composite structures"*, Composites, Vol. 19(3), pp. 229-235, 1988.

[30] A. Briggs, *"Review: Carbon fibre-reinforced cement"*, Journal of Materials Science, Vol. 12, pp. 384—404, 1977.

[31] Vernon SN, *"A single-aided eddy current method to measure electrical resistivity"*, Material Evaluation, Vol. 46, pp. 1581-1587, 1988.

[32] Ruediger Schueler, Shiv P. Joshi, Karl Schulte, *"Damage detection in CFRP by electrical conductivity mapping"*, Composites Science and Technology, Vol. 61, pp. 921-930, 2001.

[33] R. Lange and G. Mook, *"Structural analysis of CFRP using eddy current methods"*, NDT&E International, Vol. 27(5), pp. 241-248, 1994.

[34] Finlayson R D, Friesel M, Carlos M, Cole P and Lenian J C, *"Health monitoring of aerospace structures with acoustic emission and acousto-ultrasonic"*, 15th World conference on Non-destructive Testing, Rome, 2000.

[35] Gerhard Mook, Juergen Pohl and Fritz Michel, *"Non-destructive characterization of smart CFRP structures"*, Smart Material and Structure, Vol. 12, pp. 997-1004, 2003.

[36] Xavier E. Gros, *"An Eddy current approach to the detection of damage caused by low-energy impacts on carbon fibre reinforced materials"*, Materials and Design, Vol. 16(3), pp. 167-173, 1995.

[37] D. Hull and T. W. Clyne, *"An introduction to composite materials"*, 2nd Edition, Cambridge University Press UK, 1996, ISBN: 0521381904.

[38] X. E. Gros, K. Ogi and K. Takahashi, *"Eddy current, ultrasonic C-scan and scanning acoustic microscopy testing of delaminated quasi-isotropic CFRP materials: a case study"*, Journal of Reinforced Plastics and Composites, Vol. 17(5), pp. 389-405, 1998.

[39] Akira Todoroki, Miho Tanaka and Yoshinobu Shimamura *"Measurement of orthotropic electric conductance of CFRP laminates and analysis of the effect on delamination monitoring with an electric resistance change method"*, ", Composites Science and Technology, Vol. 62, pp. 619-628, 2002.

[40] M. P. Hentschel, D. Ekenhorst, K. W. Harbich and A. Lange *"New X-ray refractography for nondestructive investigations"*, Proceedings of International Symposium of Advanced Materials for Lightweight Structures , ESTEC, pp. 661-664, March 1994.

[41] R M Measures, *"Fibre optic sensing for composite smart structures"*, AGARD Conference Proceeding CP531, Smart Structures for Aircraft and Spacecraft, 1993.

[42] V. Stephen, S. Kharkkovsky, J. Nadakuduti, R. Zoughi, *"Microwave field measurement of delaminations in CFRP concrete members in a bridge"*.

[43] K Schutle, CH Baron, *"Load and failure analyses of CFRP laminates by means*

for electrical resistivity measurements", Composites Science and Technology, Vol. 36, pp. 63-76, 1989.

[44] N Muto, H Yanagida, T Nakatsiji, M Sugita, Y Ohtsuka, Y Arai, C Saito, *"Intelligent CFRP composites with self-diagnostic function for preventing fatal fracture"*, Sensors and Materials, Vol. 6, pp. 45-62, 1994.

[45] C Thiagarajan, I Sutherland, D Tunnicliffe, PE Irving, *"Electrical potential techniques for damage sensing in composite structures"*, Proceeding of 2nd Europe Conference on Smart Structure and Material, pp. 128-131, 1994.

[46] O Ceysson, M Salvia, L Vincent, *"Damage mechanisms characterization of carbon fiber/epoxy laminates by both electrical measurements and acoustic emission analysis"*, Scripta Materialia, Vol. 34, pp. 1273-1280, 1996.

[47] J.Pohl, *"Ultrasonic Inspection of Adaptive CFRP-Structure"*, NDT.net, Vol. 3 No.9, 1998.

[48] Hawkins, G. F., P. M. Sheaffer and E. C. Johnson, *"NDE of thick composites in the aerospace industry-an overview"*, Review of Progress in QNDE, Plenum Press, pp. 1591-1597, 1991.

[49] Michaels, T. E., and B. D. Davidson, *"Ultrasonic inspection detects hidden damage in composites"*, Advanced Material & Processes, Vol.3, pp. 34-38, 1993.

[50] Williams, J. H., H. Nayeb-Hashemi and S. S. Lee, *"Ultrasonic attenuation and velocity in AS/3501-6 graphite/epoxy fiber composite"*, NASA Report CR-3180, 1979.

[51] Ogihara, S., N. Takada and A. Kobayashi, *"Microscopic damage growth*

characterization in quasi-isotropic CFRP laminates by scanning acoustic microscopy", Composites' 95: Recent Advances in Japan and the United States, I. Kimpara, H. Miyairi, N. Takeda, Ed., Proc. Japan-US CCM-7, Kyoto, pp. 343-350, 1995.

[52] Ogihara, S., N. Takeda and A. Kobayashi, *"Characterization and modeling of fatigue damage in quasi-isotropic CFRP laminates with circular holes by scanning acoustic microscopy"*, Adv Composite Mater., Vol. 6(1), pp. 65-73, 1996.

[53] Libby, H. L, *"Introduction to electromagnetic non-destructive test methods"*, RE Krieger Pub. Co., 1971.

[54] Gros, X. E., *"Some aspects of electromagnetic testing of composites"*, Insight, Vol. 38(7), pp. 492-495, 1996.

[55] Owston, C. N, *"Eddy current methods for the examination of carbon fibre reinforced epoxy resins"*, Material Evaluation, Vol. 34(11), pp. 237-244,255, 1976.

[56] Kubomura, K., T. Ishida and K. Sawada, *"Eddy current inspection of broken fibers in carbon fiber reinforced plastics and the formation of current loop"*, Composites '95: Recent Advances in Japan and the United States, I. Kimpara, H. Miyairi, N. Takeda, Ed., Proc. Japan-US CCM-7, Kyoto, pp. 335-342, 1995.

[57] J. C. Moulder, E. Uzal, and J. H. Rose, *"Thickness and conductivity of metallic layers from eddy current measurements"*, Rev. Sci. Instrum., Vol. 63, pp. 3455–3465, 1992.

[58] Davis, J. M. and M. King, *"Mathematical formulas and references for non-*

destructive testing-eddy currents, First Edition", The Art Room Corporation, 1994.

[59] Gros, X. E, *"Characterization of low energy impact damage in composites"*, Journal of Reinforced Plastics and Composites, Vol. 15(3), pp. 267-282, 1996.

[60] Randolf Hanke, Theobald Fuchs and Norman Uhlmann, *"X-ray based methods for non-destructive testing and material characterization"*, Proceedings of the 9th International Workshop on Radiation Imaging Detectors, Volume 591 Issue 1, pp. 14-18, 2008.

[61] Christian Spiessberger, Alexander Dillenz and Thomas Zweschper, *"Active Thermography for Quantitative NDT of CFRP Components"*, 2nd international symposium on NDT in Aerospace, 2010.

[62] Gros, X. E, *"NDT Data Fusion"*, Edward Arnold Publisher, ISBN: 0340676485.

[63] Gerhard Mook, Rolf Lange and Ole Koeser. "*Non-destructive characterisation of carbon-fibre-reinforced plastics by means of eddy-currents*", Composites Science and Technology, 61, pp. 865-873, 2001.

[64] Gui Yun Tian, Ali Sopian. "*Reduction of lift-off effects for pulsed eddy current NDT*", NDT&E International, 38, pp.319-324, 2005.

[65] Yoshimi Hatsukade, Naoko Kasai, Hiroshi Takashima and Atsushi Ishiyama. "*Non contact SQUID-NDT method using a ferrite core for carbon-fibre composites"*, Superconductor Science and Technology, 15, pp.1728-1732, 2002.

[66] C. Bonavolonta, G. Peluso, G.P. Pepe and M. Valentino. *"Detection of early stage damage in carbon fibre reinforced polymers for aeronautical applications using*

an HTS SQUID magnetometer", European Physical Journal, B 42, pp.491-496, 2004.

[67] Andrzej Krawczyk and John A. Tegopoulos, "*Numerical modeling of eddy currents"*, Clarendon Press, Oxford, 1993.

[68] Richard L. Stoll, "*The analysis of eddy currents"*, Clarendon Press, Oxford, 1974.

[69] W Yin, P. Withers, U. Sharma and A J Peyton, "Non-contact characterization of Carbon-Fibre-Reinforced Plastics (CFRP) Using Multi-frequency Eddy Current Sensors", IMTC, 2007.

[70] D. Placko, H. Clergeot, and E. Santander, "Physical modelling of an eddy current sensor designed for real time distance and thickness measurement in galvanization industry", IEEE Trans. Magn., Vol. 25, pp. 2861–2863, 1989.

[71] Y. Nonaka, "A double coil method for simultaneously measuring the resistivity, permeability, and thickness of a moving metal sheet", IEEE Trans. Instrum. Meas., Vol. 45, pp. 478–482, 1996.

[72] A. Sethuraman and J. H. Rose, "Rapid inversion of eddy current data for conductivity and thickness of metal coatings", J. Non-destructive Eval., Vol. 14, pp. 39–46, 1995.

[73] W. Yin, A. J. Peyton, and S. J. Dickinson, "Simultaneous measurement of distance and thickness of a thin metal plate with an electromagnetic sensor using a simplified model", IEEE Trans. Instrum. Meas., Vol. 53, pp. 1335–1338, 2004.

[74] Abry JC, Choi YK, Chateauminois A, Dalloz B, Giraud G, Salvia M, "In-situ monitoring of damage in CFRP laminates by means of AC and DC

measurements", Composites Science And Technology, Vol. 61(6), pp. 855-864, 2001.

[75] C. V. Dodd and W. E. Deeds, *"Analytical solutions to eddy-current probe-coil problem"*, J. Appl. Phys., Vol. 39, pp. 2829–2839, 1968.

[76] W. Yin, A. J. Peyton, and S. J. Dickinson, *"Simultaneous measurement of distance and thickness of a thin metal plate with an electromagnetic sensor using a simplified model"*, IEEE Trans. Instrum. Meas., vol. 53, pp. 1335–1338, 2004.

[77] Raimond Grimberg, Adriana Savin, Sorin Leitoiu, Nicoleta Iftimie, Alina Bruma, Aurel Andreescu, *"Examination and monitoring of carbon epoxy composites structures"*, 4th International Conference on NDT, 11-14 October, 2007.

[78] H. Kocznarech, *"Ultrasonic detection of damage in carbon fiber reinforced plastics"*, Journal of Composite Materials, Vol. 29(1), pp. 59-95, 1995.

[79] J. W. Newman, *"Production and field inspection of composite aerospace structures with advanced shearography"*, Review of Progress in QNDE, 10B, pp. 2129-2133, 1991.

[80] C. Nageswaran, C. R. Bird and R. Takahashi, *"Phased array scanning of artificial and impact damage in carbon fibre reinforced plastic (CFRP)"*, 44th Annual British Conference on NDT, pp. 155-159, 2005.

[81] N. Angelidis, N. Khemiri and P. E. Iriving, *"Experimental and finite element study of the electrical potential technique for damage detection in CFRP laminates"*, Smart Materials and Structures, Vol.14 (10), pp. 147-154, 2005.

[82] Masahito Ueda, Akira Todoroki, Yoshinobu Shimamura and Hideo Kobayashi, *"Monitoring delamination of laminated CFRP using the electric potential change*

method (two-stage monitoring for robust estimation", Advanced Composite Material, Vol. 14(1), pp. 83-97, 2005.

[83] S. Kharkovsky and R.Zoughi, *"Application of near-field microwave and millimeter wave nondestructive testing for evaluation of fiber breakage and orientation evaluation in CFRP composite patches"*, Review of Quantitative Nondestructive Evaluation, Vol. 24, pp. 554–561, 2005.

[84] Nobuo Takeda, Yoji Okabe, Junichiro Kuwahara, Seiji Kojima and Toshimichi Ogisu, *"Development of smart composite structures with small-diameter fiber bragg grating sensors for damage detection: Quantitative evaluation of delamaination length in CFRP laminates using Lamb wave sensing"*, Composites Science and Technology, Vol. 65, pp. 2575-2587, 2005.

[85] Akira Todoroki, Miho Tanaka and Yoshinobu Shimamura, *"Electrical resistance change method for monitoring delaminations of CFRP laminates: effect of spacing between electrodes"*, Composites Science and Technology, Vol. 65, pp. 37-46, 2005.

[86] Z. Xia, T. Okabe, J. B. Park, W. A. Curtin and N. Takeda, *"Quantitative damage detection in CFRP composite: coupled mechanical and electrical models"*, Composites Science and Technology, Vol. 63, pp. 1411-1422, 2003.

[87] Gros, X. E., *"Some aspects of electromagnetic testing of composites"*, Insight, Vol. 38(7), pp. 492-495, 1996.

[88] Kubomura, K., T. Ishida and K. Sawada, *"Eddy current inspection of broken fibers in carbon fiber reinforced plastics and the formation of current loop"*, Composites '95: Recent Advances in Japan and the United States, I. Kimpara, H. Miyairi, N. Takeda, Ed., Proc. Japan-US CCM-7, Kyoto, pp. 335-342, 1995.

[89] J. C. Moulder, E. Uzal, and J. H. Rose, *"Thickness and conductivity of metallic layers from eddy current measurements"*, Rev. Sci. Instrum., Vol. 63, pp. 3455–3465, 1992.

[90] Gros, X. E, *"Characterization of low energy impact damage in composites"*, Journal of Reinforced Plastics and Composites, Vol. 15(3), pp. 267-282, 1996.

[91] C. V. Dodd, *"Research Techniques in Nondestructive Testing"*, ed R. S. Sharpe Vol. 3, Chapter 13, 1977.

[92] J. Blitz, *"Electrical and Magnetic methods of Nondestructive Testing"*, Adam Hilger, ISBN: 0-7503-0148-1, 1991.

[93] Xin Li, W Yin, Ze Liu, Philip J. Withers, A J Peyton, *"Characterization of Carbon Fibre Reinforced Plastic by Means of Eddy Current Non-Destructive Testing and FEM Modeling"*, 17th World conference of Non-destructive Testing, ShangHai, 2008.

[94] Yin W, A J Peyton, and Dickinson S J, *"Simultaneous measurement of distance and thickness of a thin metal plate with an electromagnetic sensor using a simplified model"*, IEEE Trans. Instrum. Meas., 53, pp.1335-1338, 2004.

[95] W Yin, Xin Li, Philip J. Withers, A J Peyton, *"Non-contact characterization of hybrid aluminium/carbon-fibre-reinforced plastic sheets using multi-frequency eddy-current sensors"*, Measurement and Science Technology, 21, 105708 (7pp), 2010.

[96] W Yin, Xin Li, Philip J. Withers, A J Peyton, *"Non-Contact Characterisation of Carbon Fibre Reinforced Plastics in Hybrid Aluminium / CFRP Sheets Using*

Multi-frequency Eddy Current Sensors", IEEE International Instrumentation and Measurement Technology Conference, Singapore, 2009